EFFECT OF EXOTIC MAGNETIC PHASES ON THE MAGNETO-TRANSPORT PROPERTIES OF $Fe_{80-x}Ni_xCr_{20}$ ALLOYS ($14 \leq X \leq 30$)

A Thesis Submitted

in Partial Fulfillment of the Requirements

for the Degree of

Doctor of Philosophy

by

GAUTAM SINHA

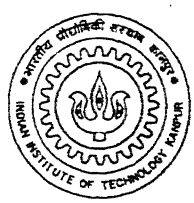

to the

DEPARTMENT OF PHYSICS

INDIAN INSTITUTE OF TECHNOLOGY KANPUR

SEPTEMBER, 1998

CERTIFICATE

It is certified that the work contained in this thesis entitled "*Effect of Exotic Magnet*
Phases on the Magneto-transport Properties of $Fe_{80-x}Ni_xCr_{20}$ *Alloys* $(14 \leq X \leq 30)$", *Gautam Sinha*, has been carried out under my supervision and that this work has not be submitted elsewhere for any degree.

Alak Kumar Majumdar 3/9/9

Dr. Alak Kumar Majumdar
Professor
Department of Physics
Indian Institute of Technology
Kanpur

September, 1998

SYNOPSIS

Magnetic alloys with competing exchange interactions exhibit long-range order (ferro- or antiferromagnetic) as well as spin-glass like ordering depending upon the concentration (C) of the magnetic component(s) present. Above a certain critical concentration (C_0) these alloys show double transitions [paramagnetic(PM) $\rightarrow$ ferromagnetic(FM) $\rightarrow$ reentrant spin glass(RSG)(where FM and spin glass(SG) orderings coexist)] with the lowering of temperature. Many interesting but often contradictory results are reported on these alloy systems (AuFe, CrFe, PdFeMn, FeNiMn, PtMn, NiMn, Co_2TiO_4, $Eu_{1-x}Sr_xS$, FeNi, FeMn, etc.). $Fe_{80-X}Ni_XCr_{20}$ alloys are one such system which shows diverse magnetic phases within the *same crystallographic phase*. These alloys exhibit a compositional phase transition from a long-range antiferromagnetic(AF) phase (X=14) to a long-range FM one (X=30), passing through intermediate phases of SG (X=19) and RSG (X=23, 26) with increasing Ni concentration. The presence of the strong competing ferro- [I(Ni-Ni), I(Fe-Ni), I(Ni-Cr), I(Fe-Cr)] and antiferromagnetic[I(Fe-Fe), I(Cr-Cr)] exchange interactions is responsible for such exotic phases. An enormous amount of theoretical and experimental effort has gone into understanding the various properties of these magnetic alloys. However, none of them contain comparative studies of these alloys in different magnetic phases, especially in the SG and the RSG phases. Taking advantage of the diverse magnetic properties of these alloys within the *same fcc γ-phase* the present work is intended to fill this void. In spite of the huge amount of work, several important questions still remain unanswered. *Is there any difference between*

an SG and an RSG at the lowest temperature? Does FM order exist in the RSG phase down to the lowest temperature? Is the transition near T_C similar to the FM to PM transition? All these motivated us to systematically study the properties of these alloys. To arrive at some meaningful conclusions, we have looked into these problems from four different angles:

1. Relaxation of magnetization,
2. Low-field magnetoresistance,
3. Linear and non-linear ac susceptibilities, and
4. Hall effect.

Chapter 1 begins with a brief historical review of magnetism followed by various theoretical models which we will be needing to explain our experimental data. We have also included a review of the present understanding of this field related to our work.

In *Chapter 2* we have given the experimental procedures in details. We have presented the phase diagram of the $Fe_{80-X}Ni_XCr_{20}$ ($10 \leq X \leq 30$) alloys along with the sample preparation and characterization. We have also described the various experimental techniques and design of cryostats.

In *Chapter 3* we present the time decay of the thermo-remanent magnetization(TRM) of the $Fe_{80-X}Ni_XCr_{20}$ ($14 \leq X \leq 30$) alloys for four different magnetic phases within the fcc γ-phase. The TRM is measured as a function of time(30 to 12,000 s) using a SQUID magnetometer(Quantum Design, MPMS) for various wait times and temperatures above and below the characteristic temperatures. We find distinct differences between the SG and the RSG phases with two different analytical forms for the time decay of the TRM. In the SG(X=19) very distinct ageing effects are observed where M(t) can be described as $M(t) = M_0(t/t_w)^{-\gamma}\exp[-(t/\tau)^{1-n}]$ for the entire time domain. In the RSG(X= 23 and 26), M(t) can be better represented by the stretched exponential with an addition of a constant term which can be explained well by the Gabay-Toulouse(GT) model. We also report the

remarkable observation of the local maximum of the TRM just above T_C in the RSG (X=23) when it passes to the PM phase from the FM phase. This is found for the first time in any polycrystalline RSG. We have tried to give an intuitive explanation for this though it's exact theoretical justification is unclear. We also observe that the values of the exponents show anomaly near the phase transitions. We observe some different features in the samples X=23 and X=26, although they undergo similar kinds of phase transitions. We find the conventional power law decay in the FM phase. The value of the magnetization is found to increase with the Ni concentration. In the AF phase the power law decay is indistinguishable from the stretched exponential as a description of the TRM.

In *Chapter 4* we present the low-field($<$ 30 gauss) magnetoresistance (LFMR) of the SG, FM and the RSG phases. We have used pulsed magnetic field in the presence of various static biasing fields for LFMR measurements. We observe that the LFMR is negative in the SG(X=19) and the PM phases and positive in the FM (X=30) phase. In the RSG (X=26), at the lowest temperature (4.5 K), the intrinsic LFMR is positive for zero biasing field, but the presence of a 18.2 gauss static biasing field makes the LFMR negative, a feature generally associated with the SG state. This suggests that the lowest temperature phase of the RSG has mixed FM and SG-type of orderings. We believe that small FM clusters are embedded in a matrix of frustrated spins of the SG. We observe hysteresis effects in the LFMR for small applied fields at the lowest temperature for the RSG sample. But such small fields do not produce any hysteresis effect in the FM phase(X=30). We find that the LFMR becomes negative around T_C for a +4 gauss pulsed field in the RSG. From the LFMR measurements, we conclude that when the RSG sample(X=26) goes from the PM to the FM phase with lowering of temperature, it passes through an intermediate phase. Here the PM(SG) phase coexists with the FM phase for a very narrow temperature interval. So with the reduction of temperature, the RSG sample passes through various magnetic phases like, $PM \rightarrow (PM(SG) + FM) \rightarrow FM \rightarrow RSG(= FM + SG)$. We also find a close resemblance between the temperature variation of the LFMR and the ac susceptibility in

the RSG(X=26).

In *Chapter 5* we present the low-field ac susceptibility and its dc field dependence in the four different magnetic phases of $Fe_{80-X}Ni_XCr_{20}$ alloys. In the SG phase(X=19) the transition temperature(T_g) varies with frequency(ν) and follows Fulcher's law of the form $\nu = \nu_0 \exp[-\frac{E_a}{k(T_g-T_0)}]$ while the non-linear susceptibility(χ_2) shows a peak at T_g. In the RSG (X=26 and 23), double transitions are clearly seen from the imaginary part of the linear susceptibility(χ_0''). The peak near the upper transition vanishes in the presence of a small dc biasing field. We compare the lower transition of the RSG with that of an SG and the upper one with that of a ferromagnet(FM). Critical exponents, γ, β, and δ are obtained from χ_0 and its dc field dependence in the RSG(X=26). They follow the scaling law obtained from the mean-field theory(MFT) although the values of the exponents are not in agreement with it. The non-linear susceptibility (χ_1) shows a peak near T_g in both the RSG's which is indicative of a long-range order. This is never observed in a pure SG, including X=19. The value of the critical exponent γ increases with the increase in Ni concentration (X=23 to 30) as the system moves towards the FM phase(X=30). In the antiferromagnet(X=14), the transition temperature (T_N) shifts towards higher temperatures in the presence of small dc fields.

The Hall effect for the four different magnetic phases of these alloys is reported in *Chapter 6*. In the SG (X=19) the Hall resistivity(ρ_H) increases with the field and does not saturate till 1.6 T. The temperature variation of ρ_H shows broad peaks around T_g for lower fields (< 0.1 T) but they disappear at higher fields(1 T). We separate the ordinary(OHC) and the extra-ordinary(EHC) Hall coefficients in the ferromagnetic sample(X=30) and show their temperature variations. In the RSG (X=26) ρ_H shows a non-linear variation with field. The temperature variation of ρ_H shows anomaly near both T_g and T_C. In the antiferromagnetic phase (X=14) ρ_H increases linearly with field and its temperature variation shows broad peaks around T_N for lower fields.

Chapter 7 presents some of the conclusions of the present work.

Acknowledgments

A doctoral project is like a broth. You have too many cooks, yet interestingly it is never spoilt. Simply because each cook is a legend in his own right. My doctoral project was no exception. Now let me introduce you to them.

Prof. Alak Kumar Majumdar was instrumental in making the project a success. His influence extended from the laboratory to the library, and from my hostel to my home. Such profound impact has left an indelible mark on my consciousness. And I treasure it.

In my laboratory I was privileged to have a team that epitomised dynamism, efficiency, and brilliance. A. Banerjee, A. Das, R. Singhal, N. Sudhakar, S. V. Sharma, Tapan, Swapan, A. Tiwari, K. P. Rajeev, Kapil, Ravindran, D. C. Banerjee, C. V. Tomy, G. D. Mukherjee, Ramprakash, and Ramashray; each of them, in their own way contributed, in some measure and each measure made the broth all the more presentable.

Beyond the laboratory, Profs. R. K. Theraja, O. P. Katyal. D. Chowdhury, Y. N. Mohapatra, V. Subrahmanyam, M. K. Verma, and K. R. Srivasthan provided those vital inputs at appropriate occasions to make the project a successful one.

Enlighted discussions with Professors R. D. Barnard and R. Chatterjee added some new flavours in it.

I am indebted to the people of physics workshop, physics office, glass-blowing center, and liquid nitrogen plant who have without exception always been most helpful.

It is pointless to enumerate who has done what. To do that would be to dishonour

them. Let not their help be measured in any M.K.S or F.P.S units, since help like gratitude is fortunately immeasurable.

It is with immeasurable love that I remember my father. He died with the belief that magnetism had changed my life, had given his son a new quest for acme. I remember him, not with just admiration, as that is too popular a sentiment all over the world, but with respect for his foresight. It is the foresight which creates history, and forbearance that builds it. My mother had the latter. To my parents goes out a silent burst of Super Nova feelings - let it not be expressed in words, and tarnished with the ink of the printer.

To make an endless list is indiscretion. The final tribute goes to those who need no mention because they live in every spoonful of the broth you are to test now.

Gautam Sinha

To those
who promote education

Contents

List of Figures

List of Tables

Chapter 1

Introduction

Magnetic alloys with competing exchange interactions exhibit long-range order (ferro- or antiferromagnetic) as well as spin-glass like ordering depending upon the concentration (C) of the magnetic component(s) present. Above a certain critical concentration (C_0) these alloys show double transitions [paramagnetic(PM) $\rightarrow$ ferromagnetic(FM) $\rightarrow$ reentrant spin glass(RSG)(where FM and spin-glass(SG) orderings coexist)] with the lowering of temperature. Many interesting but often contradictory results are reported on these alloy systems (AuFe, CrFe, PdFeMn, FeNiMn, PtMn, NiMn, Co_2TiO_4, $Eu_{1-x}Sr_xS$, FeNi, FeMn, etc.). $Fe_{80-X}Ni_XCr_{20}$ alloys are one such system which shows diverse magnetic phases within the *same crystallographic phase*[1]. These alloys exhibit a compositional phase transition from a long-range antiferromagnetic(AF) phase (X=14) to a long-range FM one (X=30), passing through intermediate phases of SG (X=19) and RSG (X=23, 26) with increasing Ni concentration. The presence of strong competing ferro- [I(Ni-Ni), I(Fe-Ni), I(Ni-Cr), I(Fe-Cr)] and antiferromagnetic[I(Fe-Fe), I(Cr-Cr)] exchange interactions is responsible for such exotic phases. An enormous amount of theoretical and experimental effort has gone into understanding the various properties of these magnetic alloys. However, none of them contain comparative studies of these alloys in different magnetic phases, especially in the SG and the

RSG phases. Taking advantage of the diverse magnetic properties of these alloys within the *same fcc γ-phase* the present work is intended to fill this void. In spite of the huge amount of work, several important questions still remain unanswered. *Is there any difference between an SG and an RSG at the lowest temperature? Does FM order exist in the RSG phase down to the lowest temperature? Is the transition near T_C similar to the FM to PM transition?* All these motivated us to systematically study the properties of these alloys. To arrive at some meaningful conclusions, we have looked into these problems from four different angles:

1. Relaxation of magnetization,
2. Low-field magnetoresistance,
3. Linear and non-linear ac susceptibilities, and
4. Hall effect.

1.1 Brief historic review

Having stated the basic objectives of the thesis, we would like to begin with a brief introduction. Magnetism is one of the oldest fields known to us. It had started with the invention of 'Lodestone' (magnetite) and its wonderful property of attracting iron pieces whose reference is found in Chinees literature of as early as 3000 B.C. The use of the magnetic compass is a pre-historic matter. Magnetism is an ever diverging field, with time it encompasses various kinds of magnetism starting from Loadstone to the most recent magnetic superconductors. The first theory of magnetism was proposed by Descartes in the beginning of 17th century. However, true understanding of magnetism came at the end of last century with the advent of Curie law(1895), Zeeman effect(1896), Langevin's theory of dia- and para-magnetism(1905), etc. On one hand the development of quantum and statistical mechanics strengthened our understanding of magnetism, on the other hand the advancement in technology helped in inventing new magnetic materials. Three decades back a new magnetic system was found

which is known today as "spin glass". *Spin glass is a random, interacting, frustrated magnetic system where no long-range order exists, yet it shows a cooperative freezing of spins, below a well-defined temperature (T_g), following a second order phase transition and marked with strong irreversibility and time dependent phenomena.* SG-like behaviour was first observed in dilute magnetic alloys(AuFe, CuMn) in the late 1960s. It took several years to experimentally identify the possibility of a phase transition in SG's through the observation of a sharp cusp in ac susceptibility measurements. In 1975, the first theoretical model came with a new order parameter to define the phase transition followed by several other models later. However, till today a complete understanding of SG's and a good correspondence between theory and experiment are not established. A new form of statistical mechanics and radically new concepts are needed to go deeper into the SG problem. The basic concepts of a SG are now-a-days successfully used in various other physical systems like, combinatorial optimization, neural networks, and biological evolution.

1.2 Theoretical models

In this thesis we will be dealing with FM, AF, SG, and RSG. Theoretical developments of FM and AF, where long-range order exists, are well established and readily available in the literature. So, here we will only briefly outline the various theoretical developments of SG and RSG which will be referred quite often throughout this thesis.

1.2.1 Edwards and Anderson model

In 1975, Edwards and Anderson(EA) proposed a model to describe the random freezing of a SG. In a SG, below the freezing temperature(T_g), each spin S_i is frozen along a preferred direction whose orientation is random over the distribution of sites i. To describe any phase transition one needs an order parameter which shows anomaly near the phase transition. As there is no long-range order or any other spatial correlation, EA proposed a new kind of

order parameter, q, which depends on the time scale. Mathematically this time correlation can be written as

$$q = \lim_{t\to\infty} << S_i(0).S_i(t) >_T >_C, \tag{1.1}$$

where $< .. >_T$ is the thermal average and $< .. >_C$ is the configurational average over all spins. It means that if a spin is frozen at site i at time t = 0, then its orientation will remain the same after a very long time($t \to \infty$). Naturally the order parameter $q = 1$ at $T = 0$ and $q \to 0$ as $T \to T_g$. So, a SG is characterised by the non-zero q where $<< S_i >_T >_C = 0$.

According to this model the Hamiltonian is given by

$$\mathcal{H} = -\sum_{ij} J_{ij} S_i.S_j - \sum_i H_i.S_i. \tag{1.2}$$

The classical spins on site i and j interact via the random exchange coupling J_{ij} which satisfy a Gaussian distribution.

$$P(J_{ij}) = \frac{1}{\sqrt{2\pi\Delta^2}} \exp\left(-\frac{J_{ij}^2}{2\Delta^2}\right), \tag{1.3}$$

where Δ is the variance. The free energy can be written as

$$F = -k_B T \ln Z = -k_B T \; Tr\left(\exp -\frac{\mathcal{H}}{k_B T}\right), \tag{1.4}$$

where Z= partition function.

This model can give solution in the limits $T \to 0$ and $T \to T_g$. The solutions are

$$q(T \to 0) = 1 - \sqrt{\frac{2}{3\pi}}\,\frac{T}{T_g}, \tag{1.5}$$

$$q(T \to T_g) = -\frac{1}{2}\left[1 - \left(\frac{T_g}{T}\right)^2\right], \tag{1.6}$$

$$\lim_{H\to 0} \chi_{ac}(T \le T_g) = \frac{(g\mu_B)^2}{3k_B T_g} - O(T_g - T)^2, and \tag{1.7}$$

$$\lim_{H\to 0} \chi_{ac}(T \to 0) = \frac{(g\mu_B)^2}{3k_B T}\sqrt{\frac{2}{3\pi}}\,\frac{T}{T_g}. \tag{1.8}$$

This model predicts an asymmetric cusp in χ_{ac} at T_g and a constant value at $T \to 0$

which is close to the experimental observations. This model was extended by Fischer using quantum spins (S=1/2) instead of classical one($S = \infty$) and a different technique. This explains the experimentally observed χ_{ac} better but it disagrees with the specific heat data.

1.2.2 Sherrington-Kirkpatrick model(SK)

In 1975, SK proposed an infinite-range mean-field theory(MFT) where every spin couples equally with every other spin. This means that the probability distribution $P(ij)$ is the same for all i-j pairs of spins independent of their spatial distribution which is an unphysical ansatz. The beauty of the MFT is that it is completely solvable and can explain experimental results to a large extent.

SK considered an Ising SG with a Gaussian distribution

$$P(J_{ij}) = \frac{1}{\Delta}\sqrt{\frac{N}{2\pi}}\ \exp\left[-\frac{N\left(J_{ij}-\frac{J_0}{N}\right)^2}{2\Delta^2}\right]. \tag{1.9}$$

This means that the spins($\#N$) interact via a Gaussian distribution of exchange forces centered at J_0(mean value) with width Δ(variance).

Using "replica trick" they found the solutions and the results are

$$q = \frac{1}{\sqrt{2\pi}}\int \exp\left[-\frac{Z^2}{2}\right]\tanh^2\left[\frac{\Delta\sqrt{q}}{k_BT^Z}+\frac{J_0m}{k_BT}\right]dZ, \tag{1.10}$$

$$and\ m = \frac{1}{\sqrt{2\pi}}\int \exp\left[-\frac{Z^2}{2}\right]\tanh\left[\frac{\Delta\sqrt{q}}{k_BT^Z}+\frac{J_0m}{k_BT}\right]dZ. \tag{1.11}$$

This model predicted three possibilities for phase transitions depending on $\frac{J_0}{\Delta}$; (i) PM $\rightarrow$ SG (ii) PM $\rightarrow$ FM and (iii) PM $\rightarrow$ FM $\rightarrow$ SG. A similar phase diagram is experimentally observed in the ternary $Pd_{1-y-x}Fe_yMn_x$ system. This model also explained the variation of χ_{ac} and its field dependence. However, there are some major drawbacks of this model like, (i) entropy becomes negative as $T \rightarrow 0$ which is unphysical, (ii) the free energy is not minimized with respect to q for the solution q= 0, $T > T_g$ and $q \neq 0$, $T < T_g$. The $q = 0$ solution (i.e. PM state) below T_g has a lower free energy than the SG state($q \neq 0$). The

reasons for these discrepancies may be because of the use of the "replica trick" and treating all the replicas as indistinguishable.

To overcome these fundamental discrepancies Thouless, Anderson, and Palmer introduced a new approach. They argued that a spin $< S_i >_T$ at site i produces a field $J_{ij} < S_i >_T$ at site j and induces a moment $J_{ij} < S_i >_T \chi_{jj}$ (χ_{jj}= local susceptibility) at that site. This induced moment in turn produces a reaction field back at site i. They included this correction term in the original mean-field equation and found the solution. Though this approach removed the fundamental discrepancies but it was far from explaining the experimental results like, specific heat.

In 1979 Parisi proposed a new scheme called replica symmetry breaking(RSB) to remove the defects of the SK solution. It gives a new Parisi order parameter, q(x), which is continuous and can be written as

$$-\lim_{n\to 0}\frac{1}{n}\sum_{\alpha\beta} q_{\alpha\beta} = \int_0^1 q(x)dx, \tag{1.12}$$

where $q_{\alpha\beta}$ is the overlap function and n is the number of replica. According to RSB model the susceptibility(χ) and the internal energy (U) can be given by

$$\chi = \frac{1}{k_B T}\int_0^1 [1 - q(x)]dx, \tag{1.13}$$

$$and\ U = -\frac{1}{2k_B T}\int_0^1 [1 - q^2(x)]dx. \tag{1.14}$$

χ(RSB) is constant for $T = T_g$ which is somewhat similar to the experimentally observed field-cooled susceptibility but not χ_{ac}. RSB when combined with the stable SK solution(above the instability line) gives an expression of M(T,H) from which it is found that the non-linear susceptibility, $\chi_{nl} = \frac{\partial^3 M}{\partial H^3}$ diverges according to the mean-field critical exponent $\gamma = 1$. This model also predicts the existence of multi-valley free energy landscape which supports the presence of different relaxation times in a SG. We will discuss this later in details while analysing our magnetic relaxation data.

1.2.3 Gabay and Toulouse model(GT)

GT proposed an m-component vector spin model where the SG order parameter is a tensor in spin space. They consider an infinite range model of N classical vector spin S_i, each of them has m components and follows normalization condition $\sum_{\mu=1}^{m} S_{i_\mu}^2 = m$. They interact via independent random interactions J_{ij} distributed according to the following law

$$P(J_{ij}) = \sqrt{\frac{N}{2\pi}} \exp\left[-\frac{N}{2}\left(J_{ij} - \frac{J_0}{N}\right)^2\right], \tag{1.15}$$

where $< J_{ij} >_b = \frac{J_0}{N}$ and $< J_{ij}^2 >_b = \frac{1}{N}$ and $< .. >_b$ means an average over the bond disorder and J_0 is the mean interaction. The Hamiltonian of this system can be given by

$$\mathcal{H} = -\sum_{ij} J_{ij} \sum_{\mu} S_{i_\mu} S_{j_\mu} - H \sum_{i} S_{ij}, \tag{1.16}$$

where H is the external field applied along $\mu = 1$ direction and sum over ij means a summation over the $\frac{N(N-1)}{2}$ distinct pairs of sites. In the limit of $J_0 \to$ *large* and positive, interactions are mainly ferromagnetic and $J_0 = 0$ interactions are random in sign and the orderings are SG like. The interesting region is near $J_0 \approx 1$ where FM and SG coexist.

For $N \to \infty$ and $J = 0$ they performed expansion of free energy F in powers of H, q_μ, and S_μ up to the fourth order and predicted a H-T phase diagram (q_μ= EA order parameter and $S_\mu = << S_\mu^2 >_b >_T - 1$ = quadrupolar deformation parameter). The line in the H-T plane where the freezing of the transverse degree of freedom of spins occurs is called the GT line which varies as $H^2 \approx 4(\frac{m+2}{m+4})(1-T)$ for $T \leq 1$ and $T \approx K_1(m) \exp\left[-\frac{H^2}{2m}\right]$ for $T \simeq 0$. This transition occurs because of the freezing of only the transverse component(w.r.t applied field) of the spin degree of freedom. Hence this cannot be observed in the Ising case where m=1. de Almeida and Thouless found a line in the H-T plane (AT line) where longitudinal spins freeze for m=1 and the breaking of replica symmetry takes place. It varies as $H^2 \approx \frac{4}{m+2}(1-T)^3$ for $T \leq 1$ and $T \approx K_2(m) \exp\left[-\frac{H^2}{2m}\right]$ for $T \simeq 0$.

But the most interesting region is the SG to FM transition where $J_0 \neq 0$ but ≥ 1. It predicts the possibility of the existence of various phases like, (i) PM $\to$ SG for $J_0 < 1$, (ii)

reasons for these discrepancies may be because of the use of the "replica trick" and treating all the replicas as indistinguishable.

To overcome these fundamental discrepancies Thouless, Anderson, and Palmer introduced a new approach. They argued that a spin $< S_i >_T$ at site i produces a field $J_{ij} < S_i >_T$ at site j and induces a moment $J_{ij} < S_i >_T \chi_{jj}$ (χ_{jj}= local susceptibility) at that site. This induced moment in turn produces a reaction field back at site i. They included this correction term in the original mean-field equation and found the solution. Though this approach removed the fundamental discrepancies but it was far from explaining the experimental results like, specific heat.

In 1979 Parisi proposed a new scheme called replica symmetry breaking(RSB) to remove the defects of the SK solution. It gives a new Parisi order parameter, q(x), which is continuous and can be written as

$$-\lim_{n\to 0}\frac{1}{n}\sum_{\alpha\beta} q_{\alpha\beta} = \int_0^1 q(x)dx, \tag{1.12}$$

where $q_{\alpha\beta}$ is the overlap function and n is the number of replica. According to RSB model the susceptibility(χ) and the internal energy (U) can be given by

$$\chi = \frac{1}{k_B T}\int_0^1 [1 - q(x)]dx, \tag{1.13}$$

$$and\ U = -\frac{1}{2k_B T}\int_0^1 [1 - q^2(x)]dx. \tag{1.14}$$

χ(RSB) is constant for $T = T_g$ which is somewhat similar to the experimentally observed field-cooled susceptibility but not χ_{ac}. RSB when combined with the stable SK solution(above the instability line) gives an expression of M(T,H) from which it is found that the non-linear susceptibility, $\chi_{nl} = \frac{\partial^3 M}{\partial H^3}$ diverges according to the mean-field critical exponent $\gamma = 1$. This model also predicts the existence of multi-valley free energy landscape which supports the presence of different relaxation times in a SG. We will discuss this later in details while analysing our magnetic relaxation data.

1.2.3 Gabay and Toulouse model(GT)

GT proposed an m-component vector spin model where the SG order parameter is a tensor in spin space. They consider an infinite range model of N classical vector spin S_i, each of them has m components and follows normalization condition $\sum_{\mu=1}^{m} S_{i_\mu}^2 = m$. They interact via independent random interactions J_{ij} distributed according to the following law

$$P(J_{ij}) = \sqrt{\frac{N}{2\pi}} \exp\left[-\frac{N}{2}\left(J_{ij} - \frac{J_0}{N}\right)^2\right], \tag{1.15}$$

where $< J_{ij} >_b = \frac{J_0}{N}$ and $< J_{ij}^2 >_b = \frac{1}{N}$ and $< .. >_b$ means an average over the bond disorder and J_0 is the mean interaction. The Hamiltonian of this system can be given by

$$\mathcal{H} = -\sum_{ij} J_{ij} \sum_{\mu} S_{i_\mu} S_{j_\mu} - H \sum_{i} S_{ij}, \tag{1.16}$$

where H is the external field applied along $\mu = 1$ direction and sum over ij means a summation over the $\frac{N(N-1)}{2}$ distinct pairs of sites. In the limit of $J_0 \rightarrow large$ and positive, interactions are mainly ferromagnetic and $J_0 = 0$ interactions are random in sign and the orderings are SG like. The interesting region is near $J_0 \approx 1$ where FM and SG coexist.

For $N \rightarrow \infty$ and $J = 0$ they performed expansion of free energy F in powers of H, q_μ, and S_μ up to the fourth order and predicted a H-T phase diagram (q_μ= EA order parameter and $S_\mu = << S_\mu^2 >_b >_T - 1$ = quadrupolar deformation parameter). The line in the H-T plane where the freezing of the transverse degree of freedom of spins occurs is called the GT line which varies as $H^2 \approx 4(\frac{m+2}{m+4})(1-T)$ for $T \leq 1$ and $T \approx K_1(m) \exp\left[-\frac{H^2}{2m}\right]$ for $T \simeq 0$. This transition occurs because of the freezing of only the transverse component(w.r.t applied field) of the spin degree of freedom. Hence this cannot be observed in the Ising case where m=1. de Almeida and Thouless found a line in the H-T plane (AT line) where longitudinal spins freeze for m=1 and the breaking of replica symmetry takes place. It varies as $H^2 \approx \frac{4}{m+2}(1-T)^3$ for $T \leq 1$ and $T \approx K_2(m) \exp\left[-\frac{H^2}{2m}\right]$ for $T \simeq 0$.

But the most interesting region is the SG to FM transition where $J_0 \neq 0$ but ≥ 1. It predicts the possibility of the existence of various phases like, (i) PM $\rightarrow$ SG for $J_0 < 1$, (ii)

PM $\rightarrow$ FM, (iii) PM $\rightarrow$ FM $\rightarrow M_1$ [M_1 is a first mixed phase where FM and SG (frozen transverse components) phases coexist], and (iv) PM $\rightarrow$ FM $\rightarrow M_1 \rightarrow M_2$ where M_2 has the spontaneous breaking of replica symmetry in addition to the coexistence. According to this model FM $\rightarrow M_1$ transition line in $T - J_0$ plane can be defined as

$$1 - T \approx \frac{1}{2}\left(\frac{m+4}{m+2}\right)(J_0 - 1)^2, \tag{1.17}$$

for $J_0 \geq 1$ where $m \neq 1$. The transition from $M_1 \rightarrow M_2$ varies as

$$1 - T \approx \sqrt{\frac{m+2}{3}}\sqrt{J_0 - 1}, \tag{1.18}$$

for $J_0 \geq 1$. Finally the transition between M_2 and SG is given by $J_0(T) = \chi^{-1}$ $(J_0 = 0)$. Experimentally the existence of M_1 phase was found in $AuFe$ by Coles et al. However, other investigators could not get any experimental evidence of the coexistence. The SK model also does not support the coexistence. The low-temperature magnetic phase where the FM and SG coexist is called the RSG phase. In this report we experimentally test the coexistence in FeNiCr alloys.

1.2.4 Droplet model

In 1986, Fisher and Huse had given a completely new phenomenological scaling theory of droplet excitations for a short-range Ising SG. The basic concept of this model is the formation of 'droplet' of length L in the ground state. All the spins inside the droplet are oriented downwards while the outside spins are oriented up. So there exists a global reversal of spins(or spin flips) inside the length scale L. This model predicts a phase transition below T_g where the global spin-reversal symmetry is broken. In each state these droplets are the dominant low-lying excitations. The free energy of the droplet can be given by $F_L \propto \gamma(T)L^{\theta}$ where γ = stiffness constant and θ = exponent. From the calculation of the distribution of droplet free energy $\rho(F_L)$ and the correlations between them, the value of the χ_{nl} was predicted which diverges at T_g for $d > (1 + \phi)\theta$ where ϕ is an exponent governing the dependence of ρ on F_L.

Annihilation and creation of droplet excitations determine the equilibrium low-frequency dynamics of the ordered phase. The characteristic time for a droplet to grow to a length L is given by $\tau = \tau_0 \exp[L^{\psi}/k_B T]$ where ψ is a new exponent $\theta \leq \psi \leq d-1$. This model predicts a logarithmic decay of the autocorrelation function, $c(t) \approx (\ln t)^{-\theta/\psi}$. According to this model $\chi'(\omega) \approx |\ln \omega|^{-\theta/\psi}$ and $\chi''(\omega) \approx |\ln \omega|^{\theta/\psi - 1}$ and $\chi_{nl}(3\omega) \approx |\ln \omega|^{[d-(1-\phi)\theta]/\psi}$ which diverges for $\omega \rightarrow 0$ if $d > (1+\phi)\theta$.

The effects of droplet fluctuation on dynamics are very interesting. When a system cools down below T_g, it tries to reduce its free energy with time. The droplets, where the spins are pointed downwards, are embedded in the up-magnetized phase. Hence the free energy of the system depends on the length of the domain wall, i.e. the amount of interface between these oppositely oriented domains of spins. Formation of larger droplets reduces the interface and hence the free energy. The characteristic length of the domain grows with time as $R_{t_a} \approx [k_B T \ \ln(t_a/t_0)/\Delta(T)]^{1/\psi}$ where t_a is the total age of the system after cooling below T_g and t_0 is a microscopic unit of time. This growth of the domains is responsible for the long-time, non-equilibrium dynamics in a SG below T_g. According to this model the decay of magnetization is given by $M(t) \approx [k_B T \ln t]^{-\lambda/\psi}$ where λ is a new dynamical exponent.

With this background of the general description of some magnetic systems, we now look into the specific observable quantities more closely.

1.3 Relaxation of magnetization

The search for magnetic relaxation began a century back when Ewing[2] observed the persistence of magnetization in soft iron for significant amount of time and a non-exponential decay. Richter[3] observed a logarithmic decay of magnetization over one decade of time in carbonised iron. Street and Woolley[4] and Néel[5] also predicted a logarithmic decay of thermo-remanent magnetization(TRM) in FM's. Several theoretical and experimental

evidences suggest that an anomalous slower relaxation of the form

$$M(t) = M_0 \exp\left[-(t/\tau)^{\beta}\right] , \quad 0 < \beta < 1 \tag{1.19}$$

is far more reasonable and common than the conventional Debye exponential form($\beta = 1$). In fact, this kind of relaxation has been observed for a wide range of phenomena and materials[6]. In 1970, Williams and Watts[7] postulated similar functions for dielectric relaxation ($\beta = 0.5$). In a review article Jonscher[8] summarized the experimental evidence on the frequency, time, and temperature dependence of the dielectric response for a wide range of solids. He also found a universality in dielectric behaviour and proposed a generalized approach of many-body interaction. The structural relaxation rate, in the case of liquid to glass transition, can be expressed as a stretched exponential ($2/3 < \beta < 1$)[9]. Also the validity of this functional form for the relaxation of TRM in SG's has been reported by a large number of investigators[10–14]. Palmar et al.[15] presented, in an elegant fashion, the whole scenario of similar kinds of relaxation in complex, slowly relaxing, and strongly interacting materials. They considered series relaxation and hierarchically constrained dynamics which is distinctly different from other approaches[16] of getting similar results. Hammann et al. proposed a phenomenological picture of the dynamic properties of SG based on fractal cluster model[17, 18]. Early decay measurements of TRM of spin glasses had shown logarithmic dependence[19]. Similar dependence was also observed in AuFe, AgMn, and ThGd spin glasses from 5 to 10^4 s[20]. Analysing the neutron diffraction and ac susceptibility data, Murani[21] found power law decay for shorter time and logarithmic decay for longer time below T_g in SG's. Bontemps and Orbach[22] measured the TRM of the insulating SG $Eu_{0.4}Sr_{0.6}S$ between $0.86T_g$ and $1.04T_g$. They found power law decay of the TRM for shorter interval of time and a stretched exponential decay beyond a well-defined cross-over time.

Recently two different theoretical models have been proposed to describe the SG behaviour. The first is the mean-field approach of Parisis's solution[23] of infinite range Sherrington-Kirkpatrick(SK)[24] model by considering hierarchical organizations of infinite

number of quasi-equilibrium states separated by finite barriers in phase space[25]. The second is the phenomenological approach based on the existence of a distribution of droplets[26] or dynamical domains[27] of correlated spins. The droplet model defines a characteristic length for the groups of correlated spins which slowly increases with time when temperature is less than T_g. However, any change in the temperature (ΔT) breaks the correlation above a certain overlap length($l_{\Delta T}$). The presence of thermally activated droplets of various sizes causes a long time non-exponential relaxation. The basic difference between these two models is the nonsymmetric behaviour of the hierarchical picture with respect to temperature change of the mean-field model in comparison with the symmetric behaviour of the droplet model where the

overlap length only depends on the absolute value of the temperature difference. Both these theories can explain reasonably well the slower SG dynamics and ageing effects. A detailed comparison between these two models was given by Lefloch et al.[28]. Huse and Fisher[26] proposed the long time decay as stretched exponential with exponent 1/2 by using droplet fluctuations in two dimensional pure Ising system with a spontaneously broken continuous symmetry. In the framework of droplet fluctuations[26], the spin autocorrelation can be described as exponentially rare in $\ln t$: $\overline{c_i(t)} = \exp[-k(\ln t)^y]$ (where $y = 1$ for random exchanges, $y = d - 2/d - 1$ for random fields) in random FM's and power of $\ln t$ in SG's. Ogielski[29] predicted that the spin autocorrelation function can be described by the product of a power law and a stretched exponential at all temperatures above T_g[30] and by a power law below T_g.

Recently, Chu et al.[31] have proposed a model in the framework of the SK mean-field theory which can explain the experimental data reasonably well. According to them the energy phase space for an experimental sample with a finite number of spins consists of quasi-degenerate metastable states separated from each other by finite energy barriers. The distance between two metastable states α and β, called Hamming distance $d_{\alpha\beta}$, is $\frac{1}{2}(q_{EA} - q_{\alpha\beta})$, where q_{EA} is the Edwards-Anderson order parameter and $q_{\alpha\beta} = \frac{1}{N}\sum_{i=1}^{N} S_i^{\alpha} S_i^{\beta}$

is the overlap of their spin configurations. The barrier height $\Delta_{\alpha\beta}$ is an exponential function of the Hamming distance. When a system is cooled to T_m ($T_m < T_g$) in the presence of a field H, it occupies a set of metastable states in the energy landscape appropriate to that temperature and field. If the field is on for t_w s (wait time), then the system will try to equilibrate among the metastable states and in this process overcomes the higher barrier heights. The time it takes to go from one valley to another is proportional to the exponential of the barrier height ($\Delta_{\alpha\beta}$). It suggests the existence of different relaxation times that can be given as $\tau_{\alpha\beta} = \tau_0 \exp(\frac{\Delta_{\alpha\beta}}{kT})$. Here, τ_0 is called the microscopic attempt time which is of the order of 10^{-13} s and is proportional to T_g^{-1}. Hence the maximum barrier height that it can overcome will be determined by the wait time $t_w(\tau_{\alpha\beta} = t_w)$. When the magnetic field is switched off($H \rightarrow 0$) the change in Zeeman energy (M.H $\rightarrow$ 0) causes a 'tilt' in the phase space which helps to drive the system towards zero magnetization states. The field-cooled states lying within the barriers of height less than or equal to the Zeeman tilt will be rapidly emptied into the M= 0 states. But the states between all the higher barriers are initially uneffected when H$\rightarrow$ 0. However, the barriers which have been tilted to zero with respect to the much lower energy, M= 0 states can now act as a diffusion sink for the states between the higher barriers. The latter diffusion is the origin of the slow time decay of the TRM observed in the experiments. Hence, larger the wait time, the slower is the decay of TRM because in that case a large number of states will be surrounded by higher barriers and it takes a longer time for the system to leave these states and decay towards the sink amongst the low barrier heights.

Ocio et al. found an analytical expression based on scaling analysis of ageing effects for the decay of TRM in the SG, $CsNiFeF_6$[32] as well as in AgMn[33]. They proposed the decay of TRM as

$$M(t) = M_0\ (\lambda)^{-\alpha} \exp\left[-(\omega\,\lambda/t_w^{\mu})^{1-n}\right], \tag{1.20}$$

$$with\ \ \lambda = (t_w/(1-\mu))[(1+t/t_w)^{1-\mu} - 1], \tag{1.21}$$

where λ is the effective time and μ is an exponent smaller than 1 . A different analysis, based on the SK mean-field model[34], suggests algebraic decay. In ferromagnets attempts have been made to explain the magnetic relaxation using a model based on magnon relaxation on a percolation distribution of finite domains[35]. The other popular prediction of relaxation is the power law[36] decay which can be obtained from scaling theories for domain growth[37] and internal dynamics[38]. Ikeda and Kikuta[39] found that there is no magnetic relaxation over 10 h in the AF $Mn_{0.45}Zn_{0.55}F_2$ at slightly lower temperatures than the transition temperature.

Despite considerable experimental work on relaxation dynamics covering enormous range of time window, no conclusive results have been found. Moreover, there is a lack of clear distinction between the SG and the RSG phases. Also, no experimental data are available on relaxation dynamics in the AF phase. All these have motivated us to study systematically the relaxation dynamics in four different magnetic phases, namely, SG, RSG, FM and AF in FeNiCr alloys *within the same crystallographic phase*, for different wait times and at different temperatures for the largest available time window.

1.4 Low-field magnetoresistance

The application of a magnetic field usually affects the transport properties of a system. The magnetoresistance(MR) of a system depends upon the relative orientation of the electric and magnetic field vectors. It is regarded as one of the most powerful tools for probing into the electronic transport processes. The MR depends upon the magnetic state of the system, hence in magnetic alloys it can give greater insight to the understanding of the magnetic phases[40].

There are different mechanisms that cause the variation of MR with field and temperature. When the magnetic field $\vec{B}$ is perpendicular to the current density $\vec{J}$, the MR is known as the transverse magnetoresistance(TMR), the space charge trajectories are deviated from

the paths of least resistance by the Lorentz force proportional to $\vec{J} \times \vec{B}$. Since the new paths are no longer necessarily the paths of least resistance, the effective mean free path (l) and the scattering life-time(τ) decrease. This gives a TMR $\frac{\Delta\rho}{\rho(0)} \approx (\frac{l}{r_L})^2$, where l is the mean free path proportional to τ and $r_L = \frac{m^* v}{eB}$ is the Larmor radius of a charge with drift velocity v. This gives the quadratic dependence in B of the TMR. This can be expressed in the general form, known as Kohler's rule, $\frac{\Delta\rho}{\rho(0)} \propto (\omega_c\tau)^2$, where $\omega_c(= \frac{eB}{m^*})$ is the cyclotron frequency and for weak magnetic fields $\omega_c\tau < 1$. The free electron theory gives zero MR in the first approximation whereas in the second approximation, it predicts a quadratic variation for small fields and a saturation in large fields[41]. Similar behaviour of the TMR was predicted from the two-band model in cases where two overlapping bands exist, like for example, in transition metals[42]. In the two-band model the MR is given by

$$\frac{\Delta\rho}{\rho_0} = \frac{\sigma_1\sigma_2(\beta_1 - \beta_2)^2 H^2}{(\sigma_1 + \sigma_2)^2 + H^2(\beta_1\sigma_1 + \beta_2\sigma_2)^2}, \tag{1.22}$$

where σ_i's are the conductivities in the two different bands and $\beta_i = \frac{e\tau_i}{m_i c}$. This means that if the two groups of carriers have either different effective masses or different charges or different relaxation times then only it gives a non-zero magnetoresistance. However, TMR can also be understood in terms of the anisotropic relaxation times and non-spherical Fermi surfaces[43].

In a metal with magnetic spins, additional quantum-mechanical effects like the suppression of the spin-flip scattering or weaklocalization can give rise to a negative MR. A conduction electron scatters by exchanging spins with magnetic moments or spin excitations. An external magnetic field increases the energy needed to flip a spin and thus decreases the amplitude of spin-flip scattering. This causes a decrease of resistivity in the presence of a magnetic field, resulting in a negative MR. Abrikosov[44] predicted the variation of MR as $\frac{\Delta\rho}{\rho(0)} = -\alpha(\mu H)^2$, where α is a positive constant and μ is the moment per magnetic scatterer, by considering the weak-field spin-flip scattering amplitude between an electron and a single local magnetic moment. The spin-flip scattering from exchange between conduction

electrons and spin excitations in an itinerant ferromagnet was considered by Herring[45]. Mookerjee[46] calculated the MR in SG's on the basis of an Edwards-Anderson-type model by considering the fact that local spins interact through the conduction electrons via the s-d exchange coupling. He predicted a negative MR at all temperatures and fields and an H^2 variation in low fields. According to him, the MR can be written as

$$\begin{aligned}\Delta\rho &= -cR_0J^2\left[M(H)\tanh(\frac{g\mu_BH}{2k_BT})+2\{Q(H)-Q(0)\}\{1-\frac{J^2}{V^2}S(S+1)\}\right.\\ &\left.+2(\frac{J^2}{V^2})Q(H)M(H)\tanh(\frac{g\mu_BH}{2k_BT})\right], \qquad (1.23)\end{aligned}$$

where $M(H)=\frac{1}{\sqrt{2\pi}}\int_{-\infty}^{\infty}\exp(-\frac{z^2}{2})\tanh\left[\alpha+\frac{\Theta M(H)}{T}+\frac{T_0}{T}Q^{1/2}(H)z\right]dz$

and

$Q(H)=\frac{1}{\sqrt{2\pi}}\int_{-\infty}^{\infty}\exp(-\frac{z^2}{2})\tanh^2\left[\alpha+\frac{\Theta M(H)}{T}+\frac{T_0}{T}Q^{1/2}(H)z\right]dz$

and Θ is the Curie temperature and $\alpha=\frac{p_{eff}\mu_BH}{k_BT}$. This was verified experimentally by Nigam and Majumdar[47] in canonical SG's. However, in a ferromagnet(FM) the presence of spontaneous magnetization and domain wall movement tend to further complicate the interpretation.

In the weak localization regime propagation of electrons between scattering events is no longer classical and therefore the quantum mechanical effects come into picture. These can be divided broadly in two parts; (i) 'localization' which considers the quantum interference between scattered waves[48–50] and (ii) 'interaction' effect which considers the modification of e-e interaction[48, 51, 52]. Details of these theories are available in the above references.

On cooling, these alloys(RSG, X=23 and 26) pass through more than two magnetic phases and hence the variation of the LFMR of these samples may not necessarily follow any of the above mechanisms. However, they are expected to show some complex interplay of the above mechanisms. The LFMR is closely connected with the state of magnetization of the alloy and is capable of providing more subtle information than, say, direct magnetization measurements. Barnard[60] observed that the LFMR (in $Au-8at.\%Mn$ and $Cu-4.6at.\%Mn$) showed dips at the freezing temperature T_g and is negative for both the

PM and the SG phases, becoming positive when FM ordering is present. Thus, LFMR can provide very useful information about the nature of the coupling between the moments in metallic magnetic alloys. To reveal the intrinsic differences in the magnetic properties of SG's and RSG's, it is necessary to do the measurements in very low fields, since larger magnetic fields can often severely disrupt the rather weak magnetic coupling existing in such alloys. Sometimes the application of larger fields is advantageous in that they might saturate an FM component, enabling the weaker SG effects to be revealed. The RSG sample shows a typical PM to FM transition as the temperature is lowered. The FM phase becomes unstable against further reduction of temperature and re-enters a SG-like state. There is a drop in the ac susceptibility and other magnetic effects show up, like the onset of magnetic viscosity and history-dependent effects. There are many controversial predictions about the nature of this lower-temperature phase. In an attempt to remove these controversies we have combined the ac susceptibility with very low-field magnetoresistance measurements thereby providing new insights into the magnetic behaviour of these alloys.

1.5 Susceptibility

The knowledge of linear and non-linear susceptibilities around the transition temperatures provides useful information and hence their systematic study including field and frequency dependence becomes very important. The other important quantities that can throw further light on these phase transitions are the critical exponents. Critical behaviour of any magnetic system near the phase transition is characterized by a set of critical exponents and amplitudes[61]. These exponents are related to each other through *scaling laws* and are independent of minute microscopic details of the system[62].

Double transitions in certain crystalline and amorphous magnetic materials are clearly seen from ac susceptibility ($\chi(T)$) measurements[63, 64]. There exists two schools of thought about the lower transition; one supports the presence of FM ordering along with SG freez-

ing(i.e., RSG) at the lowest temperature and the other does not. $\chi(T)$ increases sharply with decreasing temperature as the FM ordering temperature (T_C) is approached from the PM side, indicating a PM to FM transition. Then it shows a weakly temperature-dependent plateau in the FM regime. On further lowering of temperature $\chi(T)$ decreases sharply around T_g and the system enters the SG or the RSG regime. Theoretical models also predict similar phase transitions. However, there exists a lot of controversy about the exact nature of the RSG phase. Neutron scattering data support the existence of three distinct phases and the persistence of FM ordering down to the lowest temperature in AuFe[21] while in EuSrS no such coexistence was found[65]. It has been reported that at low temperatures the spin waves disappear in FeNi and FeCr alloys. But in NiMn the spin waves coexist with the SG ordering down to the lowest temperature. Sherrington and Krikpatrick[24](SK) predicted a similar phase with no spontaneous magnetization. Rakers and Beck[66] did not find any evidence for the presence of long-range ferromagnetism at any temperature in $Au_{82.5}Fe_{17.5}$ but observed a magneto-thermal-history effect for the entire temperature range. An infinite range model of vector spins (GT model)[67] predicts a PM to FM transition in systems where J_0(mean ferromagnetic interaction) is slightly greater than 1. It also shows a second transition at still lower temperatures to a *mixed phase* where FM ordering of the longitudinal spin components coexists with the SG freezing of the transverse components.

Investigation of non-linear ac susceptibility is one of the most important tools in understanding any magnetic phase transition. In general, the non-linearity of magnetization in the presence of a magnetic field is given by[68] the series expansion

$$m = m_0 + \chi_0 h + \chi_1 h^2 + \chi_2 h^3 + ..., \tag{1.24}$$

where m_0 is the spontaneous magnetization, χ_0 the linear and χ_1, χ_2, etc. the non-linear susceptibilities, and h the applied field. For ferromagnetic (FM) samples m has no inversion symmetry with respect to the applied field because of the spontaneous magnetization, unlike an SG. Hence for an SG, where no spontaneous magnetization is present, m can be expressed

as an odd power series in h as[69]

$$m = \chi_0 h + \chi_2 h^3 + \chi_4 h^5 + ... \quad . \tag{1.25}$$

Suzuki[69] proposed a general phenomenological theory of spin-glass transitions. He predicted singularities in non-linear responses with respect to the magnetic field and scaling relations among the critical exponents. According to this theory the non-linear susceptibility ($\chi_2 = \partial^3 m/\partial h^3$) should diverge at T_g for an SG. This divergence had been discussed by Katsura[70] in the Bethe lattice. In the Edwards-Anderson[71] model it was shown that χ_2 diverges at T_g as $h \to 0$. Therefore, a divergence of χ_2 at T_g and an absence of χ_1 are the most significant signatures of SG transitions.

1.6 Hall effect

When a magnetic field is applied along $\vec{Z}$ perpendicular to the direction of a current flowing in a specimen along $\vec{X}$, an electric field is developed across the specimen in the $\vec{Y}$ direction perpendicular to both the current and the magnetic field. This phenomenon is called the Hall effect, first observed by E. H. Hall in 1879. This field, known as Hall field(E_y), is proportional to the current density(J_x) and the magnetic induction(B_z) and the proportionality constant, R_0 is called the Hall constant, i.e.,

$$E_y = R_0 \, J_x \, B_z. \tag{1.26}$$

In the framework of the free electron theory R_0 is inversely proportional to the carrier concentration and its sign is determined by the dominant carrier type(electron/hole). However, quite often the non-linear behaviour of the Hall voltage with magnetic induction is observed in various magnetic materials like, FM and SG.

This non-linearity is observed when the contribution to R_0 comes from mechanisms other than only the Lorentz force and it has very close resemble with the magnetization. In

a FM the Hall resistivity ($\rho_H = \frac{E_y}{J_x}$) can be written as(in SI units)

$$\rho_H = R_0 B + R_s M, \tag{1.27}$$

where R_0 is the usual Lorentz term or ordinary Hall constant, R_s the extraordinary Hall constant(EHC), and M the magnetization. In high fields, when the magnetization saturates, further increase of ρ_H is only possible through the Lorentz term. Hence, the slope of the high field ρ_H gives the value of R_0 and its intersection on the ρ_H axis gives $R_s M_s$ where M_s is the saturation magnetization.

Generally, R_s is at least one order of magnitude larger than R_0 and shows a strong temperature dependence in contrast to the weak temperature dependence of R_0. It is also found that $R_s \propto \rho^n$ where ρ is electrical resistivity and $2.0 > n > 1.5$ at high temperature for ferromagnetic material like, Ni and Fe. In transition metals and alloys, $R_s = a\rho + b\rho^2$ where a and b are constants which depend on the material.

No single theory is adequate to explain all the characteristics of the extraordinary Hall effect(EHE) observed in various materials. However, the theories can be broadly classified into two categories: (i) itinerant and (ii) localized.

Karplus and Luttinger[72] considered the d-electrons itinerant in nature having unequal population for spin-up and spin-down electrons. d-spins interact with its own orbital angular momentum and lift the left-right symmetry of the electron wave function. Because of this asymmetry, a net current is produced in the presence of an electric field in the direction perpendicular to both the electric field and the average direction of the spin of the electrons. This gives rise to the extraordinary Hall effect whose coefficient varies with the square of the electrical resistivity. Similar results were also predicted by Irkhin and Shavrov[73] by considering the scattering of electrons by phonons. Kondorskii[74] found $R_s = a\rho + b\rho^2$ by considering the scattering by both impurities and phonons. He had experimentally verified this for a number of NiFe, FeMo, and FeAl alloys over a wide range of temperature and concentration.

Kondo[75] proposed a localized model where s-electrons with equal population for up and down bands are the charge carriers and the d(f)-electrons are localized at the lattice sites with their total spin contributing to the magnetization. By considering intrinsic spin-orbit interaction of the d(f)-electrons, the Hall resistivity can be given as

$$\rho_H = constant < (M- < M >)^3 >, \tag{1.28}$$

where $< (M- < M >)^3 >$ is the three spin correlation function which describes the spin-fluctuations due to thermal disorder and account for the temperature variation of ρ_H. Abel'skii and Irkhin[76] and also Kagan and Maksimov[77] considered a mixed type of spin-orbit interaction(s-orbit/d(f)- spin) along with the intrinsic one. Under the molecular field approximation for s=1/2, ρ_H is given by

$$\rho_H \approx M_s^2(0) - M_s^2(T), \tag{1.29}$$

where $M_s(T)$ is the spontaneous magnetization at a temperature T.

All the theories agree on one point that the extraordinary Hall effect arises because of some kind of spin-orbit interaction which can be explained by two distinct scattering mechanisms, (i) skew scattering and (ii) side-jump.

Smit[78] proposed that the spin-orbit(S.O) interaction break the left-right symmetry of electron wave function with respect to a plane containing the electron's spin and its incident velocity. This makes the scattering probability different towards the left and the right of this plane. This asymmetric scattering, also called the skew scattering, is observed only when it is calculated using the second Born approximation. In the case of noble metals containing rare earth impurities with localized 4f electrons, the skew scattering arises from the orbital exchange terms. Fert and Jaoul[79] proposed a different skew scattering theory based on s-d-s scattering of the free electrons. The skew scattering always predicts a linear variation of R_s with electrical resistivity. It is dominant when the electron mean free path is larger, i.e., in dilute alloys and/or at low temperatures.

Berger[80] proposed the 'side-jump' mechanism which arises because of the scattering

of the wave packet in the presence of a S.O interaction. When an electron wave packet is scattered by a potential then the locus of its center of mass, before and after scattering, can be assumed to be straight lines. But, the two trajectories before and after collision might not meet at the center of the scattering potential. The new trajectory might be displaced from the one before scattering by a finite amount. Thus at every scattering the electron wavepacket experiences a finite displacement($\approx 10^{-10} - 10^{-11}$ m for band electrons) along y-direction which contribute to the extraordinary Hall effect. This results, because the scattering potential distorts the wave function locally and thereby creates a local current density. The magnitude of the side-jump is independent of the range, strength and nature of the scattering potential. This mechanism dominates when the mean free path of the electrons is small, i.e. for concentrated alloys and/or at high temperatures. R_s arising from side-jump varies as the square of the electrical resistivity.

Kondorskii[81] proposed the first successful theory to explain the sign of R_s in ferromagnetic material like, Fe, Ni, Co. According to him, in a FM, the occupations of two sub-bands are different because the exchange interaction splits the spin-up and spin-down bands. The contribution to R_s by the carriers in different sub-bands will be different. The carrier type in a particular sub-band will be decided by the topology of that part of the Fermi surface. So the overall sign of R_s will be determined by the dominating carriers and their spins. He arrived at the expression

$$R_s = \frac{C}{I_s \sigma^2} \sum_n M_n K_n S_n, \tag{1.30}$$

where I_s is the spontaneous magnetization, σ is the electrical conductivity,M_n is the average Z-component of the magnetic moment of an electron in the nth band($M_n = \pm\mu_B$; which is positive for electrons in the up-spin band), $K_n S_n$ is some integral carried over the nth spin zone S_n, and C is a constant for a given metal. Thus if the quantity $\sum_n K_n S_n$ for the electronic part of the Fermi surface dominates over that of the hole then electrons will be

the dominating carrier for extraordinary Hall effect and vice versa. Accordingly he predicted that R_s will be positive if the dominant carriers are electron-like and are from the up-spin band and negative if they are electron-like and are from the down-spin band. For holes the signs will be just opposite of those for electrons.

In the framework of the rigid band model, Berger[80] predicted that the sign change of R_s was associated with the Fermi level crossing some degeneracy in the Ni band in NiFe and NiCo alloys. However, no such correlation was observed in CuNiFe alloys. To explain the results observed in ternary alloys Ashworth et al.[82] suggested an extreme model where all the three constituents of ternary alloys have distinctly separate sub-bands. The sign change was identified with the Fermi level crossing the top of the Ni spin-down band (or where the spin-down bands of Ni and Fe meet). This model was further extended for NiFeMe(Me= Cr, V, Ti, W, Mo, etc.) alloys. The bands for Ni are situated at the bottom in the energy scale because it is most attractive to electrons. Because of the large valence difference between Me and Ni, the bands for Me are split from the host and are placed on top in the energy scale. According to Berger's theory, the sign change of R_s is associated with the Fermi level crossing the point where the spin-down sub band of Fe and Ni meet. It was taken that the total number of states in a given 3d-sub-band is five times the concentration of the corresponding atoms. Hence, the Fermi level crossover will take place when the total number of holes in the ternary alloy system is equal to $5C_{Fe}$, i.e., when

$$5C_{Fe} = 0.55 + 2C_{Fe} - (10 + Z)C_{Me}, \tag{1.31}$$

where 0.55 is the number of holes/atom in Ni, C stands for concentration and Z is the valence difference between Me and Ni [i.e. Z= - 4 for Cr and - 5 for V]. The energy bands of Cr/V are situated above the Fermi level and they empty out all electrons into the Ni spin-down band. Hence, for calculating the contribution of electrons/holes by Cr/V atoms in Eq. (1.31) a factor (Z+10) has been used instead of only Z. However, in case of NiFeCu alloy only Z will be used.

We know that some kind of spin-orbit interaction is responsible for extraordinary Hall effect. The spin orbit coupling parameter for 3-d band electrons is given by

$$\lambda_{so}(E_F) = A_{so} X d^2 \sum_n \frac{|matrixelement|^2}{E_n - E_F}, \tag{1.32}$$

where A_{so} is the atomic spin-orbit parameter for 3d electrons, X ($\approx$ 0.1) is an overlap integral between nearest neighbour atomic 3-d states, d is the nearest neighbour distance of atoms, and E_n is the energy of a band state n. When the Fermi level E_F is in the upper half of the band, the states at E_F mostly mix with those of lower energy, thus making the denominator $(E_n - E_F)$ negative and hence R_s. The case is reversed when E_F is at the lower half of a band. Hence, R_s should change sign when E_F crosses the boundary between the two sub-bands. The split-band model can successfully explain the sign change of R_s in various binary(say, NiFe) and several ternary alloys, for example, NiFeCu[82], amorphous $Fe_{80-x}Co_xB_{20}(0 \leq x \leq 8\ at.\%)$, $Co_{40}Ni_{40}B_{20}$, $Fe_{80-x}Ni_xB_{20}(60 \geq x \geq 0)$[83].

References

[1] A. K. Majumdar and P.v. Blanckenhagen, Phys. Rev. B **29**, 4079(1984); J. Magn. Magn. Mater. **40**, 227(1983).

[2] J. A. Ewing, Phil. Trans. (London) **176**, 523(1885).

[3] G. Richter, Ann. Phys. (Leipzig) **29**, 605(1937).

[4] R. Street and J. C. Woolley, Proc. Phys. Soc. (London) A **62**, 562(1949); B **63**, 509(1950); B **69**, 1189(1956); R. Street, J. C. Woolley, and P. B. Smith, Proc. Phys. Soc. B **65**, 679(1952).

[5] L. Néel, Ann. Univ. Grenoble **22**, 299(1946).

[6] K. L. Ngai, Comments Solid State Phys. **9**, 127(1979); **9**, 141(1980).

[7] G. Williams and D. C. Watts, Trans. Faraday Soc. **66**, 80(1970).

[8] A. K. Jonscher, Nature **267**, 673(1977).

[9] M. H. Cohen and G. S. Grest, Phys. Rev. B **24**, 4091(1981).

[10] R. V. Chamberlin, G Mozurkenich, and R. Orbach, Phys. Rev. Lett. **52**, 867(1984).

[11] R. Hoogerbeets, Wei-Li Luo, and R. Orbach, Phys. Rev. Lett. **55**, 111(1985).

[12] F. Mezei and A. P. Murani, J. Magn. Magn. Mater. **14**, 211(1979).

[13] R. V. Chamberlin, J. Appl. Phys. **57**, 3377(1985).

[14] P. Nordblad, P. Svedlindh, L. Lundgren, and L. Sandlund, Phys. Rev.B **33**, 645(1986).

[15] R.G. Palmer, D.L. Stein, E. Abrahams, and P.W. Anderson, Phys. Rev. Lett. **53**, 958(1984).

[16] M.F. Schlesinger and E.W. Montroll, Proc. Natl. Acad. Sci. USA. **81**, 1280(1984).

[17] J. Hammann, M. Ocio, and E. Vincent, *in* Relaxation in Complex Systems and Related Topics, edited by I.A. Campbell and C. Giovannella (Plenum, New York, 1990), p. **11**.

[18] L. Lundgren, P. Nordblad, and P. Svedlindh, Phys. Rev. B **34**, 8164(1986).

[19] R. Tournier and Y. Ishikawa, Phys. Lett. **11**, 280(1964).

[20] S. Oseroff, M. Mesa, M. Tovar, and R. Arce, J. Appl. Phys. **53**, 2208(1982); C.N. Guy, J. Phys. F **8**, 1309(1978).

[21] A.P. Murani, J. Phys. F **15**, 417(1985).

[22] N. Bontemps and R. Orbach, Phys. Rev. B **37**, 4708(1988).

[23] G. Parisi, Phys. Lett. A **73**, 203(1979); Phys. Rev. Lett. **43**, 1574(1979); Phys. Rev. Lett. **50**, 1946(1983); M. Mezard, G. Parisi, N. Sourlas, G. Toulouse, and M. Virasoru, Phys. Lett. **52**, 1156(1984); M. Mezard, G. Parisi, and M. A. Virasoro, Spin Glass Theory and Beyond, *in* Lecture Notes in Physics, Vol. 9(World Scientific)1987.

[24] S. Kirkpatrick and D. Sherrington, Phys. Rev. B **17**, 4348(1978).

[25] P. Sibani, Phys. Rev. B **35**, 8572(1987); P. Sibani and K.H. Hoffmann, Phys. Rev. Lett. **63**, 2853(1989).

[26] David A. Huse and Daniel S. Fisher, Phys. Rev. B **35**, 6841(1987); B **38**, 373,386(1988); Phys. Rev. Lett. **56**, 1601(1986); A. J. Bray and M. Moore, Phys. Rev. Lett. **58**, 57(1987).

[27] G. Koper and H. Hilhorst, J. Phys. (Paris) **49**, 429(1988).

[28] F. Iefloch, J. Hammann, M. Ocio, and E. Vincent, Europhys. Lett., **18**(7), 647(1992).

[29] A. T. Ogileski, Phys. Rev. B **32**, 7384(1985).

[30] K. Gunnarsson, P. Svedlindh, P. Norblad, and L. Lundgren, Phys. Rev. Lett. **61**, 754(1988).

[31] D. Chu, G. G. Kenning, and R. Orbach, Philos. Mag. B **71**, 479(1995).

[32] M. Ocio, M. Alba, and J. Hammann, J. Phys. Lett. (Paris) **46**, L1101(1985).

[33] M. Alba, M. Ocio, and J. Hammann, Europhys. Lett. **2(1)**, 45(1986).

[34] H. Sompolinsky and Annette Zippelius, Phys. Rev. Lett. **47**, 359(1981).

[35] R.V. Chamberlin and D.N. Haines, Phys. Rev. Lett. **65**, 2197(1990).

[36] R.J. Borg and T.A. Kitchens, J. Appl. Chem. Solids **34**, 1323(1973).

[37] J.D. Gunton, M. Sam Miguel, and P.S. Sahui, *in* Phase Transitions and Critical Phenomenon, edited by C. Domb and J.L. Lebowitz (Academic, New York, 1983), Vol. 8.

[38] P.C. Hohenberg and B.I. Halperin, Rev. Mod. Phys. **49**, 435(1977).

[39] H. Ikeda and K. Kikuta, J. Phys. C, **17**, 1221(1984).

[40] J. M. Ziman, *Electrons and Phonons* (Clarendon, Oxford, 1960).

[41] N. H. Frank, Z. Physik **64**, 650(1930).

[42] E. H. Sondheimer and A. H. Wilson, Proc. Roy. Soc. **A190**, 435(1947).

[43] J. P. Jan, Solid State Phys. **5**, 1(1957).

[44] A. A. Abrikosov, Fundamentals of the Theory of Metals (North-Holland, New York, 1988).

[45] C. Herring, *in Magnetism*, edited by G. Rado and H. Suhl (Academic, New York, 1966), Vol. IV.

[46] Abhijit Mookerjee, J. Phys. F **10**, 1559(1980).

[47] A. K. Nigam and A. K. Majumdar, Phys. Rev. B **27**, 495(1983).

[48] B. L. Al'tshuler, A. G. Aronov, A. I. Larkin, and D. E. Khmel'nitskii, Sov. Phys. JETP **54**, 411(1981).

[49] E. Abrahamas, P. W. Anderson, D. C. Licciardello, and T. V. Ramakrishnan, Phys. Rev. Lett. **47**, 673(1979).

[50] G. Bergmann, Phys. Rev. B **28**, 294(1983).

[51] P. A. Lee and T. V. Ramakrishnan, Phys. Rev. B **26**, 4009(1982).

[52] H. Fukuyama, J. Phys. Soc. Jpn. **49**, 644(1980); Y. Isawa and H. Fukuyama, J. Phys. Soc. Jpn. **53**, 1415(1984).

[53] J. B. Bieri, A. Fert, G. Creuzet, and A. Schuhl, J. Phys. F: Met. Phys. **16**, 2099(1986).

[54] A. I. Larkin, JETP Lett. **31**, 20(1980).

[55] M. A. Howson, G. T. Morgan, A. Paja, and M. J. Walker, Z. Phys. Chem. NF, 693(1987).

[56] M. A. Howson, B. J. Hickey, and C. Shearwood, J. Phys. F **16**, L175(1986); M. A. Howson and D. Greig, Phys. Rev. B **30**, 4805(1984); S. J. Poon, E. J. Cotts, and K. M. Wong, Solid State Commun. **52**, 1080(1984).

[57] M. A. Howson and B. L. Gallagher, Phys. Report **170**, 265(1988).

[58] M. A. Howson and D. Greig, J. Phys. F: Met. Phys. **16**, 989(1986).

[59] Arisato Kawabata, J. Phys. Soc. Jpn. **49**, 628(1980); Solid State Commun. **34**, 431(1980).

[60] R. D. Barnard, J. Phys. Condens. Matter **2**, 5191(1990).

[61] S. N. Kaul, J. Magn. Magn. Mater. **53**, 5(1985).

[62] D. J. Amit, Field Theory, The Renormalization Group, and Critical Phenomena (World Scientific, 1993).

[63] G. A. Takzeĭ, A. M. Kostyshin, and K. V. Chuistov, JETP Lett. **39**, 459(1984).

[64] G. A. Takzeĭ, A. M. Kostyshin, Yu. P. Gerbenyuk, and I. I. Sych, Sov. Phys. JETP **62(6)**, 1259(1985).

[65] H. Maletta, G. Aeppli, and S. M. Shapiro, Phys. Rev. Lett. **48**, 1490(1982); H. Maletta and P. Convert, Phys. Rev. Lett. **42**, 108(1979).

[66] L. D. Rakers and P. A. Beck, Phys. Rev. B **36**, 8622(1987); P. A. Beck, Phys. Rev. B **32**, 7255(1985).

[67] M. Gabay and G. Toulouse, Phys. Rev. Lett. **47**, 201(1981).

[68] T. Sato and Y. Miyako, J. Phys. Soc. Jpn. **51**, 1394(1982).

[69] M. Suzuki, Prog. Theor. Phys. **58**, 1151(1977).

[70] S. Katsura, Prog. Theor. Phys. **55**, 1049(1976).

[71] S. F. Edwards and P. W. Anderson, J. Phys. F **5**, 965(1975).

[72] R. Karplus and J. M. Luttinger, Phys. Rev. **95**, 1154(1954).

[73] Yu. P. Irkhin and V. G. Shavrov, Sov. Phys. JETP **15**, 854(1962).

[74] E. I. Kondorskii, A. V. Cheremushkina, and N. Kurbaniyazov, Sov. Phys. Solid State **6**, 422(1964).

[75] J. Kondo, Prog. Theoret. Phys. (Japan)**27**, 772 (1962).

[76] Sh. Sh. Abel'skii and Yu. P. Irkhin, Phys. Met. Metall. **14**, 1(1962).

[77] Yu. Kagan and L. A. Maksimov, Sov. Phys. Solid State **7**, 422(1965).

[78] J. Smit, Physica **24**, 39(1958).

[79] A. Fert and O. Jaoul, Phys. Rev. Lett. **28**, 303(1972).

[80] L. Berger, Phys. Rev. B **2**, 4559(1970); Physica **30**, 1141(1964).

[81] E. I. Kondorskii, Sov. Phys. JETP **28**, 291(1969).

[82] H. Ashworth, D. Sengupta, G. Schnakenberg, L. Shapiro, and L. Berger, Phys. Rev. **185**, 792(1969).

[83] R. C. O'Handley, Phys. Rev. B **18**, 2577(1978).

Chapter 2

Experimental details

Having stated the objectives and identifying the problems we are now looking for their solutions. For this we have to measure several quantities. This is the most important and difficult part, yet this is the smallest chapter. Here we describe the sample preparation and their characterization and the experimental techniques including the cryostat design.

2.1 Sample preparation and characterization

The alloys $Fe_{80-X}Ni_XCr_{20}$ with X= 14, 19, 23, 26, and 30 were prepared[1] by induction melting in an argon atmosphere. The starting materials were of 99.999% purity obtained from M/s Johnson Matthey Inc., England. It is not possible to have AF $\gamma - phase$ of Fe below 1180 K due to $\gamma \rightarrow \alpha$ transformation. Introduction of Cr stabilizes the $\gamma - phase$ and allows one to study in $FeNiCr$ alloys a complete transition region from AF($Fe - rich$) to FM($Ni - rich$) within the same crystallographic fcc phase. The magnetic phase diagram of $Fe_{80-X}Ni_XCr_{20}(10 \leq X \leq 30)$ alloys is shown in the Fig. 2.1. The alloys were homogenized at 1323 K for 100 h in an argon atmosphere, and then quenched in oil. This thermal treatment is very important in preventing any possible chemical clustering and also the α- phase. All

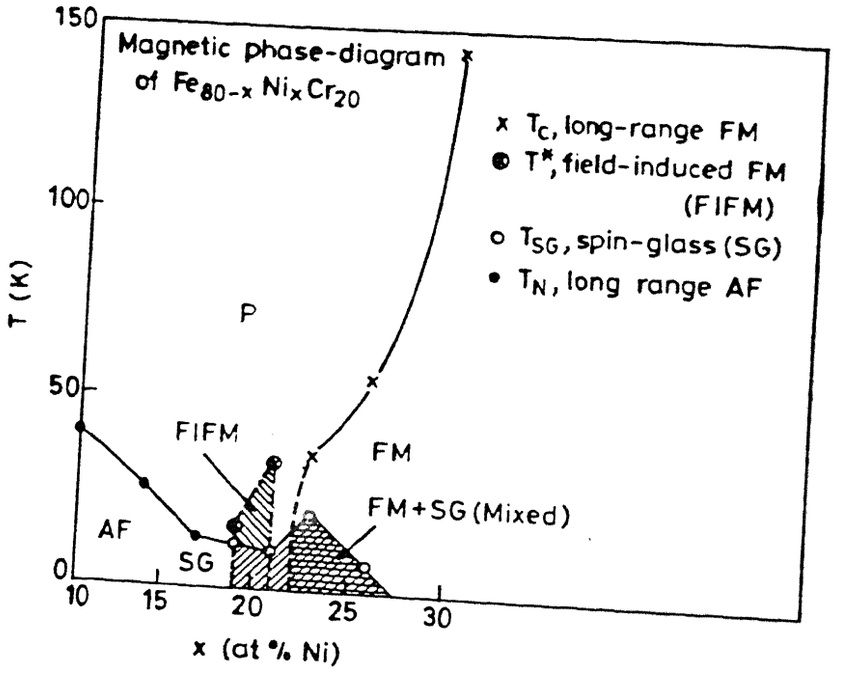

Figure 2.1: Magnetic phase diagram of $Fe_{80-X}Ni_XCr_{20}(10 \leq X \leq 30)$ alloys in the temperature-concentration (Ni) plane.

the homogenized alloys in bulk form were then cold rolled in the form of sheets and cut into thin rectangular strips as well as in needle forms for various transport and magnetic measurements. All the pieces were then finally annealed in argon atmosphere for 24 h at 1323 K to reduce the strain introduced due to the cold work, and then quenched in water.

Chemical analysis of Ni and Cr shows that the compositions of the alloys are within ± 0.5 at. % of their nominal values. X-ray diffraction data at room temperature in powdered samples reveal that these are single-phase fcc (γ) alloys with lattice parameter a=3.60 $\AA$. Neutron diffraction data[1] show the presence of single-phase fcc (γ) structure down to 2 K for the alloy with X=19.

2.2 Experimental techniques

2.2.1 Magnetic relaxation

To study the relaxation dynamics, we applied a small magnetic field (10 gauss) at a temperature greater than the characteristic temperatures T_{ch} (T_g, T_C, T_N), cool (t_C = cooling time) the system to a temperature T_m which is less than the characteristic temperature. This field-cooled system will attain a metastable state (which is not an equilibrium state), then after waiting for definite amounts of time t_W (t_W varies from 60 to 3600 s) the magnetic field is removed, the system is allowed to relax towards the equilibrium state and then the thermo-remanent magnetization(TRM) is measured with time (30 to 12,000 s) using a SQUID magnetometer (Quantum Design, MPMS) at National Research Institute for Metals, Japan. Immediately after switching off the magnetic field an instantaneous drop in the magnetization is observed. The subsequent decay of the TRM is measured where 0 s is the time when the field is switched off. To see the effect of temperature, we also measured TRM at several temperatures, T_m, both above and below the characteristic temperatures for constant wait time, t_W = 180 s. We have very carefully subtracted the background noise. We repeated a few experiments with an applied field of 20 gauss and obtained similar results within the experimental error.

2.2.2 Low-field magnetoresistance(LFMR)

In a metallic system, the change of electrical resistivity in the presence of a magnetic field is exceedingly small for small fields (< 30 gauss). To detect the minute change of resistivity in fields comparable with those used in ac susceptibility experiments, Barnard[2] devised a state of the art instrument which can measure LFMR with a resolution of 10^{-8}. The LFMR, in the present investigation, was measured using this instrument. The LFMR is normally obtained by measuring the voltage developed across a current carrying sample with and without the presence of a magnetic field, applied either in a longitudinal or a transverse

direction with respect to the current. Now the LFMR can be defined as the ratio of the change of the voltage ΔV ($\propto \Delta\rho$) to the voltage in zero field, $LFMR = \frac{V(B)-V(B=0)}{V(B=0)} = \frac{\Delta\rho}{\rho(0)}$. For low fields, ΔV is very small and hence its detection against a large background voltage($V = I.R$) is very difficult. The fundamental feature of this new method is to separate ΔV from V. If a very stable dc current (from batteries) passes through a sample and an unidirectional pulsed or oscillating magnetic field is applied, then the change of the voltage in the presence of the oscillatory field will also be oscillatory in nature. This small ac voltage could then be amplified and measured using a lock-in amplifier(LIA). Hence very small LFMR voltages could be detected which are not coupled with the large dc voltage across the sample. A schematic diagram of the measuring circuit is shown in the Fig. 2.2.

The capacitor, C is used so that the dc voltage, V can not flow through the primary of the transformer T. The value of C is large ($\approx 10,000\mu F$) so that it can provide very low impedance to the square wave signal(40 - 200 Hz). The transformer is necessary to match the low-source resistance of the sample to the high-input impedance of the LIA. It also gives noiseless amplification of the MR signal by a factor of 100. It was made from a toroid of super-mumetal with a primary wound from 16 swg wire to give an inductance of 50 mH. The secondary was wound with 40 swg wire, the turns ratio being 100:1. When a square-wave current passes through a solenoid, it produces a magnetic field which may have small spikes at the edges. This can be removed by applying a similarly generated signal of opposite sign via the variable mutual inductance M which is driven by the same current that generates the pulsed field. This operation has to be done when no current flows through the sample. We have measured the LFMR in two different kinds of external fields but the field was always parallel to the direction of the current(i.e. , the longitudinal magnetoresistance). In one case an unidirectional square-wave pulse produced the magnetic field whose amplitude could be varied. In the other case a small constant square wave pulse was applied with an additional dc biasing field whose magnitude could be varied.

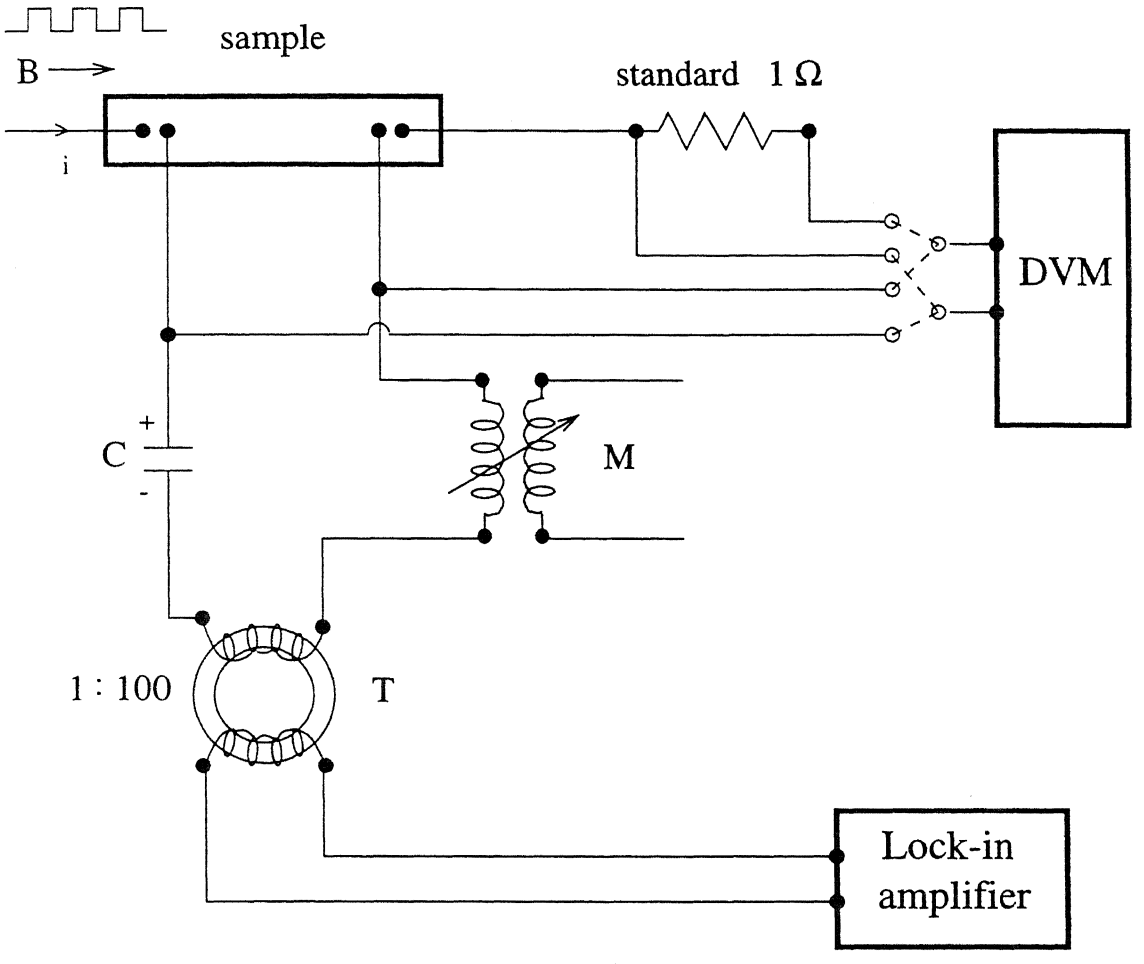

Figure 2.2: Schematic diagram of the circuit used for LFMR measurements.

2.2.3 AC susceptibility

The ac susceptibility measurement facility was developed as a part of my thesis work. An ac mutual inductance bridge was locally made[3]. There are two secondaries which are connected in series opposition so that the output of the bridge is nearly balanced without any sample. If the two secondaries are identical then the output should be zero. However, for all practical cases there is always some off-balance signal present which we balance electronically. The working principle of the bridge is simple. We take a small signal accross R which is in phase with the primary signal(Fig. 2.3). This is resolved into a set of reference and quadrature components by using a low-pass(A2) and a high-pass(A3) Butterworth active filters having the same time constant. These are separately amplified using two different variable gain amplifiers(A4 and A5). We have used decade resistance boxes(DRB) of General Radio which show very good frequency characteristics($\frac{\Delta R}{R} < 1\%$) for the gain variation. After amplification these are passed through an adder(A6) and then fed to the secondaries. Here we can independently null the in-phase and the quadrature components of the secondary signal without any sample by using amplifiers A4 and A5. The inverter A1 is there to match the polarity to null the off-balance signal in the secondary, if required. When a sample is placed inside one of the secondaries, the induced voltage in the coil is given by

$$\begin{aligned} E &= -nAf\frac{dm}{dt} \\ &= -nAf\omega h_0[(\chi_0 + \frac{3}{4}\chi_2 h_0^2 + \frac{5}{8}\chi_4 h_0^4 + ...)sin\omega t + (\chi_1 h_0 + \chi_3 h_0^3 + \\ &\quad \frac{15}{16}\chi_5 h_0^5 + ...)sin2\omega t + (\frac{3}{4}\chi_2 h_0^2 + \frac{15}{16}\chi_4 h_0^4 + ...)sin3\omega t + ...] \\ &= -nAf\omega h_0(\chi_0^t sin\omega t + \chi_1^t h_0 sin2\omega t + \frac{3}{4}\chi_2^t h_0^2 sin3\omega t + ...), \end{aligned} \tag{2.1}$$

where n is the number of turns per unit length, A the cross-sectional area of the secondary coil, f a filling factor, $h = h_0 cos\omega t$ and

$$\begin{aligned} \chi_0^t &= \chi_0 + \frac{3}{4}\chi_2 h_0^2 + \frac{5}{8}\chi_4 h_0^4 + ..., \\ \chi_1^t h_0 &= \chi_1 h_0 + \chi_3 h_0^3 + \frac{15}{16}\chi_5 h_0^5 + ..., \end{aligned}$$

$$\frac{3}{4}\chi_2^t h_0^2 = \frac{3}{4}\chi_2 h_0^2 + \frac{15}{16}\chi_4 h_0^4 + ..., etc. \quad (2.2)$$

For small fields we can write $\chi_0^t \approx \chi_0, \chi_1^t \approx \chi_1, \chi_2^t \approx \chi_2$, etc. Driving the primary coil at a frequency ω and detecting the secondary coil signal at frequencies ω, 2ω, 3ω, etc. using a lock-in amplifier, we can find linear (χ_0) and non-linear ($\chi_1, \chi_2, etc.$) susceptibilities. Actually what we detect is the coefficient of $\sin\omega t$, $\sin 2\omega t$, $\sin 3\omega t$, etc. of Eq. (2.1). These are proportional to the linear and non-linear susceptibilities for small fields. We measure both real and imaginary components for all terms of the susceptibility, i.e, $\chi_0 = \chi_0' + i\chi_0''$. In spin glasses m is expressed as an odd power series in h. Hence χ_1, χ_3, χ_5, etc. will not be present in an SG where there is no spontaneous magnetization.

The measurements are performed in the temperature range of 1.2 to 100 K and in a frequency range of 30 to 800 Hz, using an ac field range of 0.1 to 1.5 Oe. One additional coil is present to produce a dc magnetic field up to 150 Oe. Samples are placed vertically such that the magnetic field is parallel to their largest dimension. Needle or cylindrical-shaped samples are used with maximum diameter and length of 2.5 and 15 mm, respectively. The cryostat assembly consists of a glass dewar and a double-walled quartz tube(Fig. 2.4). Primary and secondary coils are wound on a bakelite former which surrounds this quartz tube. These coils always remain dipped in liquid helium and all the electrical connections (inside and outside the cryostat) are made by using miniature coaxial cables (Lake Shore) to reduce ac drift of the bridge. A perspex sample holder is connected to a stainless steel(SS) tube which goes inside the quartz tube. A heater, wound on an OFHC copper block, is attached to the same SS tube and placed 5 cm away from the sample so that it does not produce any extra signal. Exchange gas is used to heat the sample uniformly. Temperature is measured with a silicon diode sensor (D087111, Lake Shore) using a Lake Shore temperature controller(DRC-93C). In-phase and out-of-phase components of the susceptibilities are measured by using a dual phase lock-in amplifier(PAR 5208). All the instruments are connected to a PC through a GPIB(IEEE 488) card. Data are taken at an interval of a few mK by a computer-controlled

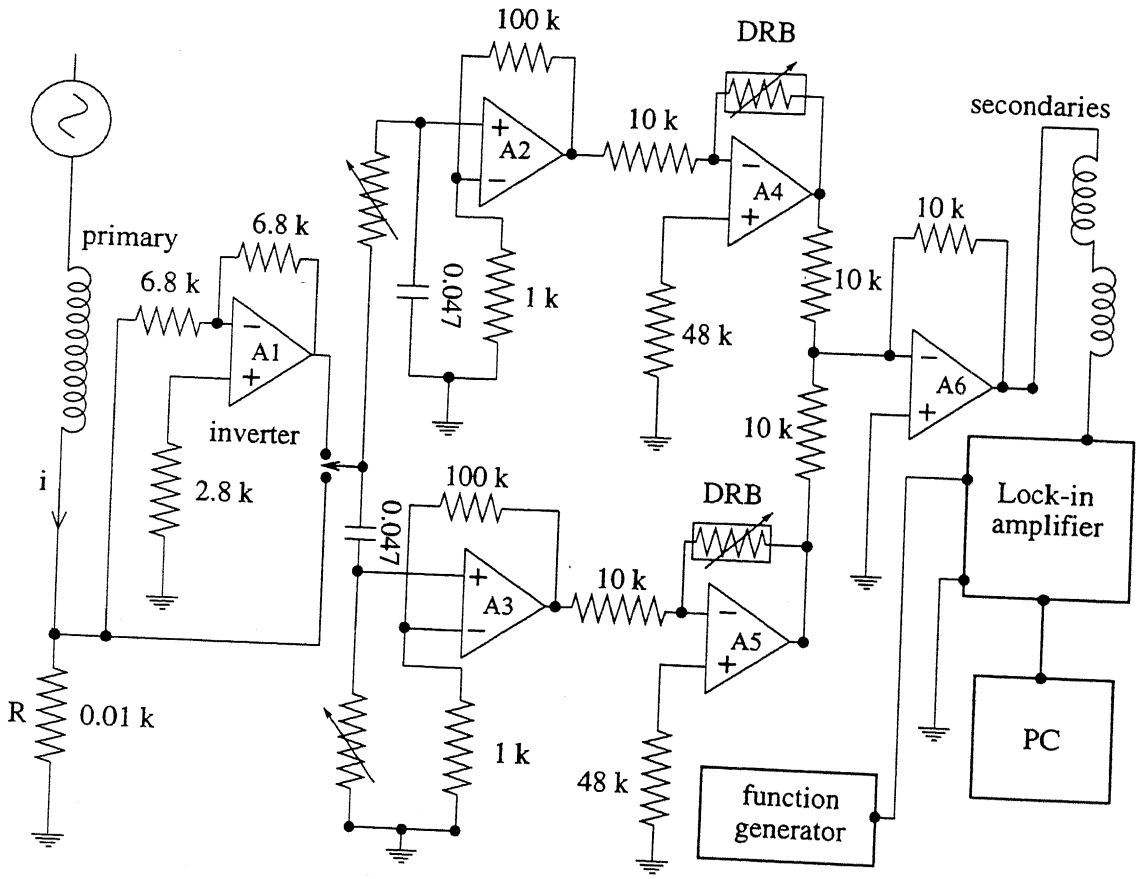

Figure 2.3: Detailed circuit diagram of the balancing bridge. All ICs are 741, resistances are in Ω and capacitances are in μF and DRB are the decade resistance boxes(General Radio 1432B).

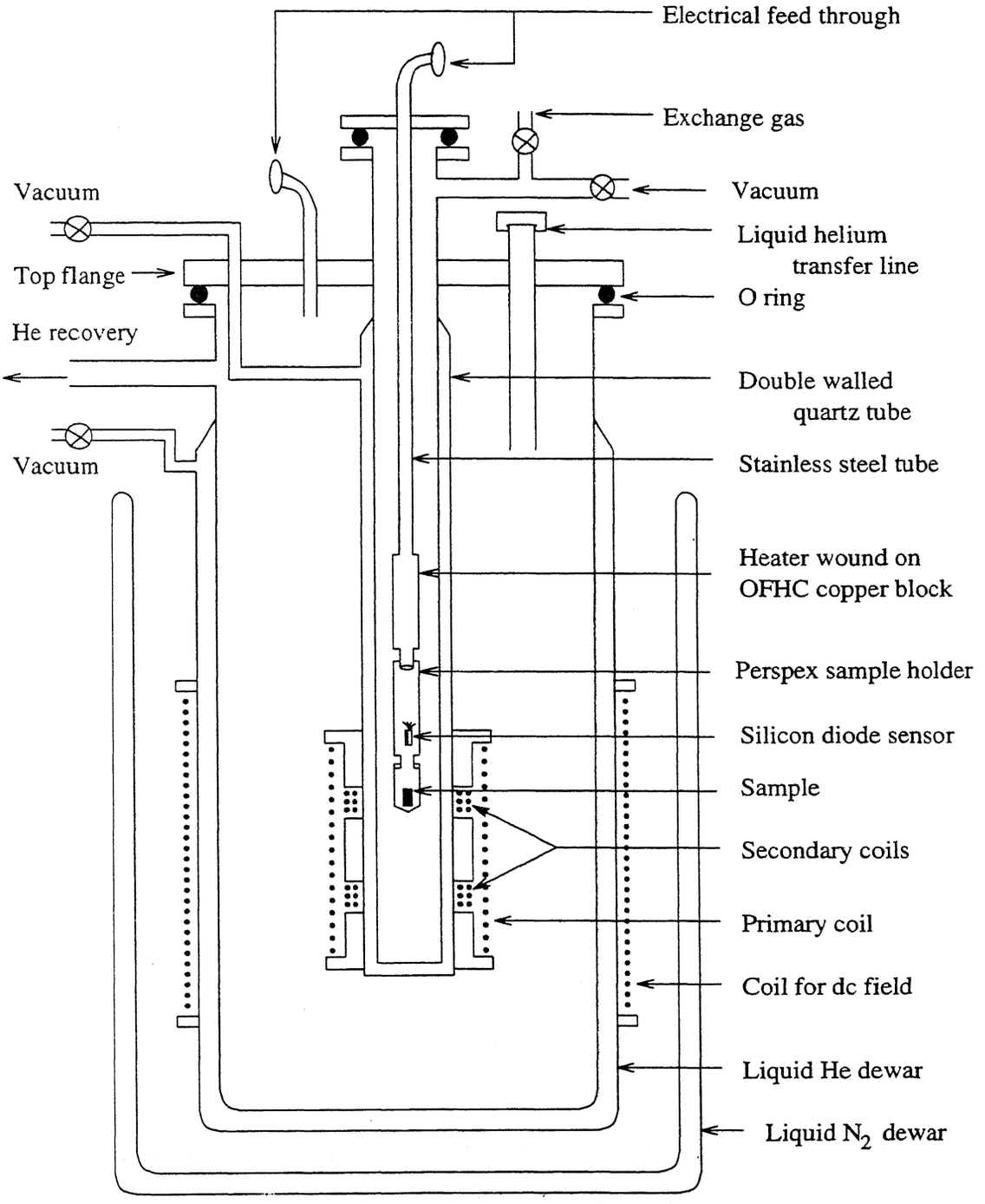

Figure 2.4: Schematic diagram of the cryostat assembly.

automatic data acquisition system developed by us.

2.2.4 Hall effect

The Hall voltage in metals is small, only a few microvolts for moderately high magnetic field and current. Therefore, to detect this small signal special care has been taken while designing the cryostat and wiring the circuit. We have used a sample current of 100 mA and the maximum field of 1.7 T for Hall measurements in the temperature interval of 1.5 to 300 K. We have used a five-probe dc method for the Hall voltage measurements to minimize the resistive voltage arising from the misalignment of the voltage probes. We have shown the measurement set-up schematically in Fig. 2.5. A and B are the current probes connected to a Keithley 220 programmable current source. E and F are the voltage leads which go to a Keithley 182 nanovoltmeter. A 10 $K\Omega$ potentiometer is connected between the terminals C and D from where one of the voltage probes is trapped(F). By adjusting the position of the voltage probe F one can reduce the misalignment voltage to less than 10 nV at any temperature. The distance between the probes C and D is less than a mm. We have used four different combinations of current and magnetic field to get the Hall voltage after eliminating the thermal and misalignment voltages. If the magnetoresistance of a sample is small then one can afford to measure the Hall voltage even without reversing the magnetic field. For our sample an error of $\approx$ 40 nV arises if we do not reverse the magnetic field whereas our typical Hall voltage is around 5 microvolts. We have thinned down our sample to less than 0.1 mm to get higher Hall voltage. The magnitude of the Hall voltage also depends on the length to width ratio. If this ratio is less than 5 then a part of the Hall voltage gets shorted through the current electrodes and hence the magnitude of the Hall voltage reduces for a given thickness of a sample. Typical dimensions of our sample are (17 x 3 x 0.09) mm^3. We have firmly placed the sample on the sample holder to prevent any noise arising from the small movement of the sample due to the magnetic field. We applied GE varnish to fix the sample and also apply Apiezon grease on it. The latter becomes very hard at lower

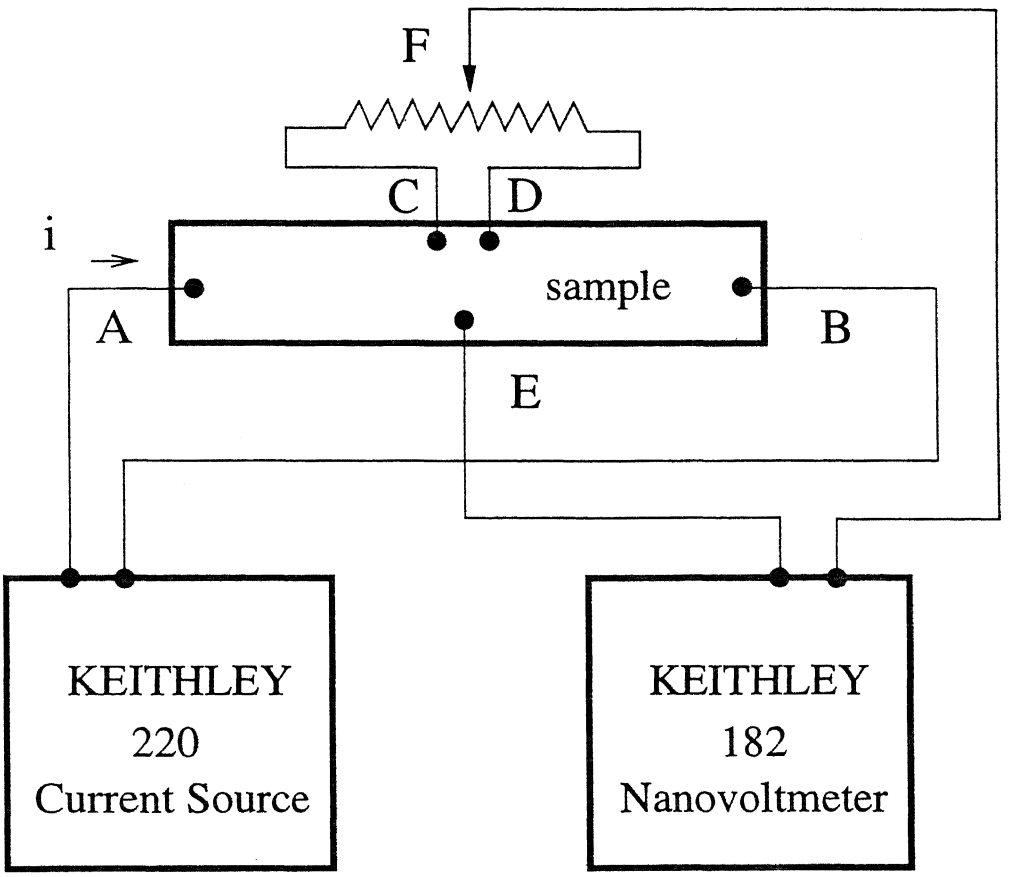

Figure 2.5: Schematic diagram of the Hall effect measurement apparatus.

temperatures and holds the sample firmly against the sample holder. All the connecting wires are twisted and pass through properly grounded shielded cables to minimize pick up of any external signal. After taking all these precautions we are able to reduce the noise to ± 5 nV.

References

[1] A. K. Majumdar and P.v. Blanckenhagen, Phys. Rev. B **29**, 4079(1984); J. Magn. Magn. Mater. **40**, 227(1983).

[2] R. D. Barnard, J. Appl. Phys. **73**, 6846(1993).

[3] A. Banerjee, A. K. Rastogi, M. Kumar, A. Das, A. Mitra, and A. K. Majumdar, J. Phys. E: Sci. Instrum. **22**, 230(1989).

Chapter 3

Relaxation of thermo-remanent magnetization

In this chapter we present the time decay of the thermo-remanent magnetization(TRM) of $Fe_{80-X}Ni_XCr_{20}$ ($14 \leq X \leq 30$) alloys for four different magnetic phases within the fcc γ-phase. The TRM is measured using a SQUID magnetometer(Quantum Design, MPMS). In the spin-glass phase(SG)(X=19) very distinct ageing effects are observed where M(t) can be described as $M(t) = M_0(t/t_w)^{-\gamma}\exp[-(t/\tau)^{1-n}]$ for the entire time domain. In the reentrant spinglass(RSG)(X= 23 and 26), M(t) is well represented by the stretched exponential with an addition of a constant term which can be well explained by the Gabay-Toulouse(GT) model. In the RSG(X=23), the TRM shows a minimum near T_C and a local maximum just above T_C. In the FM phase (X=30), the popular prediction of the power law decay of the TRM is observed. The latter is indistinguishable from the stretched exponential in the antiferromagnetic(AF) phase (X=14).

[1]This chapter is mainly based on the published work by G. Sinha, R. Chatterjee, M. Uehara, and A. K. Majumdar, J. Magn. Magn. Mater **164**, 345(1996).

3.1 Results and discussion

The most salient feature of the present work is to demonstrate how by changing the composition by small amounts in $Fe_{80-x}Ni_xCr_{20}$ alloys (X = 14 AF, X = 19 SG, X = 23,26 RSG, X = 30 FM) one can tune the relaxation dynamics. This is the only experimental report which presents a complete scenario of the relaxation spectrum in various kinds of interesting magnetic phases and throws new light on this area of interest to theoreticians as well as experimentalists.

3.1.1 Spin glass(X=19)

We observe remarkable results of ageing effects in the SG where each isotherm strongly depends upon wait time t_w (time of exposure in the magnetic field below T_g). The magnetization can be well represented by an equation of the form

$$M(t) = M_0(t/t_w)^{-\gamma} \exp\left[-(t/\tau)^{1-n}\right] \tag{3.1}$$

for the entire available time domain. Figure 3.1 shows the time decay of TRM, M(t), for different wait times (t_w = 60, 240, 1200, 1800, 3600 s) below T_g(12 K) at T_m = 5 K for the SG (X = 19) and the solid lines are the best fits of the experimental data to Eq. (3.1) ($\chi^2 = (1/n)\sum_{i=1}^{n}(Raw\ data_i - Fitted\ data_i)^2/Raw\ data_i^2 \leq 10^{-6}$). We have purposefully plotted our data on a linear time scale because if we plot on a log scale, for longer time interval, the plot will contract and the fits will apparently look better. However, goodness of fit is better judged from the value of χ^2. From these fits, the value of the initial TRM, M_0, the characteristic time constant, τ, and the exponents, n and γ, are found. The most significant feature of this analysis is that M_0 ($\approx$ 0.04 emu/g) is not varying with t_w[1–3] while the exponent, n, gradually increases with the increase of t_w. This indicates that larger time exposure below T_g in a magnetic field makes the system more reluctant to come back to an equilibrium state from a metastable one. According to Chu et al.[4] (discussed in Chapter 1), larger the wait time, the slower is the decay of TRM because in that case a

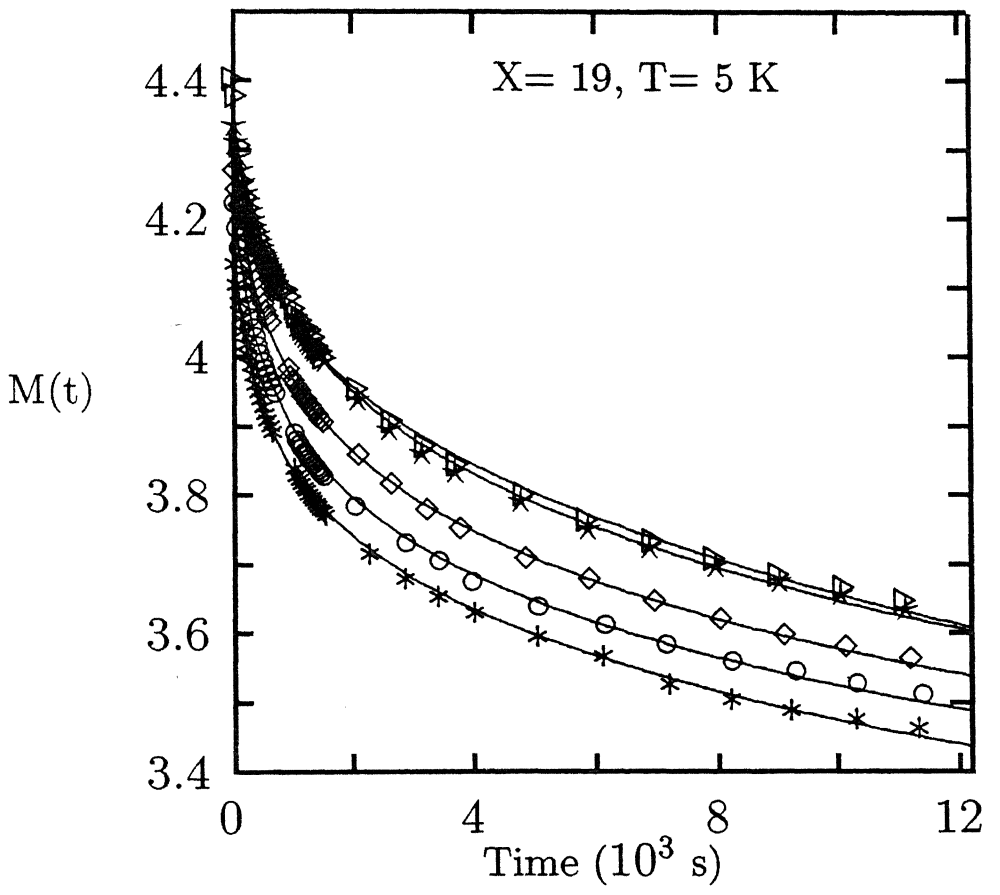

Figure 3.1: TRM, M(t) (10^{-2} emu/g), as a function of time in the SG (X=19) at 5 K for t_w = 3600, 1800, 1200, 240 and 60 s, from top to bottom, respectively. Solid lines are the best fits of the data to Eq.(3.1).

large number of states will be surrounded by higher barriers and it takes a longer time for the system to leave these states and decay towards the sink amongst the low barrier heights. Other investigators[1, 2] reported n independent of wait time but we found that it varies from 0.63 to 0.77. The power law exponent, γ, remains constant (0.022 $\pm$ 0.004) except t_w = 60 s where γ is 0.03.

Figure 3.2 shows the variation of TRM, M (t), with time for different temperatures at a constant wait time (t_w =180 s). From the best fit to Eq. (3.1) the temperature variations of n, M_0, τ, and γ are found which broadly match with the previous observations[1–3, 5]. The value of n increases linearly from 0.8 to 0.9 from 0.5T_g to T_g and then it starts falling beyond T_g (Fig. 3.3). It is reported that in the SG AgMn and CuMn, n remains constant at lower temperatures and then it starts rising from a temperature T =T_0, which strongly depends on the anisotropy energy of the sample[6] and hence can vary from sample to sample.

Non-availability of lower temperature data(less than 0.4T_g) prevented us from verifying the constancy of n. The prefactor, M_0, shows (Fig. 3.3) a linear decrease with increasing temperature for T < 0.75 T_g and the rate of decrease becomes slower for T > 0.75 T_g, in good agreement with the earlier findings[1]. The power law exponent γ increases with the increase of temperature up to 0.75 T_g. At T_g and beyond it starts decreasing with temperature (Fig. 3.3). It is difficult to tell exactly the temperature from which it has started falling, but the earlier prediction was that it should increase as one approaches T_g[3]. Figure 3.4 shows how the inverse of the characteristic relaxation time τ decreases with the increase of the reduced temperature T_g/T for X=19. This was also observed by Alba et al.[3] in AgMn.

Figure 3.4 also reflects the general tendency observed by others[2, 5]. Fewer number of data points prevents us from finding the functional form. Apparently, to check the exponential form as predicted earlier[2], we need to probe even at lower temperatures. We can try to explain the variation of τ with temperature by considering hierarchically organized metastable states in phase space[7] within the framework of Parisi's mean-field solution of the infinite range SK model. The states are continuously splitting into new states with the

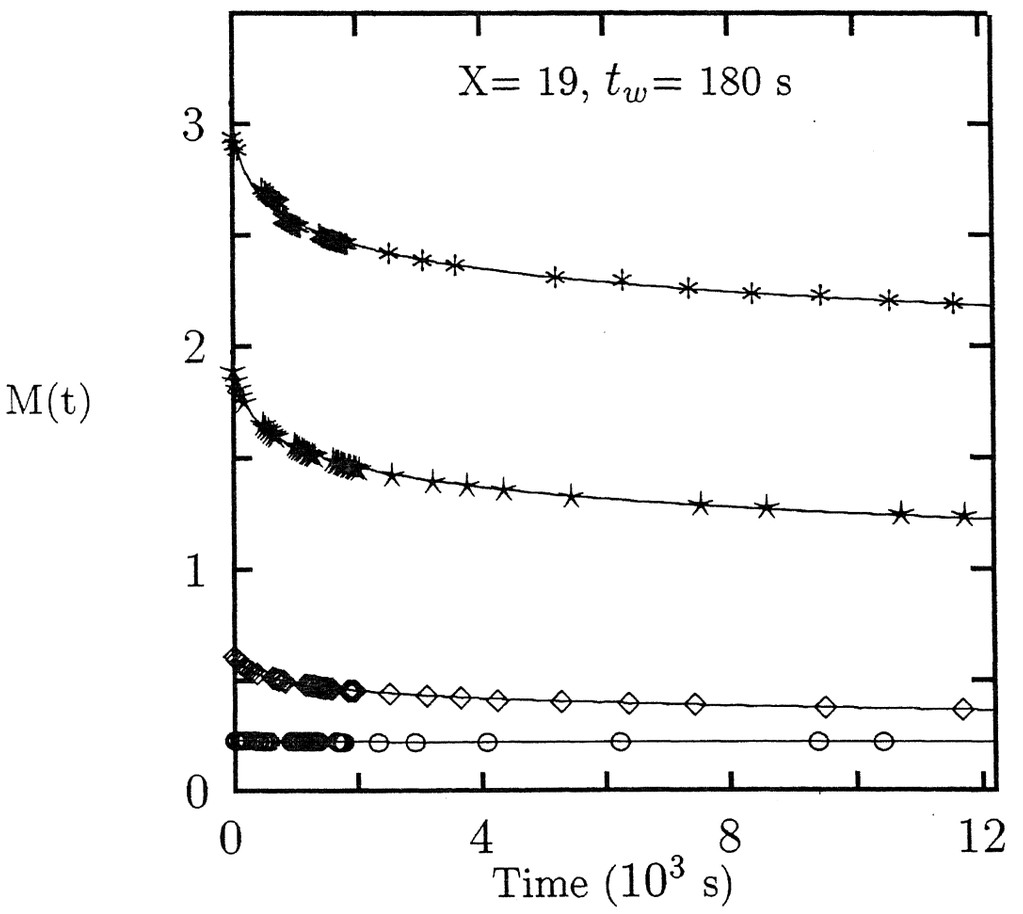

Figure 3.2: TRM, M(t) (10^{-2} emu/g), as a function of time in the SG (X=19) for t_w = 180 s for different temperatures, T_m = 7, 9, 12 and 15 K, from top to bottom, respectively. Solid lines are the best fits of the data to Eq. (3.1).

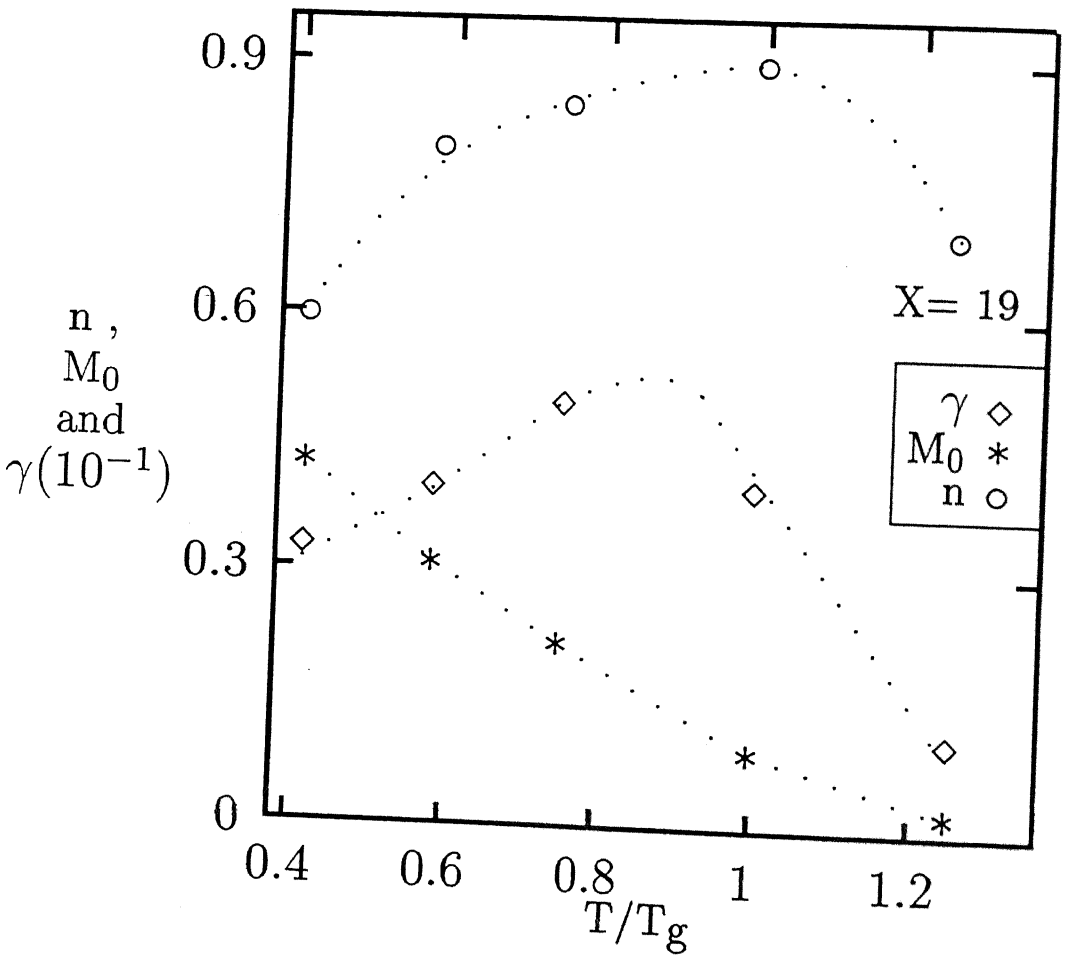

Figure 3.3: Temperature variation of the exponents, γ and n, and the initial magnetization, $M_0(10^{-1}\text{emu/g})$, for $t_w = 180$ s in the SG(X=19). Dotted lines are just guides to the eye.

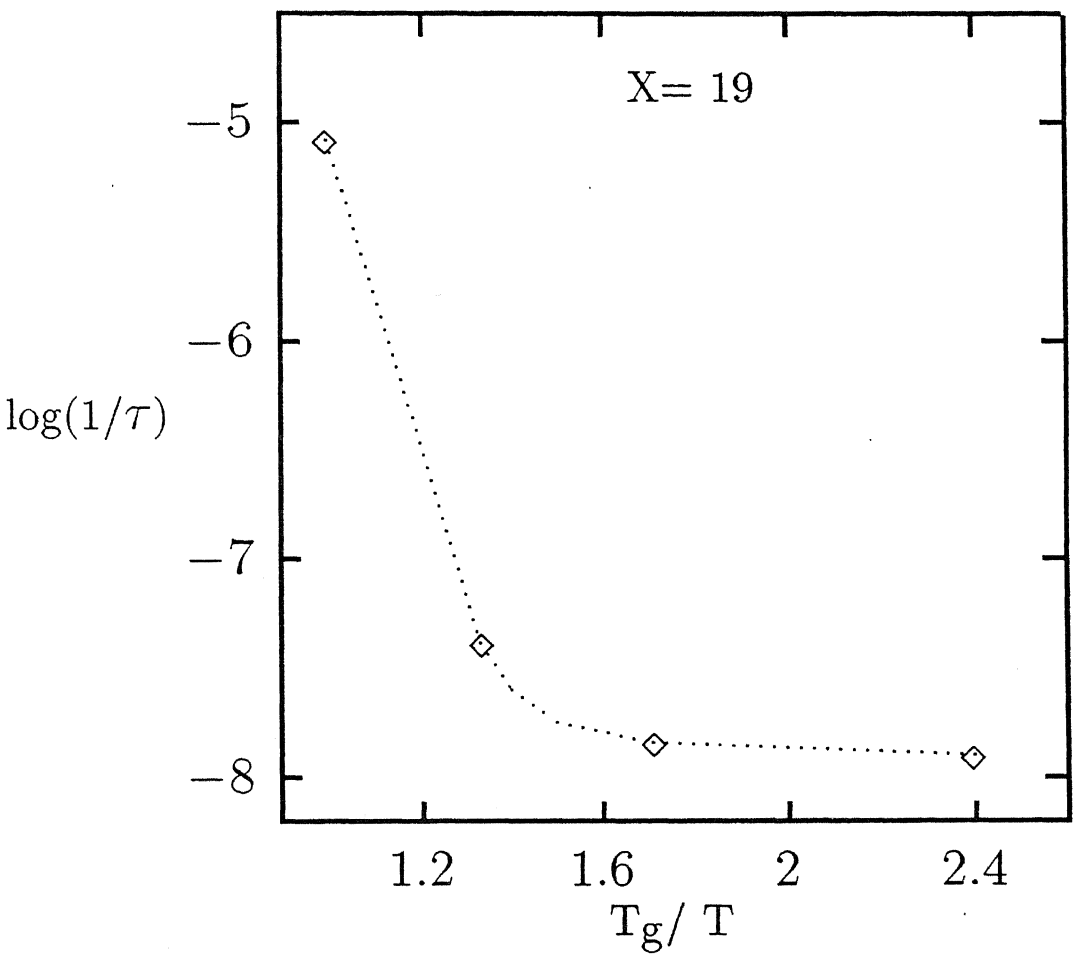

Figure 3.4: Temperature variation of the inverse of the characteristic relaxation time, $1/\tau$, (semi-log) for t_w = 180 s in the SG(X=19). Dotted line is just a guide to the eye.

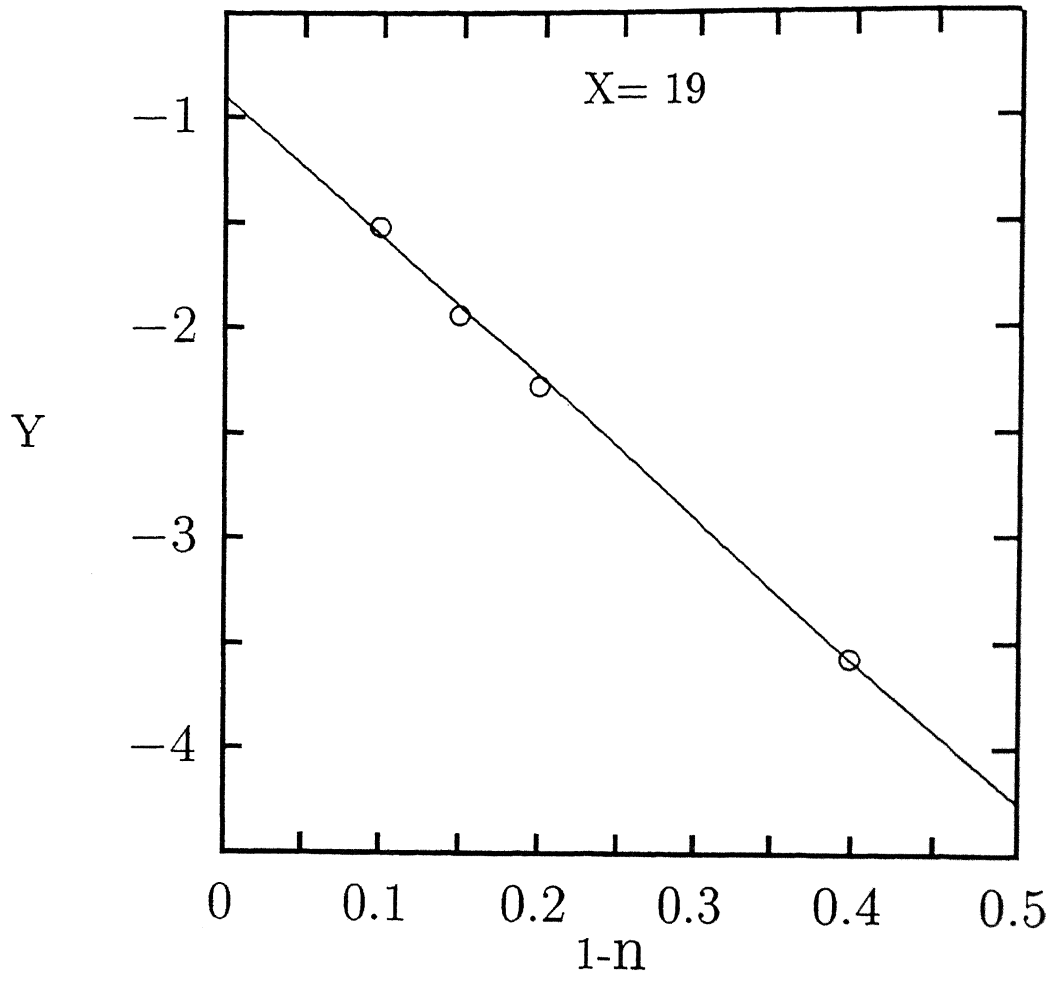

Figure 3.5: Y = log ((1-n)$(1/\tau)^{(1-n)}$) = log (c ω^{1-n}) as a function of (1-n) for different temperatures for t_w = 180 s in the SG(X=19). Solid line is the best fit for getting ω.

lowering of temperature and are separated by barriers. These barrier heights strongly vary inversely with temperature. That is, at lower temperatures, barrier heights increase and separate different metastable states into mutually inaccessible states which makes τ larger at lower temperatures. Using values of n and τ from Figs. 3.3 and 3.4, respectively and plotting $\log(1-n)(1/\tau)^{1-n}$ versus (1-n) by writing this function as $(1-n)(1/\tau)^{1-n} = c\omega^{1-n}$, we get the value of the relaxation frequency ω from the slope of the best-fitted curve (Fig. 3.5) as 1.9×10^{-7} s^{-1} and the constant, c, is 0.13. These values are much lower than those predicted earlier[1]. Analysis of M(t), considering only the stretched exponential, i.e., with-

out the power law part of Eq. (3.1), shows unusually small ($\approx$ 10 times smaller) values of n and a poor $\chi^2(\approx 10^{-5})$. Fits are even worse in cases of other mathematical forms, like only the power law. So, we find that Eq. (3.1) is the simplest analytical form that can represent our experimental data of the decay of TRM in the SG phase for the available time domain.

We should mention here that Eq. (3.1) is a simpler version of the earlier prediction of scaling analysis of ageing process[3, 8] (Eq. (1.20)). Instead of t they used λ which is a function t and t_w and $\lambda \rightarrow$ t for t << t_w. But we find that Eq. (3.1) is valid for the entire available time domain. FeNiCr alloys show some unconventional behaviour in different magnetic phases. From our magnetoresistance(MR) measurements[9] we concluded that these alloys do not show distinctive features of any pure magnetic phase. This could be understood in terms of very strong competing antiferro(Fe-Fe, Cr-Cr) and ferromagnetic(all other pairs) interactions which prevent the formation of well-defined pure magnetic phases. Hence the direct comparison of Eq. (1.20) with our result is difficult. Ogielski[10] predicted similar analytical form to describe the spin autocorrelation function in SG at all temperatures above T_g for both short and long time scales. However, other investigators[1, 5, 6] found only the stretched exponential form for the decay of TRM for the SG phase.

Chu et al.[4] in a recent paper, reported that for longer wait times remanence should be large and the decay of TRM becomes slower as we had observed. They also calculated the field dependence of the exponent (n) which does not vary significantly from 4 to 30 gauss. For fields > 50 gauss, n increases significantly. We have repeated some of our experiments in 20 gauss field and could not observe any change in the exponents.

3.1.2 Reentrant spin glass(X= 23 and 26)

SG has been the focus of attention for quite sometime, but not much attention has been paid to the RSG phase. The sample with X = 23, below 35 K, enters an FM phase from a random paramagnetic(PM) phase. On further lowering of temperature below 22 K it enters once again a new random phase where FM and SG orderings coexist[11]. It shows most of

the SG-like behaviour (frustration, irreversibility, etc.). This phase is known as the RSG.

We observe in the RSG the best representation of TRM is

$$M(t) = M_1 + M_0 \exp\left[-(t/\tau)^{1-n}\right] \quad . \tag{3.2}$$

The additional small term M_1 can easily be explained in the framework of the GT model[12] where only transverse spin freezing occurs in the RSG while the longitudinal spins can produce diffuse background effect.

Figure 3.6 represents the variation of M(t) with time at T_m=5 K for different wait times (t_W = 60, 1200, 1800, and 3600 s) in the RSG phase (X=23) and the solid lines are the best fitted curves which are of the form of Eq. (3.2)($\chi^2 \approx 10^{-6} - 10^{-7}$). The salient feature of this figure is that the initial magnetization, $\sigma_0 = M_0 + M_1$, increases with the increase of wait time (Fig. 3.7). This is not observed in the SG phase but the variation of n is similar. We also observe that M_1, which is arising because of the presence of the FM ordering[12], is not changing at all with wait time and the values of M_1 are 84% to 94% of the total magnetization depending on wait time (total magnetization changing with wait time). It is quite natural that if the ferromagnetic component is embedded in the SG phase, then the major contribution of the total magnetization should come from the ferromagnetic component. Similar expression (Eq. (3.2)) also reported earlier for the decay of TRM in SG's as well as in RSG's[13]. But they did not find any difference between the RSG and the SG phases. We find that Eq. (3.2) is only valid for the RSG and distinct differences exist between the SG and the RSG phases.

Figures 3.8 and 3.9 depict the variation of M(t) with time at different temperatures (T_m = 10, 15, 20, 25, 30, and 38 K) for constant wait time (180 s). From the fits of the data to Eq. (3.2), the value of σ_0 and the exponent, n, are found. The exponent increases with temperature and approaches unity as one approaches T_g, in exact agreement with the previous observations[1, 2] in SG's, the only difference is that the present values are slightly higher. If we increase the temperature even more, a sudden change takes place around 20 K.

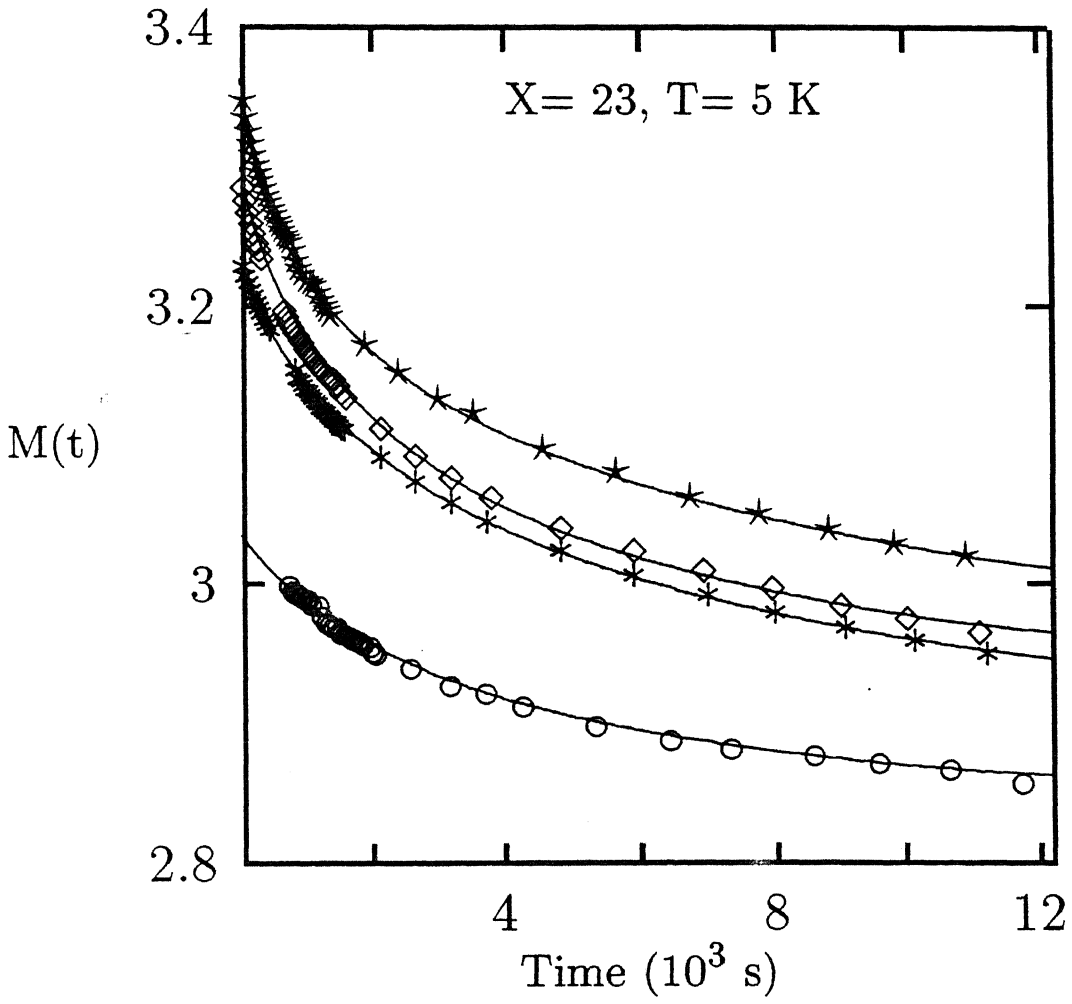

Figure 3.6: TRM, M(t) (10^{-1}emu/g), as a function of time in the RSG (X=23) at 5 K for t_w = 3600, 1800, 1200 and 60 s, from top to bottom, respectively. Solid lines are the best fits of the data to Eq. (3.2).

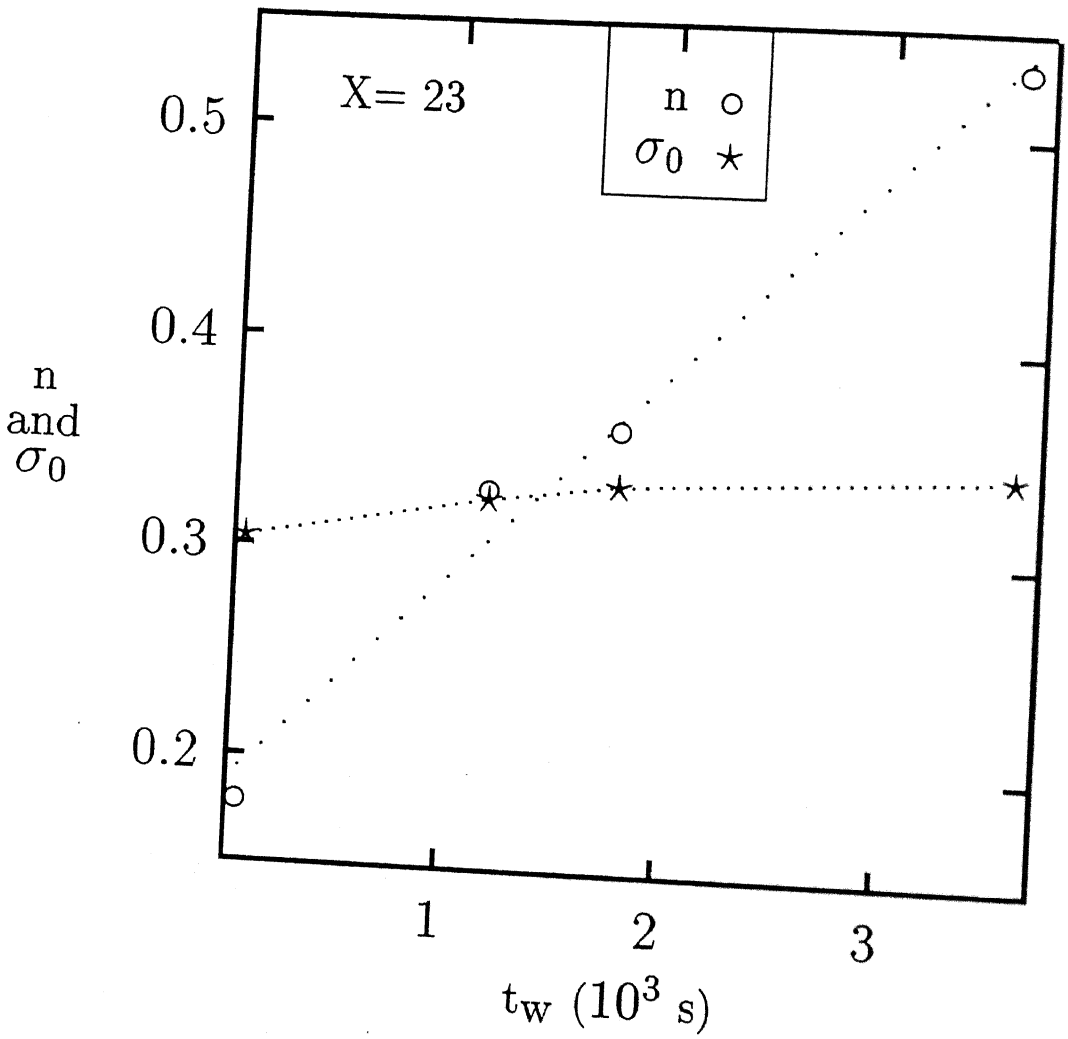

Figure 3.7: Wait time dependence of the exponent, n, and the initial magnetization, σ_0(emu/g), at 5 K in the RSG(X=23). Dotted lines are just guides to the eye.

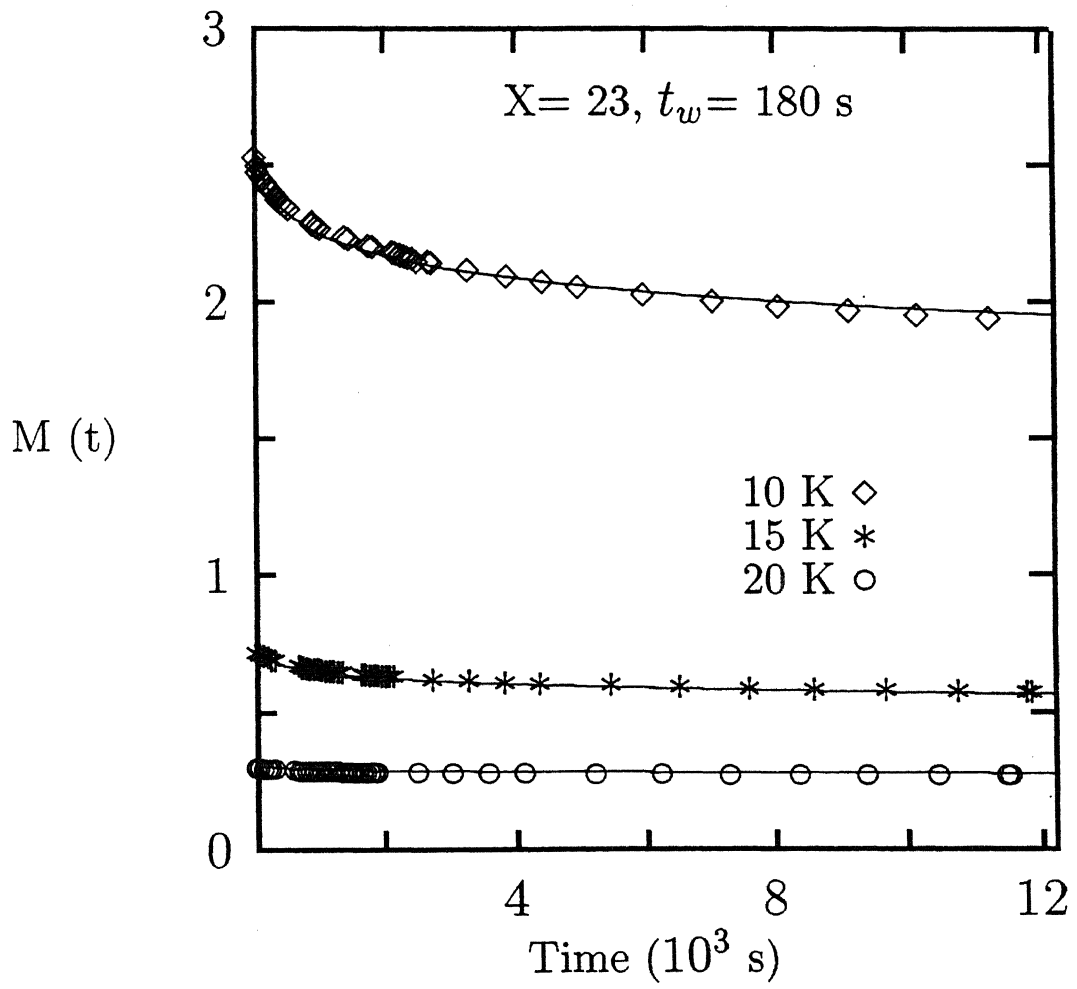

Figure 3.8: TRM, M(t) (10^{-1}emu/g), as a function of time in the RSG (X=23) for t_w = 180 s for different temperatures, T_m = 10, 15 and 20 K, from top to bottom, respectively. Solid lines are the best fits of the data to Eq. (3.2).

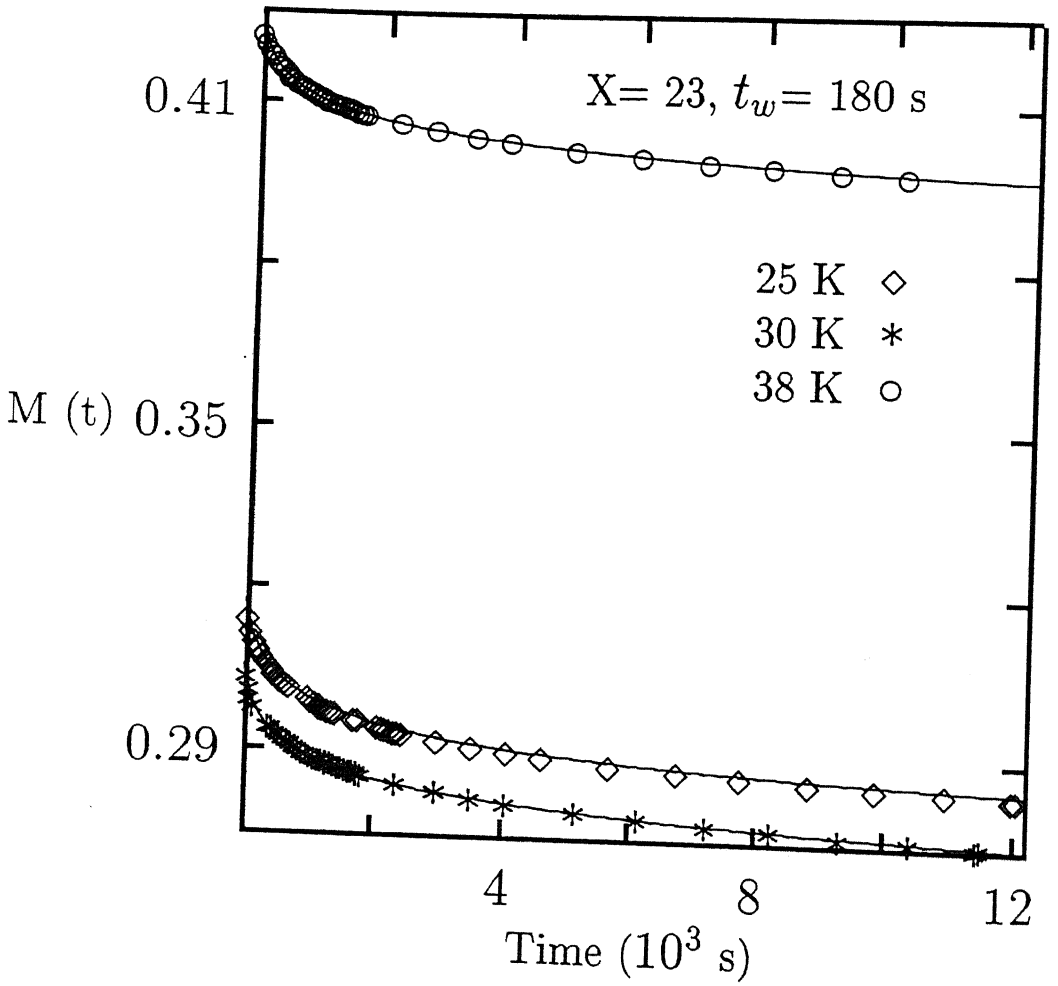

Figure 3.9: TRM, M(t) (10^{-1}emu/g), as a function of time in the RSG (X=23) for t_w = 180 s for different temperatures, 38, 25 and 30 K, from top to bottom, respectively. Solid lines are the best fits of the data to Eq. (3.2).

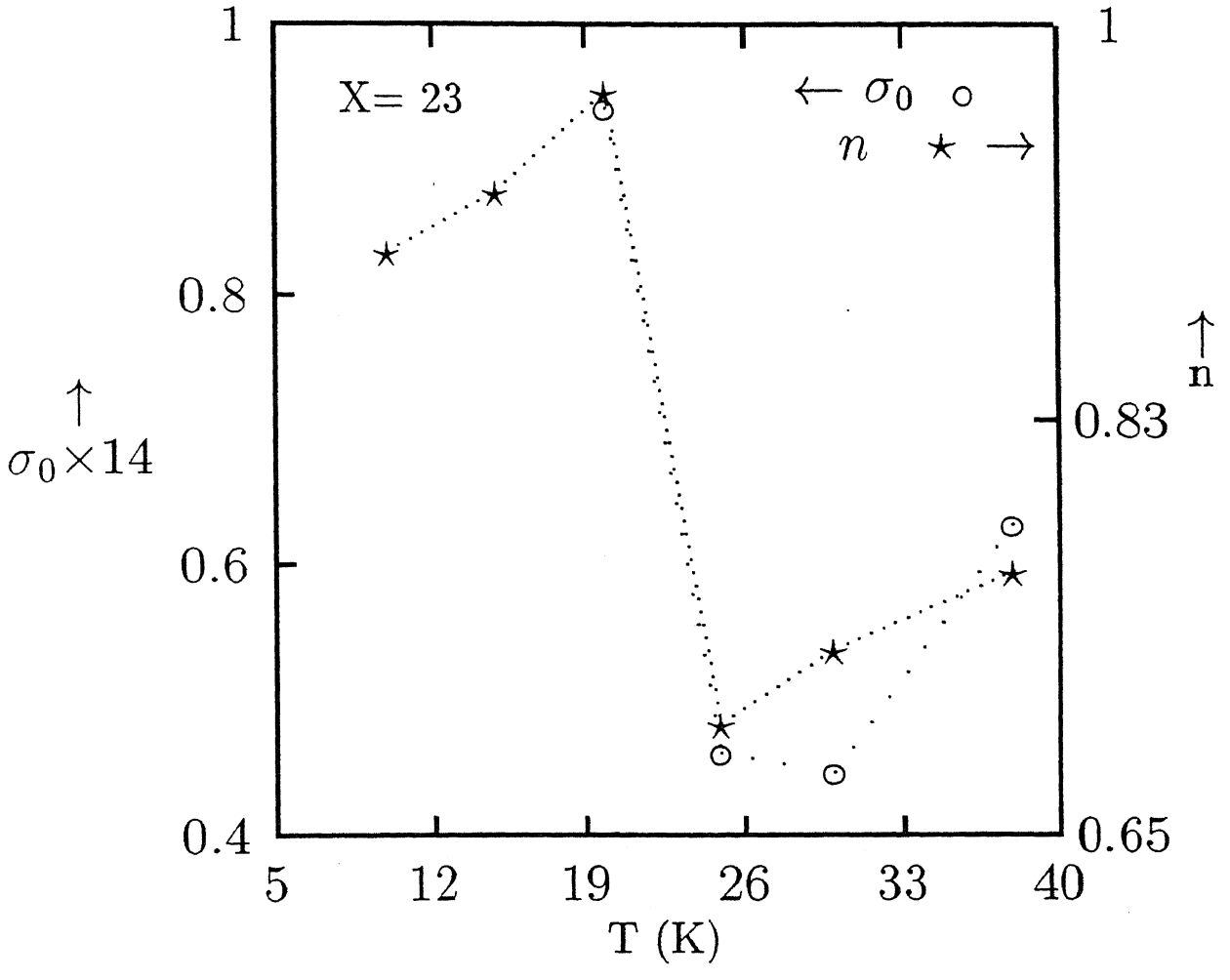

Figure 3.10: Temperature variation of the exponent, n, and the initial magnetization, σ_0(emu/g), for t_w = 180 s in the RSG(X=23). Dotted lines are just guides to the eye.

A drop in the value of n indicates a phase change. Moreover, at lower temperatures it shows a better fit to Eq. (3.2) but at higher temperatures power law fit is better than the stretched exponential. This supports the onset of the FM phase. This could also be an indication of the switch-over from nonequilibrium dynamics to equilibrium dynamics when it passes from the RSG to the FM phase. The power law behaviour in the FM phase (having an exponent ≈ 0.06) is quite consistent with the Huse and Fisher theory[14].

The rate of increase of the exponent also changes somewhat beyond 30 K where it passes from the FM to the PM state at 35 K. The value of the exponent increases by 4.6 % in the

temperature interval of 8 K (30 to 38 K)(Fig. 3.10). This is above the error bar which is less than 1 %. The error bar (Fig. 3.10) is of the order of the size of the symbol. The value of the exponent shows anomaly near two temperatures, 22 K and 35 K, which are nothing but T_g and T_C, respectively[11]. But the variation of n near T_c is not as prominent as that near T_g. We also find that in Eq. (3.2) the additional term , M_1, which is the value of the residual magnetization, $M(\infty)$, decreases with the increase of temperature below T_g (0.0067 emu/g at T_g) and suddenly increases to 0.027 emu/g when it enters the FM phase, as expected. The most striking observation is the variation of the initial magnetization, σ_0, with temperature (Fig. 3.10). σ_0 decreases monotonically with the increase of temperature up to 20 K beyond which the rate of decrease reduces significantly and at 25 K and 30 K it becomes almost constant (0.033 and 0.032 emu/g, respectively) and then there is a sudden rise at 38 K (0.045 emu/g) which makes the scenario most interesting. The value of σ_0 changes by about 40% in this temperature interval (30 to 38 K). This kind of remarkable observation of switching of magnetization while passing from FM to PM phase was reported earlier only by Chamberlin and Holtzberg[15] in ferromagnetic EuS single crystal. They tried to explain this in terms of the percolation theory[16]. So we observe that the TRM in the RSG (X=23) shows a minimum near T_C and a local maximum just beyond T_C. At lower temperatures ($< T_C$), the finite size domains try to orient themselves with the direction of the local field which need not be in the same direction as the applied field. These domains are dynamically strongly correlated (forming a strong viscous medium). These FeNiCr alloys have shown very large high-field susceptibility[17], i.e., even at very high magnetic fields the orientation of these domains with the direction of the applied field is not complete because of the presence of strong anisotropy. Near T_C the correlation between finite domains gets disrupted. Just above T_C, the domain magnetization still remains but the domains become less viscous and they try to orient themselves along the direction of the applied field, thus increasing the magnetization. Further increase of temperature randomizes the spin orientations. We repeated the experiment to confirm this unusual observation and found a similar behaviour.

The sample with X= 26, below 56 K , enters a FM phase from a random PM phase. On further lowering of temperature below 7 K it enters an RSG phase[11]. We observe some different features in the samples X= 23 and X= 26, though they undergo similar kinds of phase transitions(PM $\rightarrow$ FM $\rightarrow$ RSG). M(t) data at 5 K, similar to those shown in Fig. 3.6 but now for the sample X= 26, when fitted to Eq. (3.2) ($\chi^2 \approx 10^{-6} - 10^{-7}$), shows that the initial magnetization, $\sigma_0 = M_0 + M_1$, does not change with wait time ($\approx$ 0.5 emu/g). The value of the exponent, n, increases from 0.55 to 0.64, with the increase of wait time from 240 to 3780 s. We have observed similar variation in the SG(X=19) phase whereas in the other sample, X=23, σ_0 increases with wait time in the RSG phase. The value of σ_0 is larger for the sample X=26 than that for the sample X=23 and smaller than that for the sample X=30(FM, described below). Hence the value of the initial magnetization, σ_0, increases gradually with the increase of Ni concentration as we move towards the FM phase. The variation of n is similar in both the SG(X=19) and the RSG(X=23) samples.

Figures 3.11 and 3.12 display the variation of M(t) with time at different temperatures (T_m = 6, 8, 10, 20, 30, 40, 50, and 60 K) for constant wait time (180 s) for the sample X= 26. From the fits ($\chi^2 \approx 10^{-6} - 10^{-7}$) of the data to Eq. (3.2), the values of the initial magnetization, σ_0, and the exponent, n, are found. σ_0 decreases at a faster rate up to 20 K and then continues to decrease slowly till 60 K (Fig. 3.13). Here we have not observed the local maximum above T_C as in the case of X=23. To observe this we need to probe at a temperature closer to T_C(56 K). The exponent, n, increases abruptly when the system undergoes a transition from the RSG to the FM phase at 7 K. Then it starts to decrease up to 20 K and beyond this again increases till 50 K. Further increase of temperature reduces the value of n and the system passes from the FM to the PM phase (Fig. 3.13). The variation of n is not well understood, specially the dip around 20 K. Interestingly, we have also observed around this temperature some striking features in the low-field magnetoresistance and a.c susceptibility measurements[18]. These features have kept the field wide open for further work. We also observe that at higher temperatures (T$\geq$30 K, much higher than T_g) M(t)

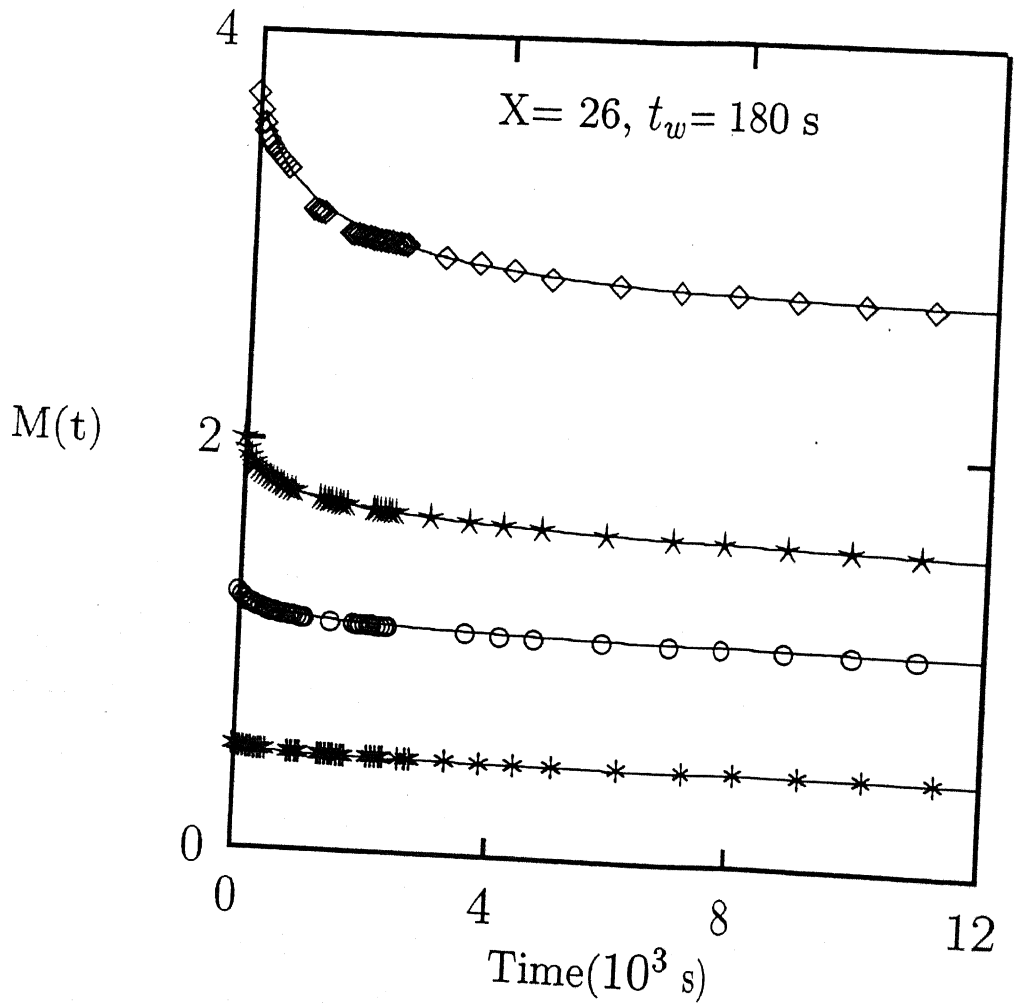

Figure 3.11: TRM, M(t) (10^{-1}emu/g), as a function of time in the RSG (X=26) for t_w = 180 s for different temperatures, T_m = 6, 8, 10, and 20 K, from top to bottom, respectively. Solid lines are the best fits of the data to Eq. (3.2).

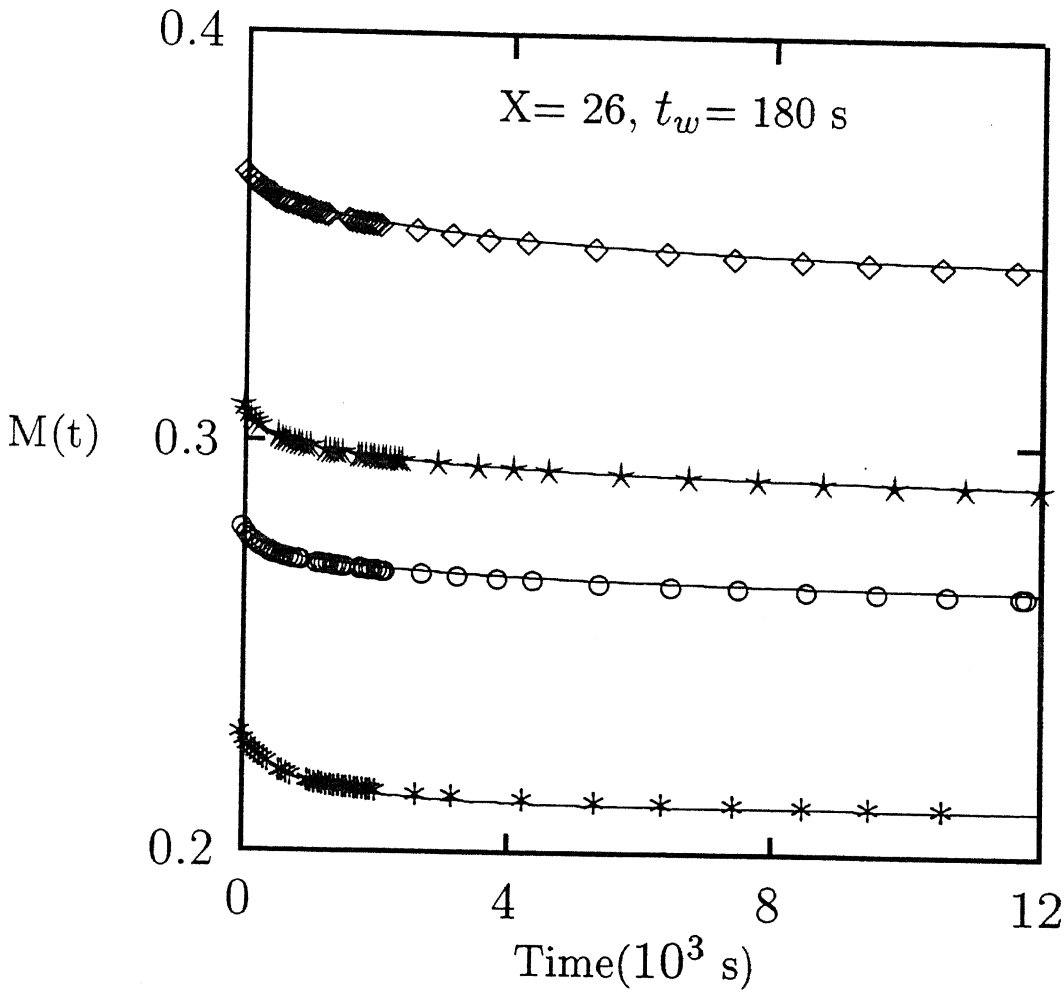

Figure 3.12: TRM, M(t) (10^{-1}emu/g), as a function of time in the RSG (X=26) for t_w = 180 s for different temperatures, 30, 40, 50, and 60 K, from top to bottom, respectively. Solid lines are the best fits of the data to Eq. (3.2).

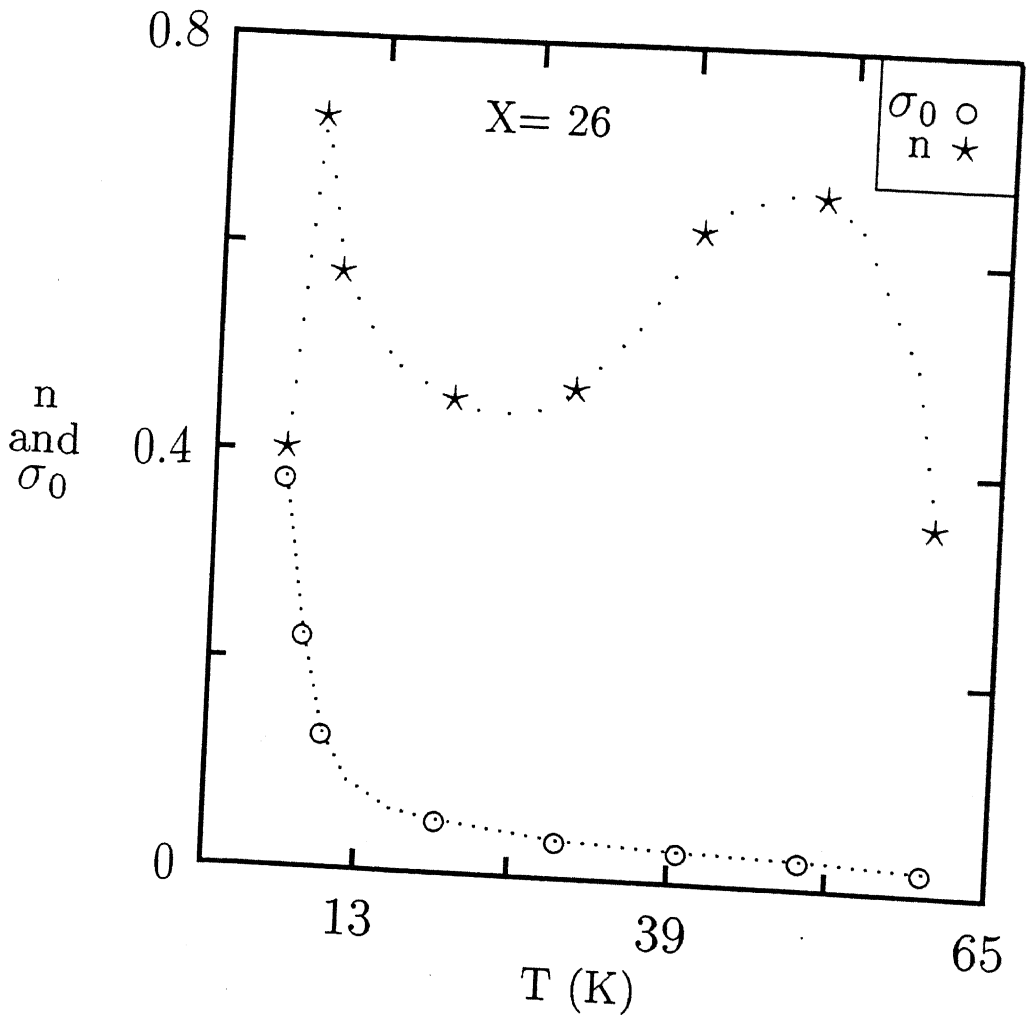

Figure 3.13: Temperature variation of the exponent, n, and the initial magnetization, σ_0(emu/g), for t_w = 180 s in the RSG(X=26). Dotted lines are just guides to the eye.

data show better fits to the power law compared to the stretched exponential (Eq. (3.2)). For X=23, we observe similar behaviour for $T \geq T_g$.

3.1.3 Ferromagnet(X= 30) and antiferromagnet(X= 14)

Figure 3.14 shows the variation of TRM with time at 5 K in the FM phase (X=30) for different wait times (t_w = 240, 1380, 1980, 3780 s). We find that

$$M(t) = M_1 + M_0\, t^{-\gamma} \tag{3.3}$$

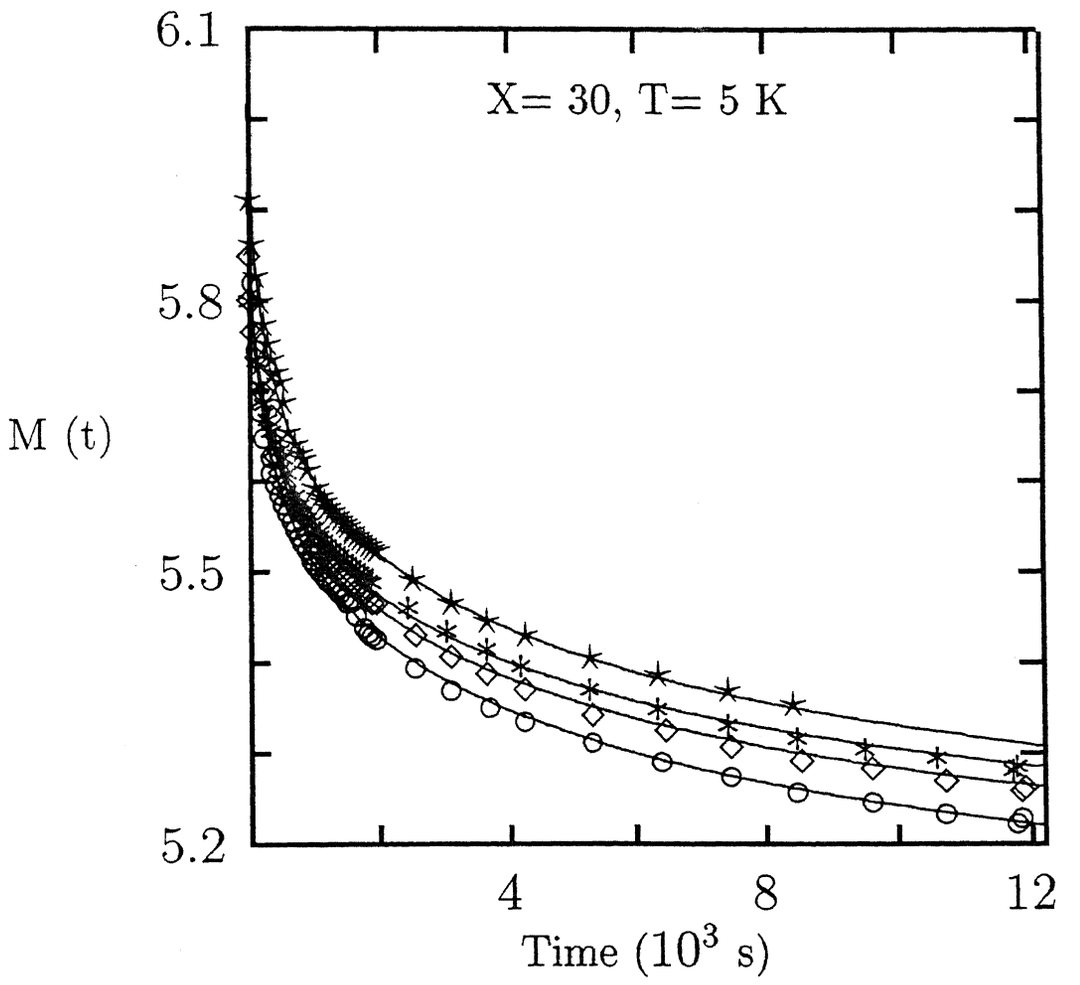

Figure 3.14: TRM, M(t) (10^{-1}emu/g), as a function of time in the FM (X=30) at 5 K for t_w = 3780, 1980, 1380 and 240 s, from top to bottom, respectively. Solid lines are the best fits of the data to the power law (Eq. (3.3)).

Table 3.1: Best fitted parameters for the power law (Eq. (3.4)) fit for different wait times at 5 K for X=14. Solid lines in Fig. 3.15 are the best fitted curves. $\chi^2 = (1/n)\sum_{i=1}^{n}(Raw\ data_i - Fitted\ data_i)^2/Raw\ data_i^2$.

t_W (10^3 s)	M_0 (10^{-4} emu/g)	γ (10^{-4})	χ^2 (10^{-7})
0.18	20.58	44.0	0.59
1.32	20.57	43.5	1.03
1.98	20.62	41.6	2.22
3.78	20.61	38.2	3.30

gives the best fit of the experimental data (solid lines in the graph) and from the fits ($\chi^2 \approx 10^{-6} - 10^{-7}$) the values of M_1, M_0 and γ are found. It does not show much wait-time dependence, the values of M_1 and M_0 remain almost constant ($\approx$ 0.29 and 0.35 $\pm$ 0.01 emu/g, respectively) while the exponent, γ, decreases inversely with wait time (from 0.049 to 0.036). With the increase of temperature the value of the initial magnetization reduces drastically (0.65 emu/g at 5 K to 0.094 emu/g at 80 K) and the exponent also becomes smaller (0.049 at 5 K to 0.00036 at 80 K).

Figure 3.15 shows the time decay of TRM, M(t), for different wait times (t_W = 180, 1320, 1980, 3780 s) below T_N=26 K (T_m = 5 K) for the AF(X = 14) sample and the solid lines are the power law fits of the form

$$M(t) = M_0 t^{-\gamma}. \tag{3.4}$$

From these fits the values of M_0 and γ are obtained (Table 3.1). M_0 ($\approx$ 0.00206 emu/g) does not change with wait time whereas γ decreases with the increase of wait time (0.0044 to 0.0038). Figure 3.16 shows the time decay of TRM, M(t), at different temperatures for constant wait time (180 s) and the solid lines are the power law fits from which the value of

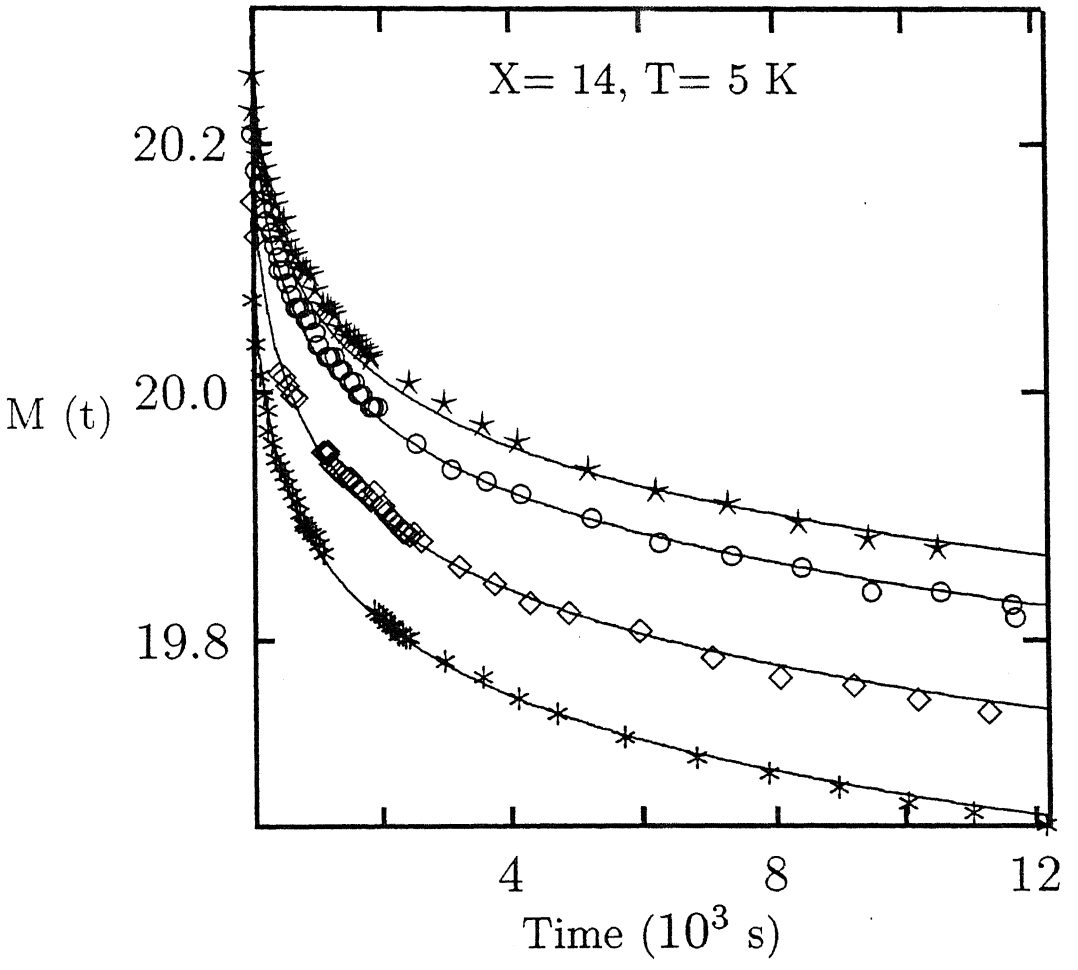

Figure 3.15: TRM, M(t) (10^{-4}emu/g), as a function of time in the AF(X=14) at 5 K for t_w = 3780, 1980, 1320 and 180 s, from top to bottom, respectively. Solid lines are the best fits of the data to the power law (Eq. (3.4)).

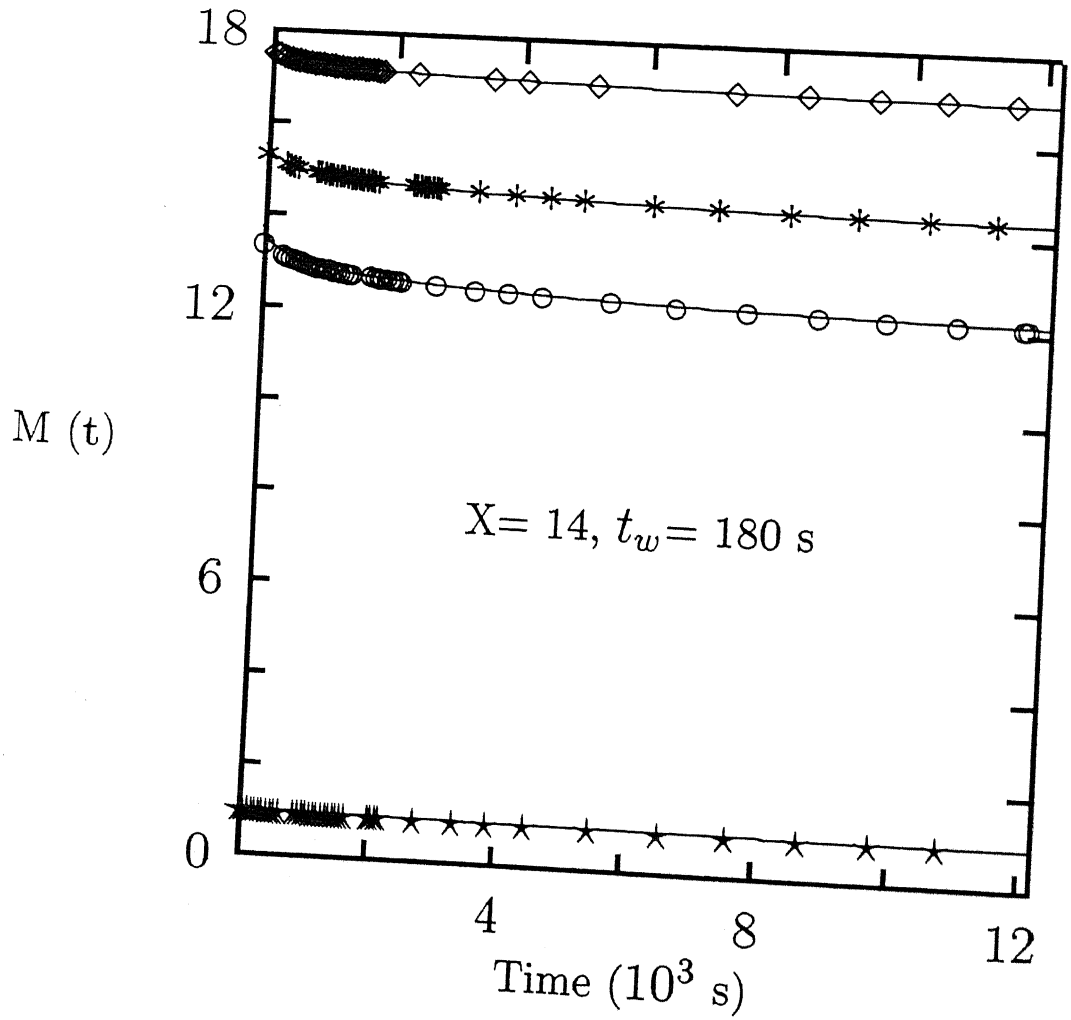

Figure 3.16: TRM, M(t) (10^{-4}emu/g), as a function of time in the AF (X=14) for t_w = 180 s for different temperatures, T_m = 10, 18, 24 and 30 K, from top to bottom, respectively. Solid lines are the best fits of the data to the power law (Eq. (3.4)).

Table 3.2: Best fitted parameters for the power law fit (Eq. (3.4)) at different temperatures for constant wait time (180 s) for X=14. Solid lines in Fig. 3.16 are the best fitted curves.

T (K)	M_0 (10^{-4} emu/g)	γ (10^{-3})	χ^2 (10^{-7})
5	20.5	4.0	0.59
10	18.2	7.0	0.63
18	16.3	14.0	3.39
24	14.9	21.7	3.90
30	1.2	30.4	34.0

M_0 and γ are found (Table 3.2).

The value of M_0 decreases linearly with the increase of temperature up to T_N (0.0015 emu/g at 24 K) and then suddenly falls to a much lower value (0.00012 emu/g at 30 K) as shown in Fig. 3.17. The exponent, γ, increases with temperature and the rate of increase changes somewhat when it passes to the PM phase (Fig. 3.17). In the case of the AF phase we need not add any constant term (unlike the FM phase) and the value of the exponent is an order of magnitude lower than that in the FM phase. We also observe that the stretched exponential function, Eq.(1.19), shows reasonably good fits to the TRM in the AF phase. The values of the best-fitted parameters and the χ^2 are given in Tables 3.3 and 3.4. The value of the exponent, β, is almost two orders of magnitude smaller than that in the SG phase (0.004 and 0.37, respectively). It increases monotonically (Table 3.4) with temperature (0.004 at 5 K to 0.029 at 30 K) in contrast to that in the SG phase where β decreases with the increase of temperature up to T_g (0.37 at 5 K to 0.1 at 12 K obtained from Fig. 3.3 using β = 1-n). So, we find that the M(t) data for the AF fit well to both the power law (Eq. (3.4)) and the stretched exponential (Eq. (1.19)). We have given the values of χ^2 in Tables 3.1 - 3.4 for comparison. They are comparable for both the above mathematical

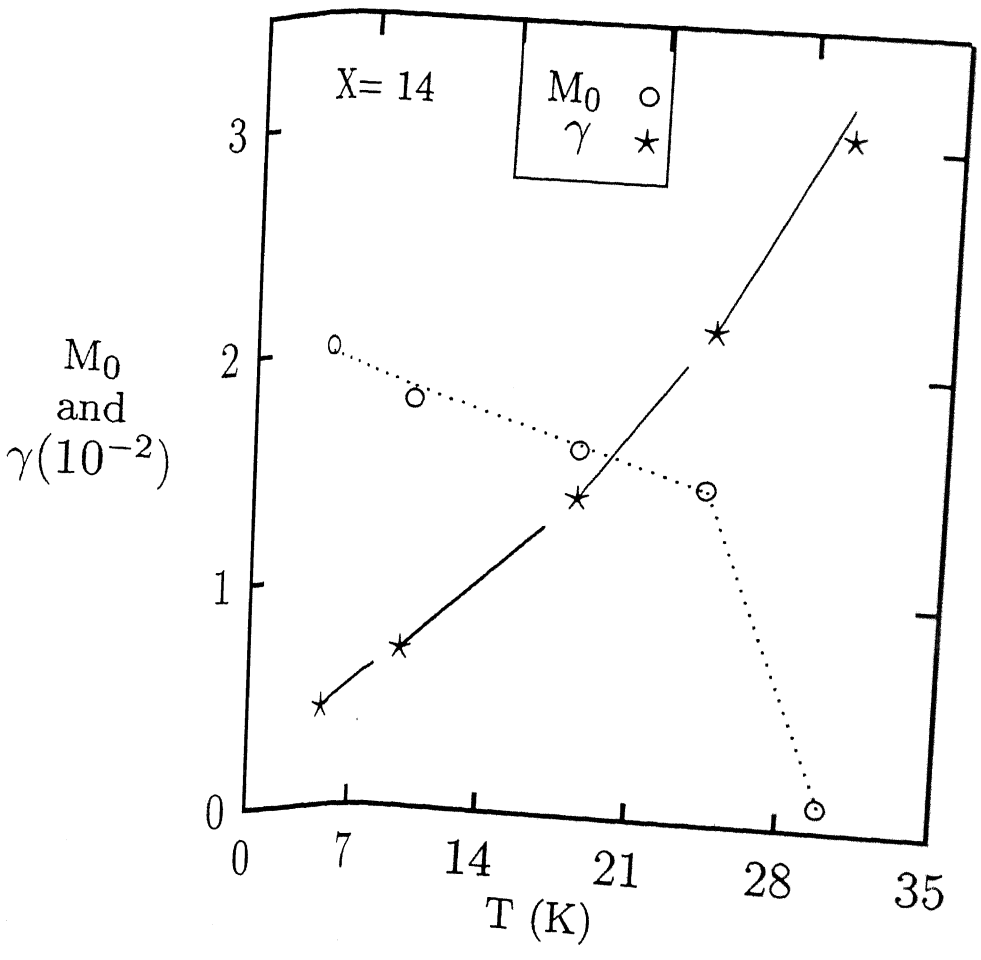

Figure 3.17: Temperature variation of the exponent, γ, and the initial magnetization, $M_0(10^{-3}\text{emu/g})$, for t_w = 180 s in the AF(X=14). Dotted lines are just guides to the eye.

forms. Hence it is difficult to describe the exact nature of the decay of the TRM in the AF phase. More experimental work is needed to arrive at a more definitive conclusion.

3.2 Conclusions

We have measured the TRM in $Fe_{80-x}Ni_xCr_{20}$ ($14 \leq X \leq 30$) alloys for four different magnetic phases within the *same crystallographic phase* and from their wait time and temperature variations tried to establish a correspondence with the magnetic phase diagram. We

Table 3.3: Best fitted parameters for Eq. (1.19) for different wait times at 5 K for X=14.

t_w (10^3 s)	M_0 (10^{-4} emu/g)	β (10^{-4})	χ^2 (10^{-7})
0.18	53.9	43.8	0.63
1.32	54.0	43.6	2.62
1.98	54.1	43.4	1.09
3.78	54.2	39.7	3.40

Table 3.4: Best fitted parameters for Eq. (1.19) at different temperatures for constant wait time (180 s) for X=14.

T (K)	M_0 (10^{-4} emu/g)	β (10^{-3})	χ^2 (10^{-7})
5	53.9	4.4	0.63
10	47.1	7.0	0.71
18	40.0	14.0	2.50
24	35.0	19.0	79.0
30	2.4	29.0	27.0

find distinct differences between the SG and the RSG phases with two different analytical forms for the time decay of the TRM. We also observe the presence of the FM ordering in the RSG below T_g which is consistent with the GT model. We also report the remarkable observation of the local maximum of the TRM just above T_c in the RSG (X=23) when it passes to the PM phase from the FM phase. This is found for the first time in any polycrystalline RSG. However, it's exact theoretical justification is unclear. We also observe that the values of the exponents show anomaly near the phase transitions. We observe some different features in the samples X=23 and X=26, though they undergoes similar kinds of phase transitions. We find the conventional power law decay in the FM phase. The value of the magnetization is found to increase with the Ni concentration. In the AF phase the power law decay is indistinguishable from the stretched exponential as a description of the TRM. More experimental work is needed to arrive at a more definite conclusion about the decay of TRM in an AF.

References

[1] R. V. Chamberlin, G Mozurkenich, and R. Orbach, Phys. Rev. Lett. **52**, 867(1984).

[2] R. Hoogerbeets, Wei-Li Luo, and R. Orbach, Phys. Rev. Lett. **55**, 111(1985).

[3] M. Alba, M. Ocio, and J. Hammann, Europhys. Lett. **2(1)**, 45(1986).

[4] D. Chu, G. G. Kenning, and R. Orbach, Philos. Mag. B **71**, 479(1995).

[5] D. Chu and G.G. Kenning, and R. Orbach, Phys. Rev. Lett. **72**, 3270(1994).

[6] R. V. Chamberlin, J. Appl. Phys. **57**, 3377(1985).

[7] F. Iefloch, J. Hammann, M. Ocio, and E. Vincent, Europhys. Lett., **18**(7), 647(1992).

[8] M. Ocio, M. Alba, and J. Hammann, J. Phys. Lett. (Paris) **46**, L1101(1985).

[9] T. K. Nath and A. K. Majumdar, J. Appl. Phys. **70**, 5828(1991).

[10] A. T. Ogileski, Phys. Rev. B **32**, 7384(1985).

[11] A. K. Majumdar and P.v. Blanckenhagen, Phys. Rev. B **29**, 4079(1984); J. Magn. Magn. Mater. **40**, 227(1983).

[12] M. Gabay and G. Toulouse, Phys. Rev. Lett. **47**, 201(1981).

[13] P. Mitchler, R. M. Roshko, and W. Ruan, J. Phys. I France, **2**, 2299(1992); D. Li, R. M. Roshko, and G. Yang, Phys. Rev. B **49**, 9601(1994).

[14] David A. Huse and Daniel S. Fisher, Phys. Rev. B **35**, 6841(1987); B **38**, 373, 386(1988); Phys. Rev. Lett. **56**, 1601(1986); A. J. Bray and M. Moore, Phys. Rev. Lett. **58**, 57(1987).

[15] R.V. Chamberlin and F. Holtzberg, Phys. Rev. Lett. **67**, 1606(1991).

[16] D. Stauffer, A. Caniglio, and M. Adam, Adv. Polim. Sci. **44**, 103(1982).

[17] T. K. Nath, N. Sudhakar, A. K. Majumdar, and E. J. Mcniff, Jr., Annual Report, Francis Bitter National Magnet Laboratory, Massachusetts Institute of Technology (1991-1992), p. **77**.

[18] G. Sinha, R. D. Barnard, and A. K. Majumdar, Phys. Rev. B **55**, 8982(1997).

Chapter 4

Low-field Magnetoresistance

In this chapter we present the low-field(< 30 gauss) magnetoresistance (LFMR) of the spin-glass(SG), ferromagnetic(FM) and the reentrant spin-glass (RSG) phases of fcc $Fe_{80-X}Ni_XCr_{20}$ ($19 \leq X \leq 30$) alloys. We find close resemblance between the temperature variation of the LFMR and the ac susceptibility in the RSG (X=26). Hysteresis effects in the LFMR have been found in the RSG for both increasing and decreasing temperatures. The presence of a dc biasing field at different temperatures alters the sign of the LFMR in the RSG at the lowest temperatures. This supports the idea of the existence of mixed FM and SG phases at the lowest temperature in the RSG. In the SG(X=19), the LFMR becomes negative while in the FM(X=30) it remains positive. These measurements of LFMR throw new light on our understanding of the various couplings between the moments in such magnetic systems.

[1]This chapter is mainly based on the published work by G. Sinha, R. D. Barnard, and A. K. Majumdar, Phys. Rev. B **55**, 8982(1997).

4.1 Results

Usually when the LFMR is measured for both forward and reversed pulsed magnetic fields these values are equal, i.e., the LFMR is symmetric for both the field directions. However, if some finite magnetization exists in the sample, which modifies the actual field seen by the electrons, then the LFMR becomes asymmetric with respect to the field direction. In such cases considerable care must be taken to determine the sign of the LFMR. To understand this it will be convenient to consider a material in which the intrinsic LFMR is proportional to the square of the magnetization(M).

Generally for small fields $M \propto H$ and hence LFMR $\propto H^2$. Here whether H is positive or negative, a positive LFMR results. The same variation will also hold when the H field is a pulsed square wave as in our experiments. This is the simplest system where the same variation is observed on both increasing or decreasing H. Under these conditions the sign of the LFMR is unambiguous. This case is shown in Fig. 4.1(a) where the LFMR is clearly positive but obviously a negative LFMR is also possible (shown by the dotted curve). In the above, the *static point* of the sample is the origin where no field is applied to the sample. However, if we consider an additional constant field H_0 which might be present in the sample, the *static point* is now at A and the pulsed field will be with respect to this point. The observed variation of LFMR will now look like that shown in Fig. 4.1(b) in which apparently there is a negative LFMR though no *intrinsic* negative LFMR is really associated with the sample. It should be mentioned here that the field H_0 may not necessarily be an externally applied field; it may be an internal field present in the sample. In such cases the determination of the sign of the LFMR(intrinsic) can be difficult. Let us now examine the case where an internal field H_0 is present and an external biasing field H_1 is also applied which may be positive or negative [Fig. 4.1(c)]. With H_0 and positive H_1 we observe a *static point* at B while if H_1 is negative then point C will be the *static point*. If H_1 is large and negative then the *static point* C could move to D. The variation of the LFMR for the static

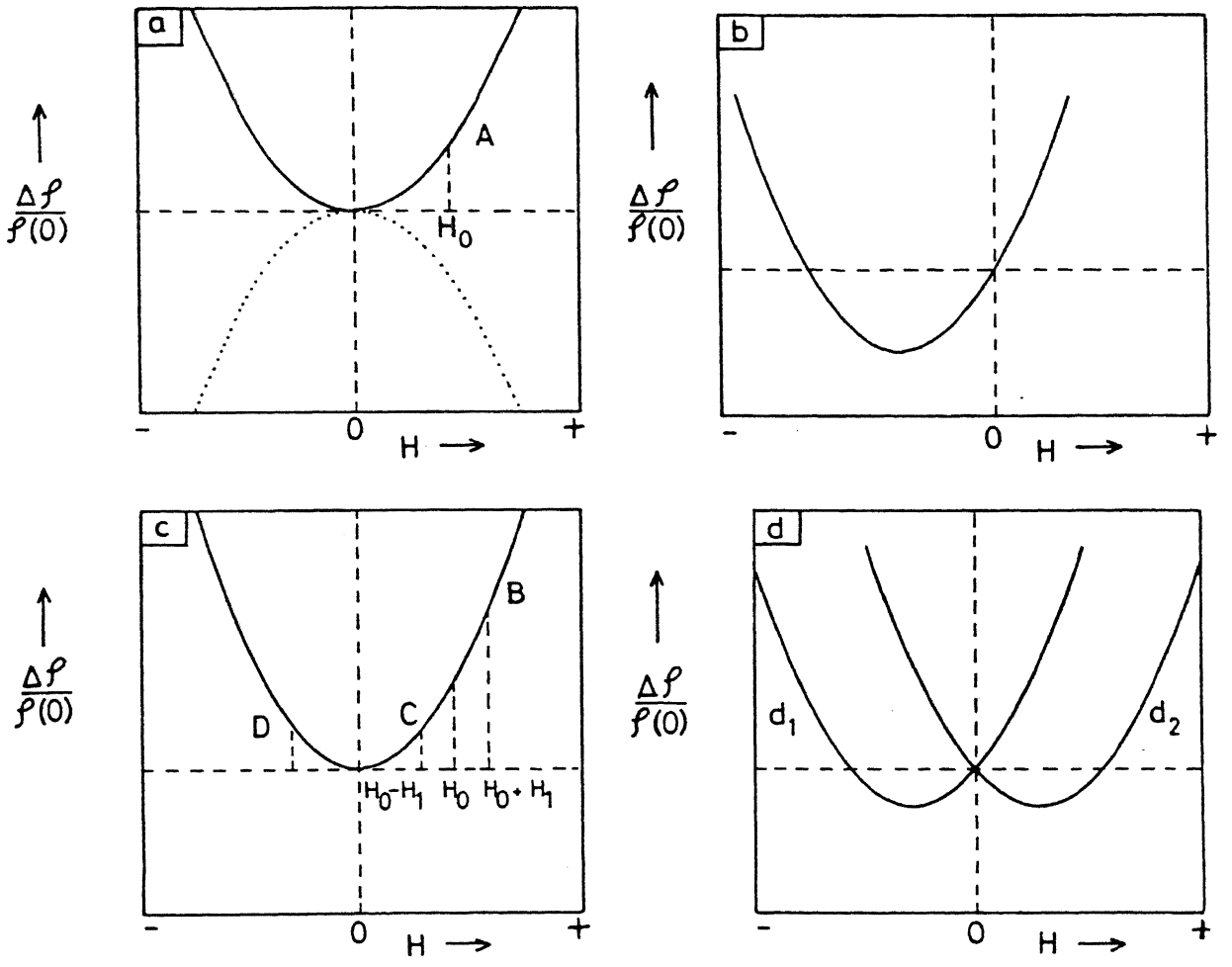

Figure 4.1: (a) Variation of MR with field which goes as H^2 with the origin as the static point. (b) Presence of a constant field(H_0) in the sample shifts the static point to A from the origin and the MR becomes asymmetric. (c) If there is an internal field present in the sample and an external field $\pm H_1$ is applied then the static point will shift from the origin to B and C, respectively. If H_1 is large then the static point will shift from C to D. (d) d_1 and d_2 are the variation of the MR with field for the static points at C and D, respectively.

points C and D will look as shown in Fig. 4.1(d), curves d_1 and d_2, respectively.

So to find the intrinsic LFMR one has to choose the static point in a way that will enable one to observe the effect of only the external magnetic field which, in our case, is an unidirectional pulsed field of frequency 38 Hz and not of the internal field or any other biasing field present prior to the application of the pulsed external field. If there is no internal field present in the sample, then the LFMR will be symmetric with respect to the origin for small fields and the origin *will* be the proper static point. If the LFMR is not symmetric with respect to the origin indicating the presence of some extra field(internal), then one has to apply an appropriate biasing field H_1 in order to nullify the effect of the internal field on the LFMR. This will *make* the LFMR symmetric with respect to the origin. In other words one has to shift the axes of the graph $\frac{\Delta\rho}{\rho(0)}$ vs H in such a way that the LFMR becomes symmetric with respect to the new origin and this point is called the proper *static point.*

The sample with X=26 undergoes a double transition, one from PM to FM at 68.89 K and the other from FM to RSG at 16.68 K on further lowering of temperature. These double transitions are clearly seen from the ac susceptibility(χ) measurements. The real part of the susceptibility shows a double knee while the imaginary part shows two distinct peaks at T_C and T_g, respectively (Fig. 4.2). The temperature variation of the LFMR also shows a behaviour (Fig. 4.3) somewhat similar to the real part of the susceptibility. According to Kohler's rule MR $\frac{\Delta\rho}{\rho(0)} = f(\frac{B}{\rho(0)})$. In magnetic samples B is no longer equal to H but $B = H + KM = H(1 + K\chi)$ where K is a constant. Therefore for constant H, MR should be a function of χ, i. e. , $\frac{\Delta\rho}{\rho(0)} = f(\chi)$. $\rho(0)$ has its own temperature dependence which is very weak compared to that of χ in the interval of 4.2 to 80 K where $\rho(0)$ changes by only $\approx 4\%$. So the temperature variation of $\rho(0)$ can be neglected. Hence there must be some relation between the temperature variation of MR and χ. We also observed that in the other RSG sample (X=23), the temperature variation of susceptibility and LFMR follow a similar behaviour (not shown) indicating a close relationship between the two. Similar behaviour was also reported in $FeNiMn$ RSG by Barnard et al.[1].

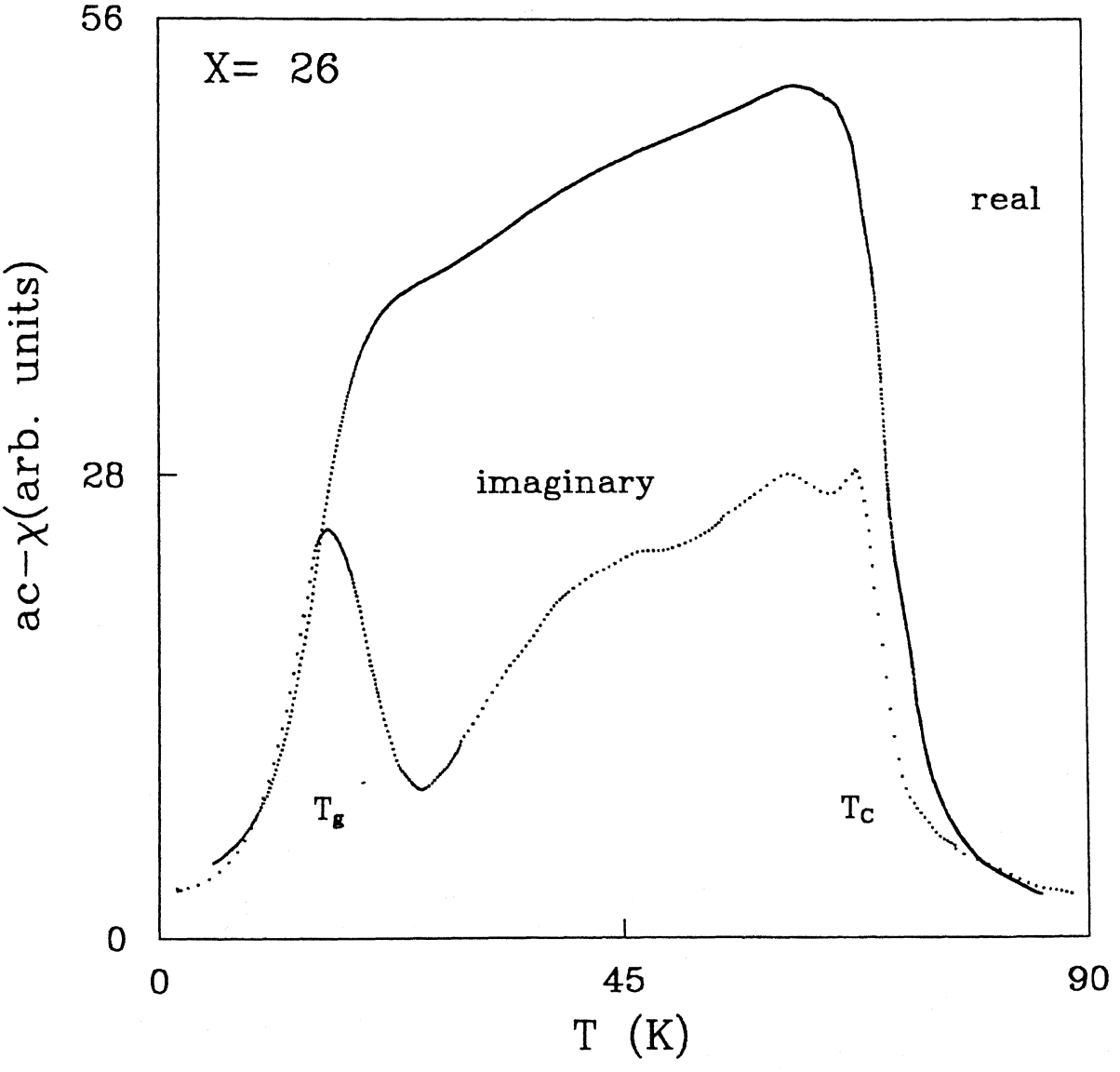

Figure 4.2: Temperature variation of the real and imaginary part of the ac-susceptibility for X=26 measured in a field of 242 Hz and 0.6 gauss.

The most interesting feature of the LFMR of X=26 is that it shows two different curves for +4 and -4 gauss square-wave fields(Fig. 4.3). To obtain these curves we have cooled the sample in unidirectional square-wave pulsed fields of ±4 gauss and frequency 38 Hz. This occurs because of the presence of some internal field which modifies the field seen by the sample. This is discussed later in this chapter. The internal field is also a function of temperature. In the temperature interval between 25 and 39 K it seems that the internal field vanishes as the two curves coincide. For +4 gauss field the LFMR becomes negative around 71 K which is above the T_C obtained from the ac susceptibility measurements. Similar behaviour has been observed in other RSG's ($\underline{Au}Fe$, $(Fe_{0.65}Ni_{0.35})_{1-x}Mn_x, x = 11.36at.\%$)[2, 1] near the PM to FM transition.

The LFMR shows thermal hysteresis effects at lower temperatures for a +4 gauss pulse square-wave field (Fig. 4.4). To see thermal hysteresis we have cooled the sample down to 4.2 K in zero field and then applied a +4 gauss pulsed square-wave field of frequency 38 Hz. Then we increased the temperature up to 20 K (A→ B of Fig. 4.4), then cool it down slowly to 4.2 K (B→ C) and again increased the temperature up to 30 K (C→ D). Through out the operation (A→ B → C→ D) the square-wave pulsed field of +4 gauss was on. So the curve C→ D of Fig. 4.4 is essentially the same as shown in Fig. 4.3 for +4 gauss field up to 30 K. With the increase of temperature it shows a negative LFMR, a feature generally associated with the SG state, then a dip around 10 K followed by a sharp increase and finally it becomes positive. On reducing the temperature it starts bifurcating at 17 K but retains the positive value to the lowest temperature. Afterwards, it shows a reversible behaviour with thermal cycling. It is to be noted that thermal hysteresis is only observed in the RSG phase and not in the FM phase ($T > T_g$) with this small applied field. The dip around 10 K is a new finding which we could not trace in our susceptibility measurements. The magneto-thermal-history effect in SG's has also been reported by Raker and Beck[3].

To further investigate the magnetic hysteresis effect we measured the LFMR with varying pulsed field at 4.5 K (Fig. 4.5). It shows hysteresis and for small fields the LFMR is

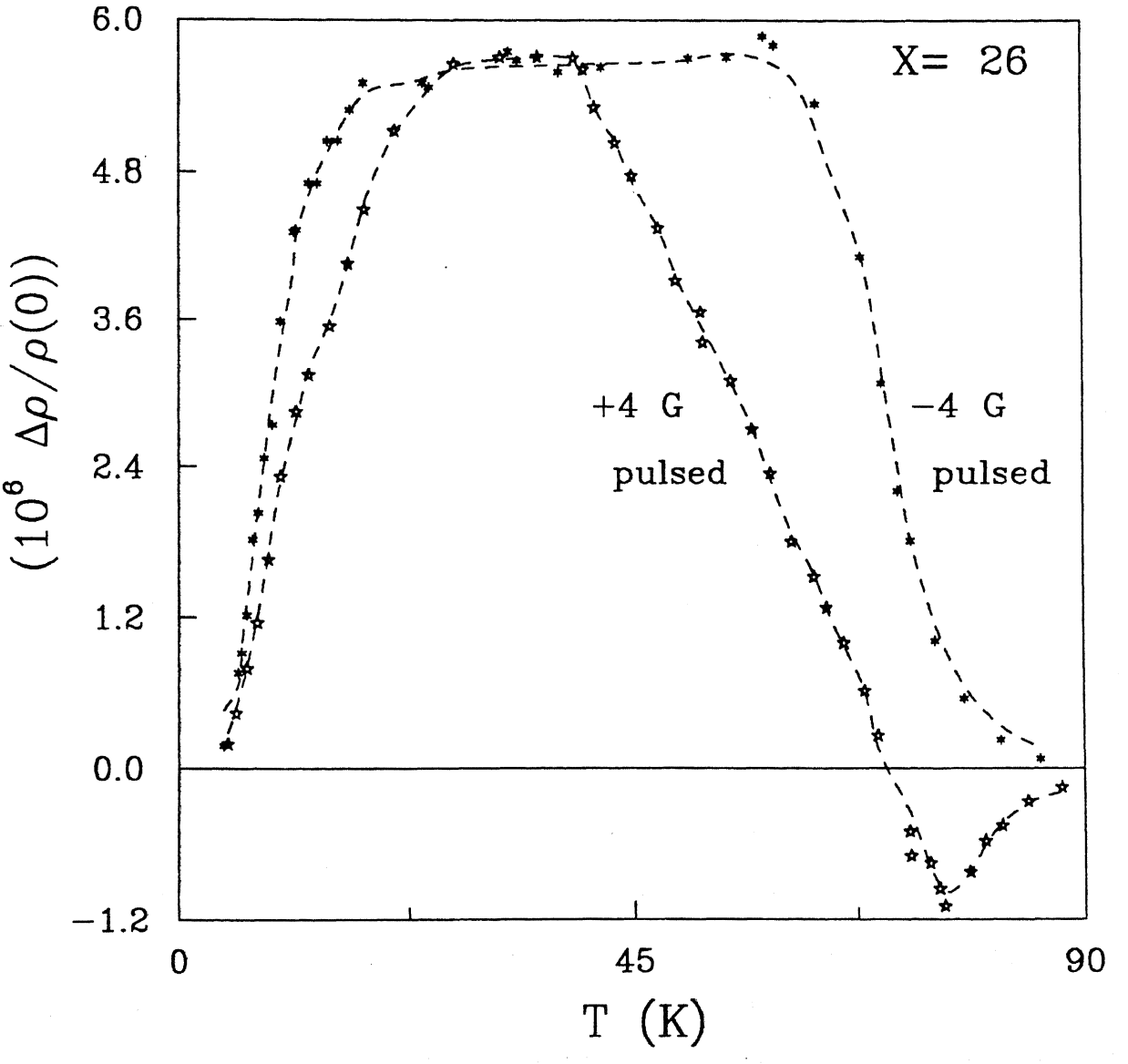

Figure 4.3: Temperature variation of the LFMR for X=26 measured in ±4 gauss pulsed square-wave fields.

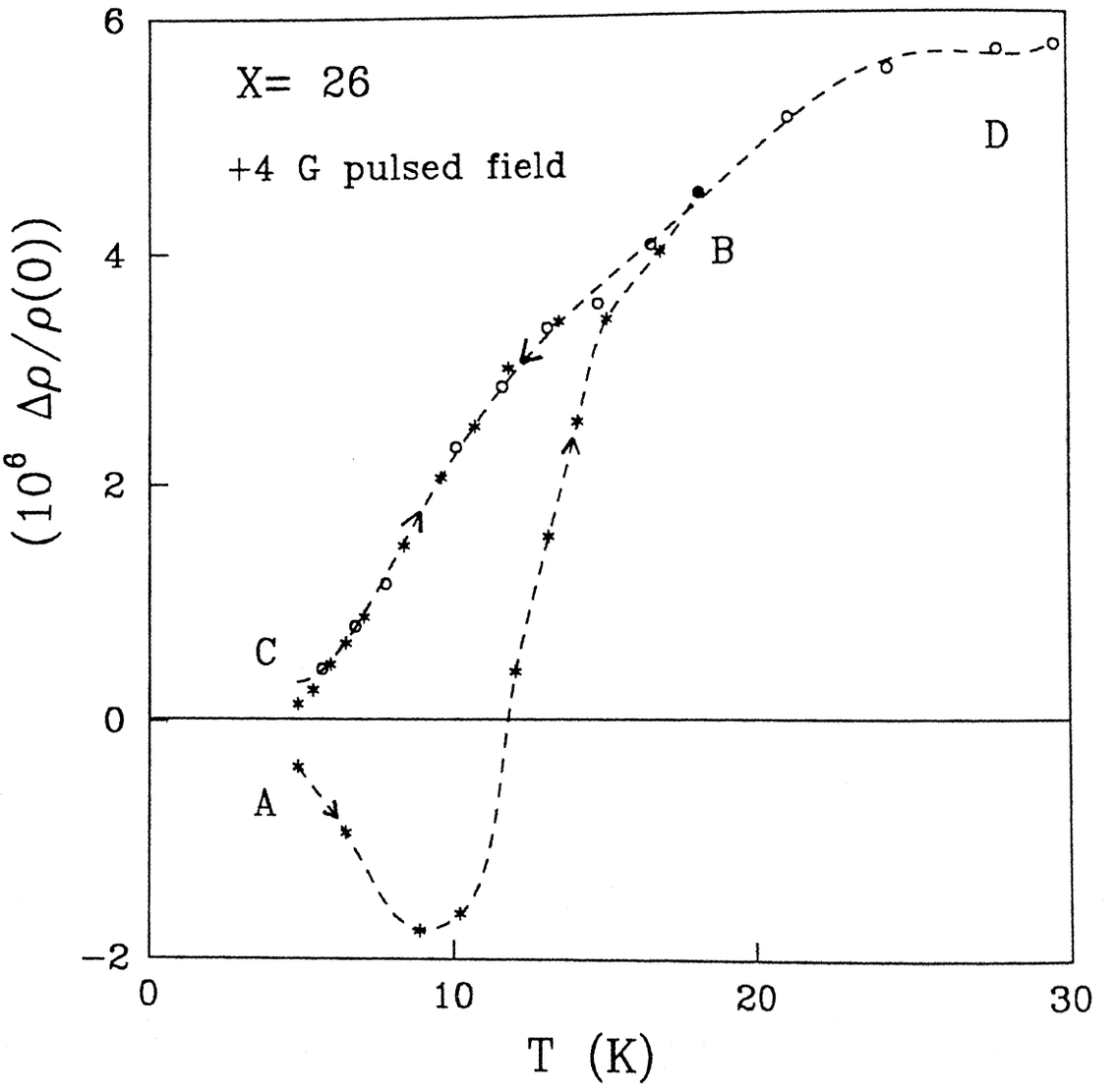

Figure 4.4: Temperature variation of the LFMR for X=26 for various thermal cycles, measured in a +4 gauss pulsed square-wave field. Initially the temperature was increased from A to B, then it was decreased to C and then increased again to D. The arrows in the figure show the cycles.

negative. We think that the presence of small (negative) internal fields shifts the *static point* and makes the LFMR apparently negative, but the intrinsic MR always remains positive. Here the magnetic history effect is somewhat similar to the thermal history effect. After one cycle it followed a reversible path. Initially the LFMR is positive above B≈10 gauss. On reducing the field the LFMR always remained positive and reduced to zero as the field was reduced to zero. Then for a negative field, it followed a reversible path. Hysteresis effects were also observed in other RSG samples[1], where their appearance for smaller fields, followed by a reversible behaviour at higher fields, further complicated the situation.

Figure 4.6 shows the variation of the LFMR at 4.5 K in the presence of different static fields on top of the variable pulsed field. In the presence of ±18.2 gauss static fields it shows a negative LFMR along with hysteresis effects. The curves are also not symmetric for the positive and negative applied fields. In the RSG phase, both FM and SG types of clusters are present and the LFMR is the combined effect of all these clusters. In zero static field the LFMR arising from the FM clusters predominates and makes the resultant LFMR positive(Fig. 4.5). But the application of a sufficiently high static field effectively locks the FM clusters and only the SG component can then follow the pulsed field which reveals itself as a negative MR. Hence the LFMR provides strong evidence for the presence of FM ordering down to the lowest temperature, a conclusion we had reached earlier from our magnetic relaxation and ac susceptibility measurements[4]. However, the reason behind the asymmetry in the curves for positive and negative pulsed fields and the exact nature of the different types of clusters present and their interactions seem to be quite complicated. One possible explanation is that the ±18.2 gauss static fields are insufficient to fully saturate the FM component but nevertheless are sufficient to block the rest of the positive LFMR. That there is still some hysteresis in the curves shown in Fig. 4.6 strongly suggests near, but not complete, saturation.

We concluded earlier that the internal field was absent at around 25 K. Further measurements on X=26 at 25 K of the variation of the LFMR in zero and ±18.2 gauss biasing

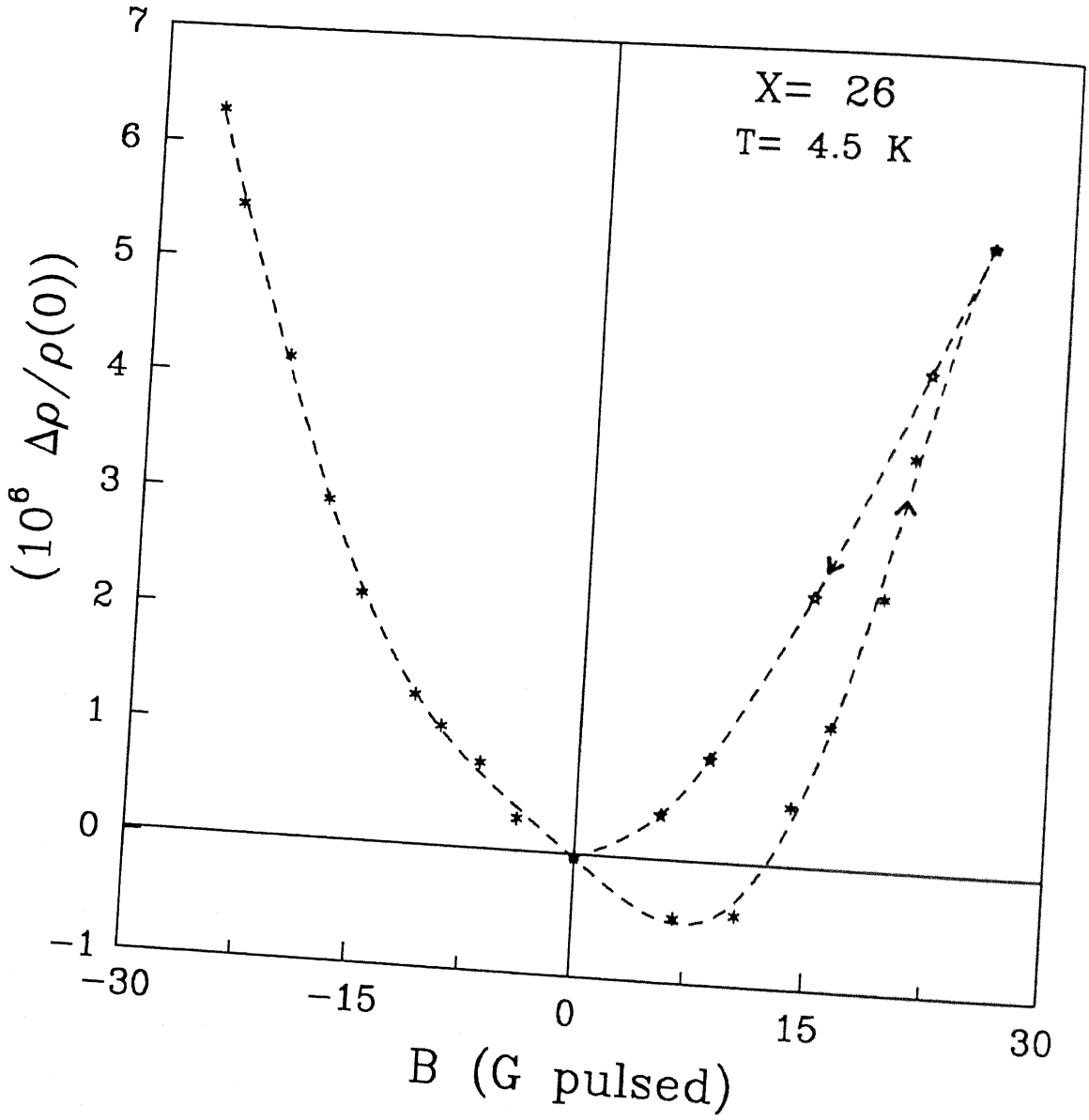

Figure 4.5: Variation of the LFMR for X=26 at 4.5 K with the increase and decrease of pulsed square-wave fields(the arrow indicating the direction).

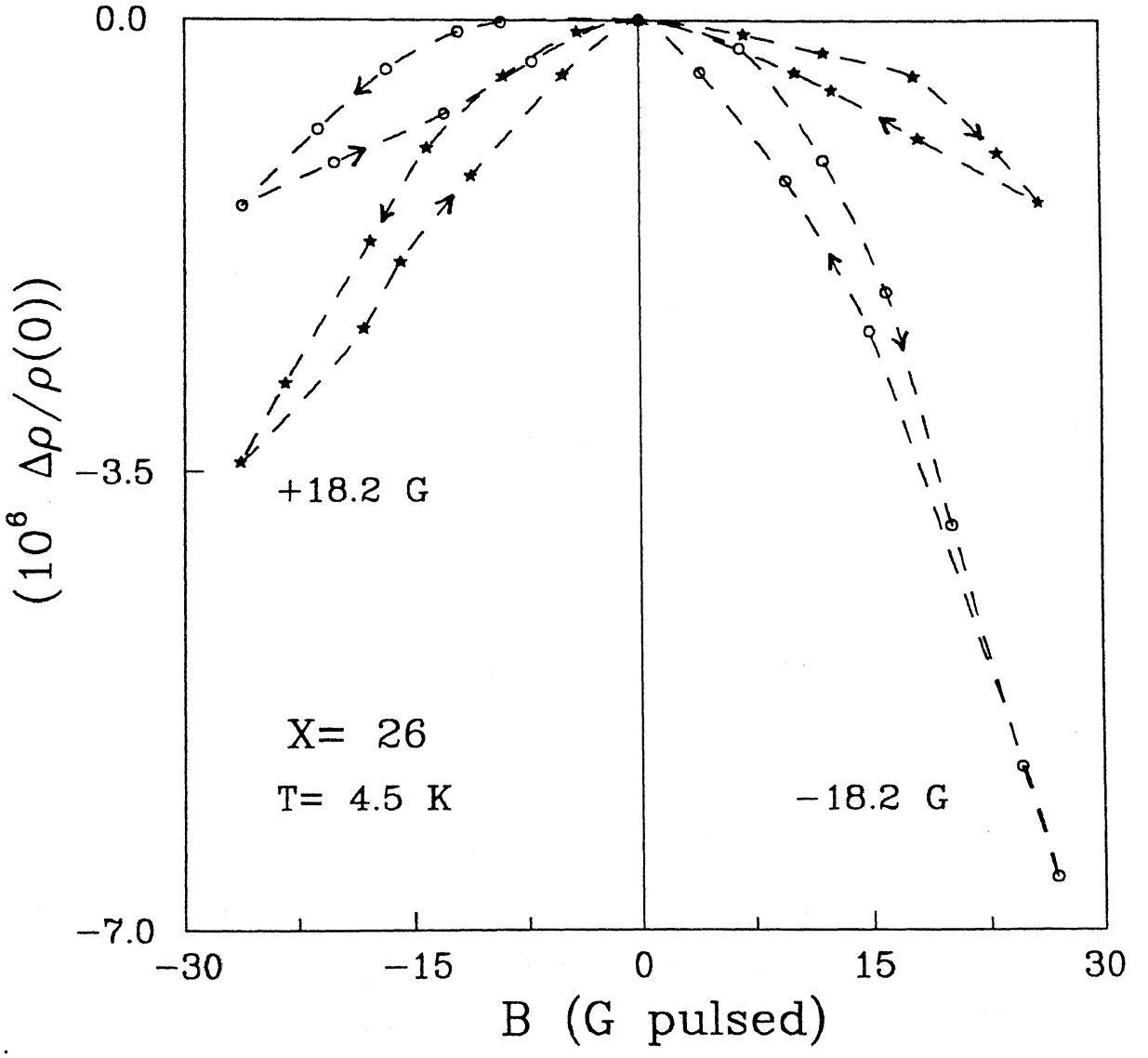

Figure 4.6: Variation of the LFMR for X=26 at 4.5 K with the pulsed square-wave field in the presence of ±18.2 gauss static biasing field. The biasing field makes the LFMR negative.

fields are shown in Fig. 4.7. For zero biasing field, the LFMR is always positive, and the curve is symmetrically placed about the origin. With the biasing field of ± 18.2 gauss the LFMR curves are shifted by equal amounts on either side of the origin. By choosing the proper *static point* through shifting of the graphing axes, discussed earlier, we can show that here the LFMR is positive. At 25 K the sample is in a FM phase, hence a positive LFMR is expected. However, in the presence of ± 18.2 gauss biasing field the LFMR indicates saturation for higher fields. It may be that at higher fields it reverses its slope and becomes negative. Our high field data (0.1 to 17 kGauss) for the other RSG sample(X=23) shows negative MR in the FM phase[5]. Therefore it is very important to do low-field measurements to reveal the true nature of the magnetic state. It is only through the positive LFMR that we are able to conclude that the ferromagnetic phase persists even below the lower transition temperature in the RSG. At still higher fields (up to 7 T) Banerjee and Raychaudhuri[6] had shown that the MR can be expressed as $\frac{\Delta\rho}{\rho(0)} = A(T)H^2 - B(T)H^m$, where A(T) and B(T) are constants at a given temperature and the exponent, m, is less than 1. They concluded that the negative contribution has a magnetic origin.

The measurements at 78 K, in the PM region, show negative MR (Fig. 4.8). But to get a symmetric curve we need to apply a -9.1 gauss biasing field. For zero and other biasing fields, we have to shift the static points to get the intrinsic LFMR, which is negative in this case. So in the PM region, we observe a negative LFMR and a small internal field of about 9 gauss. At 4.5 K the LFMR curve (LFMR intrinsically positive) is shifted to the right of the origin for zero bias(Fig. 4.5) but here it shifts to the left of the origin.

Figure 4.9 depicts the variation of the LFMR at 63.5 K for zero and some biasing fields. At this temperature the LFMR starts showing asymmetric behaviour. For zero biasing field the static point is very close to the origin indicating the presence of a very small (negative) internal field. The LFMR initially increases with field but around 30 gauss it shows a tendency to saturate. With positive and negative 9.1 gauss biasing fields the LFMR shifts by unequal amounts along the $(-\frac{\Delta\rho}{\rho(0)})$-axis unlike that at 25 K (Fig. 4.7). For -18.2 gauss

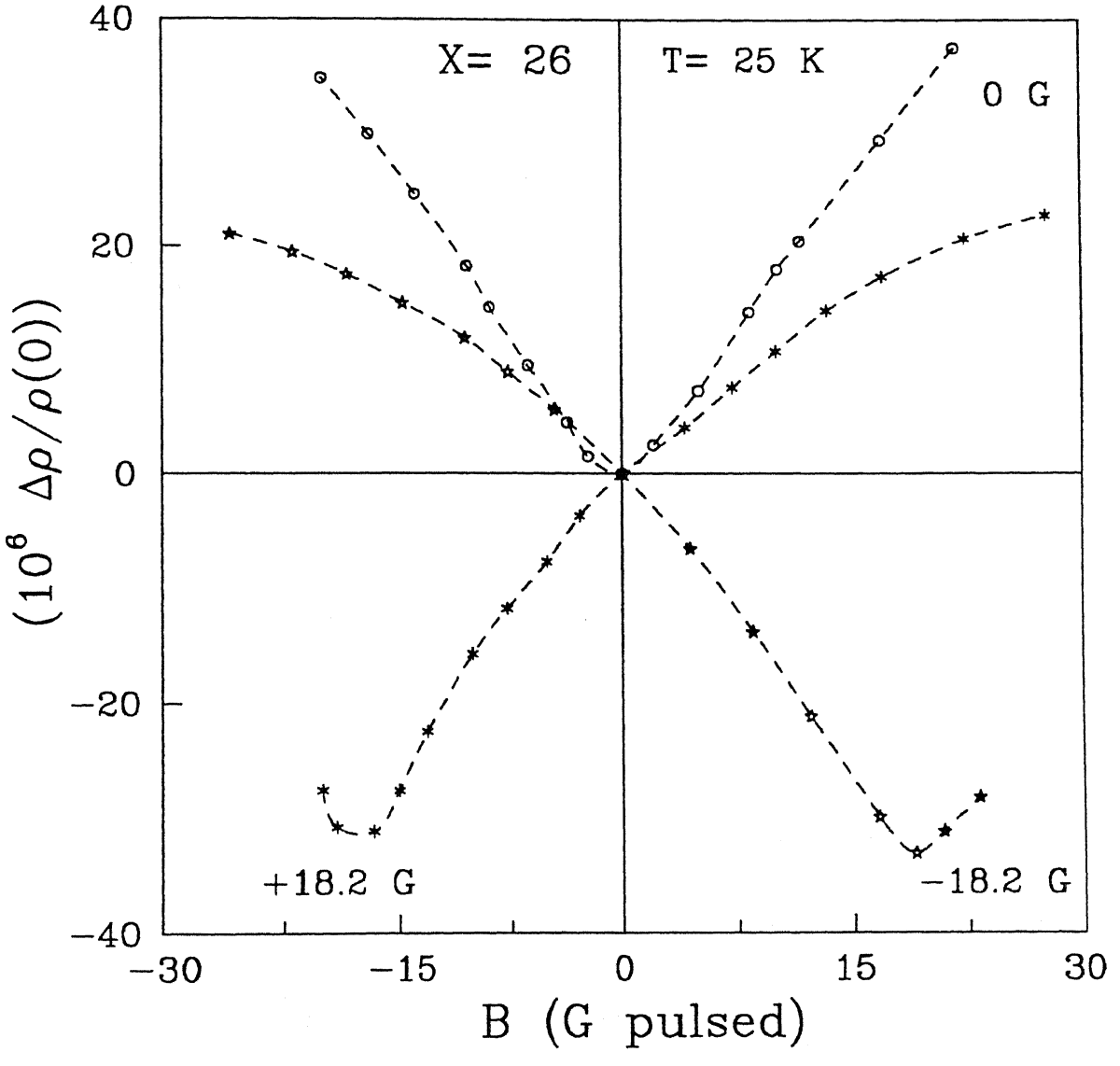

Figure 4.7: Variation of the LFMR for X=26 at 25 K with the pulsed square-wave field in the presence of 0 and ±18.2 gauss static biasing fields.

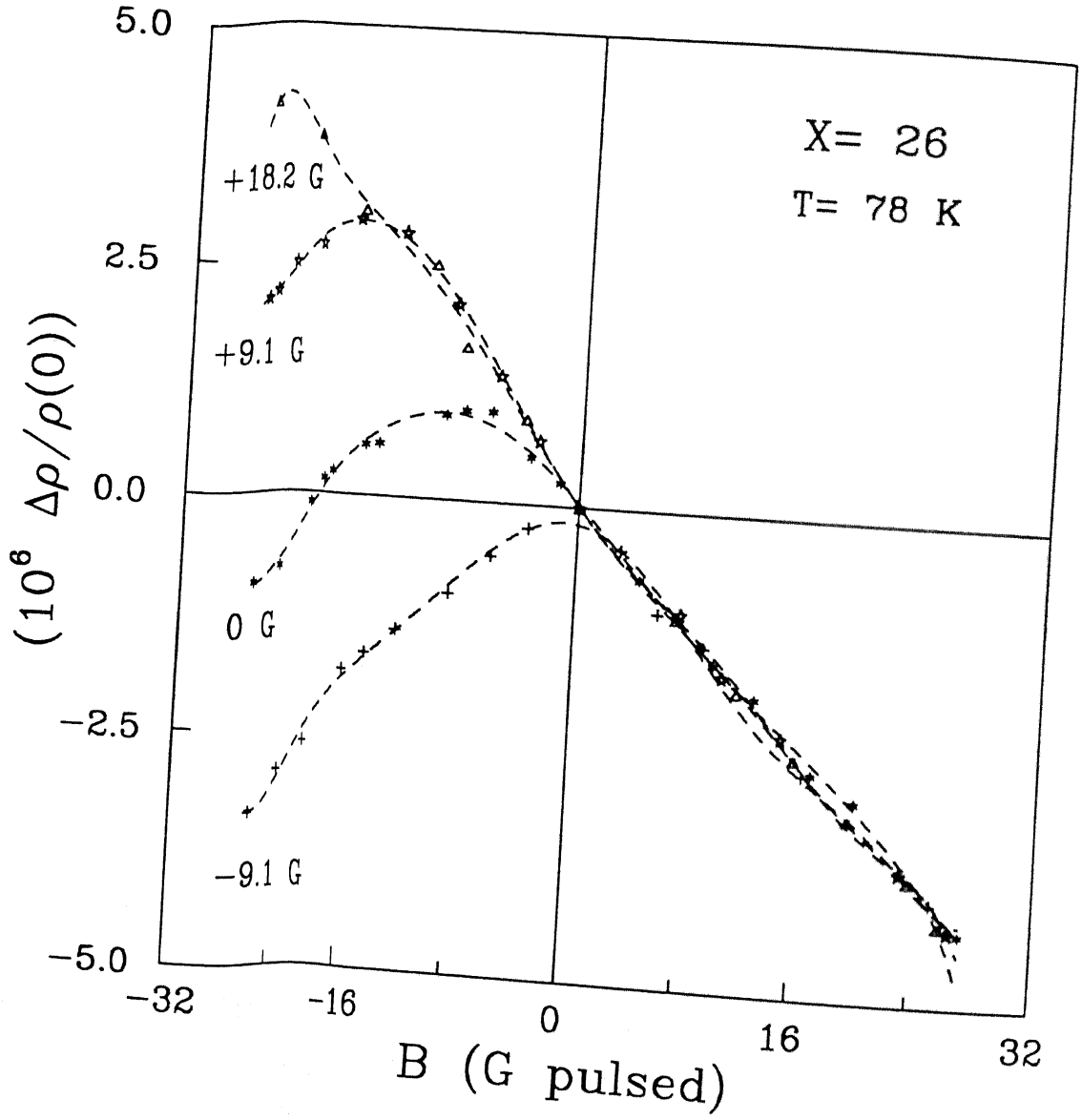

Figure 4.8: Variation of the LFMR for X=26 at 78 K with the pulsed square-wave field in the presence of +18.2, +9.1, 0, and -9.1 gauss static biasing fields. -9.1 gauss biasing field brings the static point to the origin.

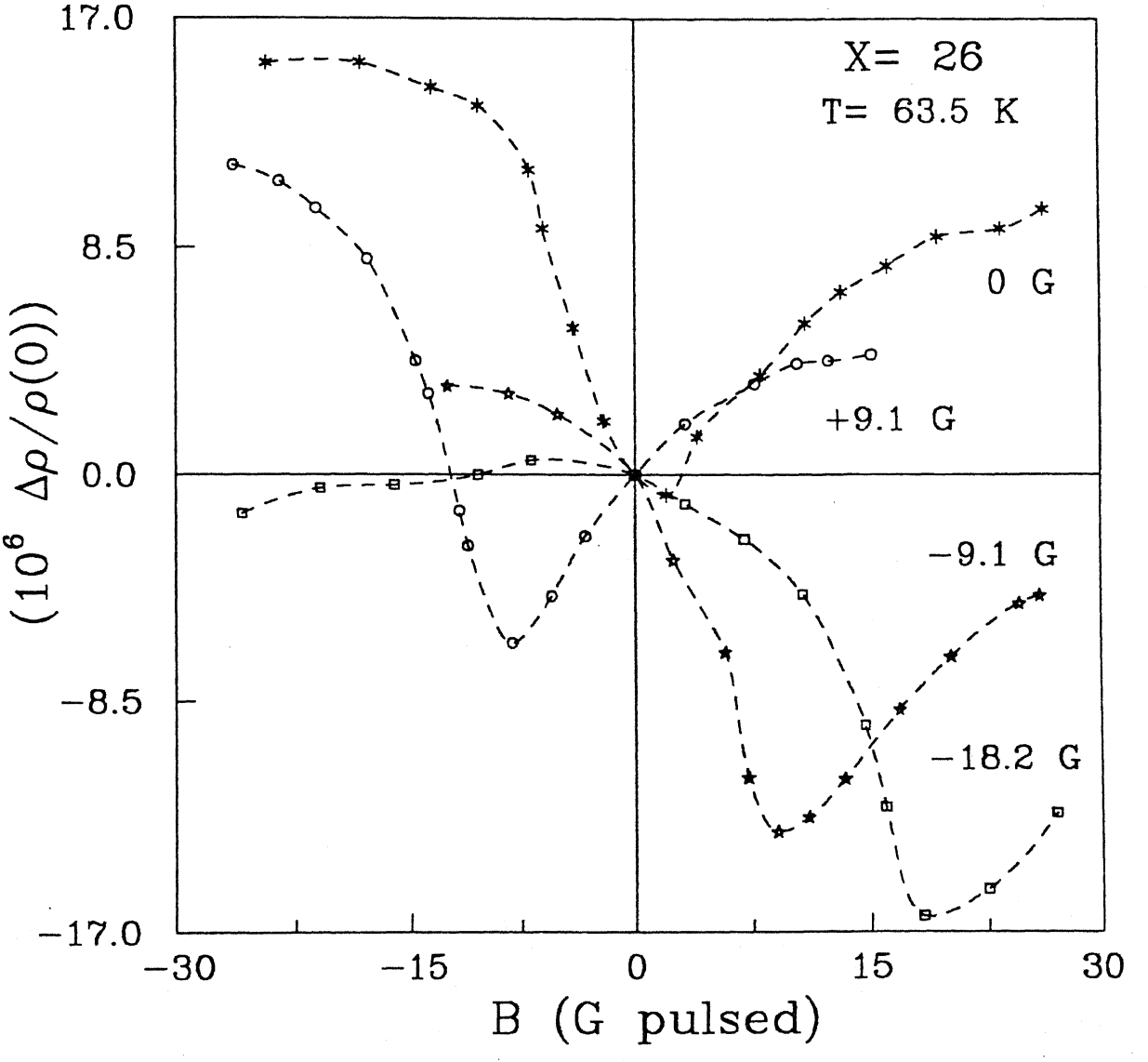

Figure 4.9: Variation of the LFMR for X=26 at 63.5 K with the pulsed square-wave field in the presence of +9.1, 0, -9.1 and -18.2 gauss static biasing fields.

biasing field the *static point* is now on the right of the origin and is $\approx$ 18 gauss away along the B axis. With respect to this new origin the slope of the LFMR curve is positive. But when the field increases along the negative direction the LFMR reverses its slope and finally becomes negative. As we have already applied a biasing field of -18.2 gauss, the effective field along the negative direction is still larger. The reason behind this asymmetric behaviour of the LFMR for positive and negative fields is not clear.

At 70 K, very close to the critical temperature, the LFMR has a very complicated behaviour. Figure 4.10 shows the variation of the LFMR for different biasing fields. The LFMR is not symmetric, nor can a graphical shift of the *static point* make it symmetric. Therefore the choice of the static point is very difficult here. Very close to the critical temperature (T_C), the complex interplay of different magnetic constituents and the absence of any pure magnetic phase further complicates the situation. According to our criterion, for zero biasing field, the origin is the so-called static point. Hence for positive biasing fields, the static point is expected to be on the left of the origin and on the right for negative biasing fields. For smaller fields(zero bias case) the slope of the LFMR is positive but around -20 gauss field, it reverses its slope indicating a negative LFMR. So, even in the zero bias, the LFMR can have both positive and negative components. In the presence of a +18.2 gauss biasing field, the LFMR indeed becomes positive (seen after choosing the proper *static point* which is now at the left of the origin). But with the increase of the field along the positive direction, the LFMR becomes negative. Actually, when the *static point* shifts towards the left of the origin, the actual field seen by the sample is larger than the applied field along the positive direction. The nature of the LFMR curves is different for positive and negative 18 gauss biasing fields. At this point it seems that the LFMR has two components, one positive and the other negative. Starting from the high-temperature side, prior to the establishment of the FM phase there may be a mixed phase where a PM or even a SG phase coexists with a FM phase. The positive contribution is coming from the FM ordering while the PM or SG ordering gives a negative LFMR. However, the resulting nature of the LFMR curve will

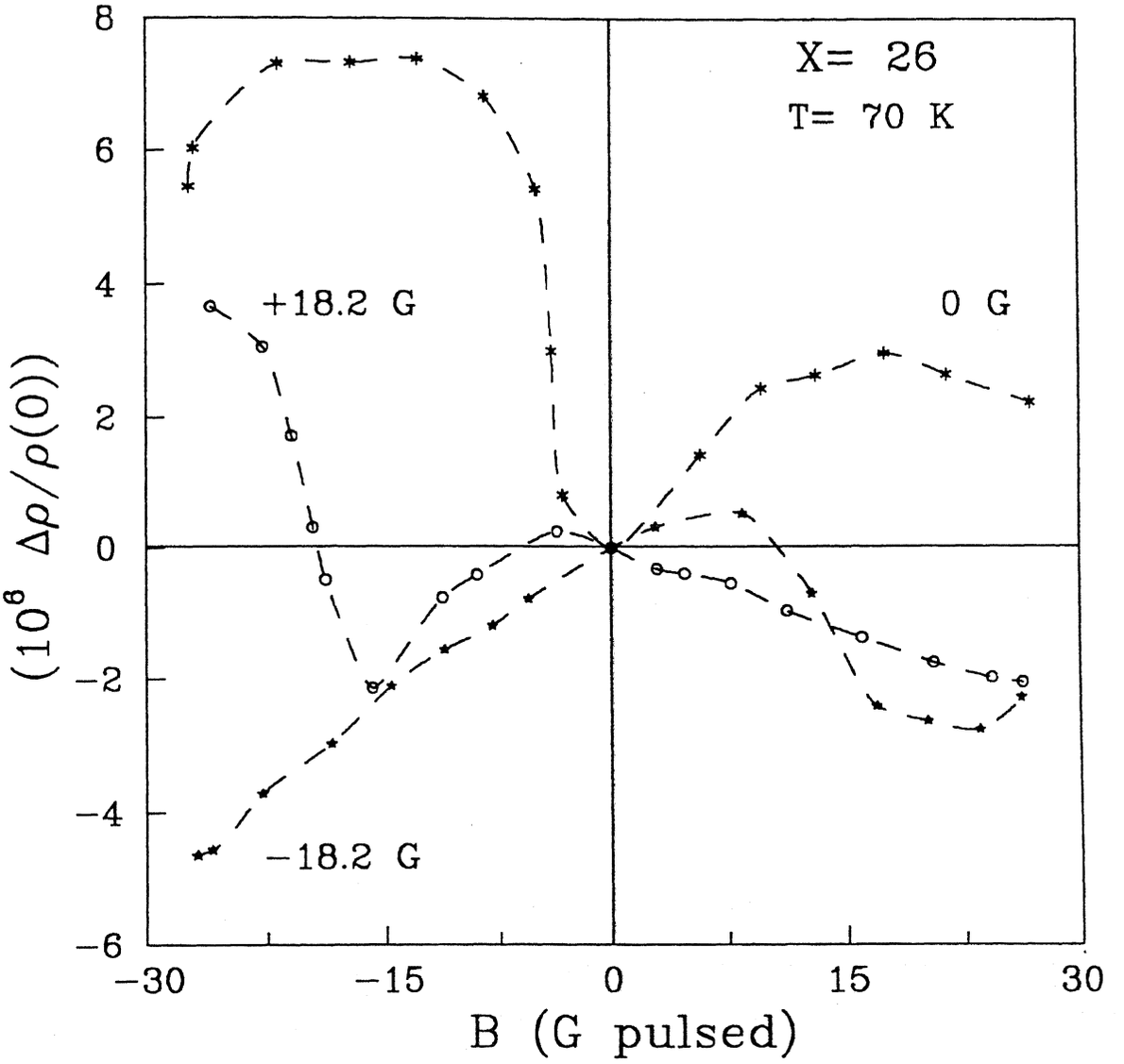

Figure 4.10: Variation of the LFMR for X=26 at 70 K with the pulsed square-wave field in the presence of 0 and ±18.2 gauss static biasing fields.

depend on their relative contributions. Here the LFMR for zero bias is somewhat similar to that observed in $(Fe_{0.08}Ni_{0.92})_{77}Si_{10}B_{13}$ RSG near T_C[2].

Figure 4.11 shows the variation of the LFMR for X=30 at 78 K (T_C = 130 K). X= 30 is a ferromagnet, and thus the LFMR is positive and symmetric for both the positive and negative pulsed fields. It also does not show any hysteresis effects for the small applied fields used. In the FM phase where long-range order exists, smaller fields do not show non-linear effects which give rise to hysteresis in magnetization and therefore in magnetoresistance. For small fields, the LFMR in X=30 shows reversible paths, unlike the SG phase, where at lower temperatures we have observed that the LFMR in X=26 follows irreversible paths for small fields.

Figure 4.12 shows the temperature variation of the LFMR for the sample with X= 19, which is a SG. For small applied fields, the LFMR is very small and it is about the limit of our experimental resolution. We get rather scattered data, even after applying a pulsed field of 20 gauss. We can barely resolve a dip at the transition temperature. Nevertheless, we can definitely conclude that the LFMR in X= 19 remains negative both in the SG and the PM phase (up to $\approx 2T_g$).

4.2 Discussion

The LFMR results in the RSG (X=26) presented in this chapter under very low-field conditions (< 30 gauss) show at 4.2 K, a negative LFMR, a characteristic of a SG. It has a negative dip around 10 K, then it increases and finally becomes positive. But the LFMR retains a positive value when the temperature is lowered with the field on. For the RSG (X=26) at 4.5 K and zero bias, the intrinsic LFMR is positive. If the lower temperature phase is a pure SG, then the LFMR should be negative. So the presence of FM clusters at the lower temperature is strongly suggested. Now, to see the SG-type of behaviour we have to suppress or block the contributions coming from the FM clusters. Application of a biasing field locks

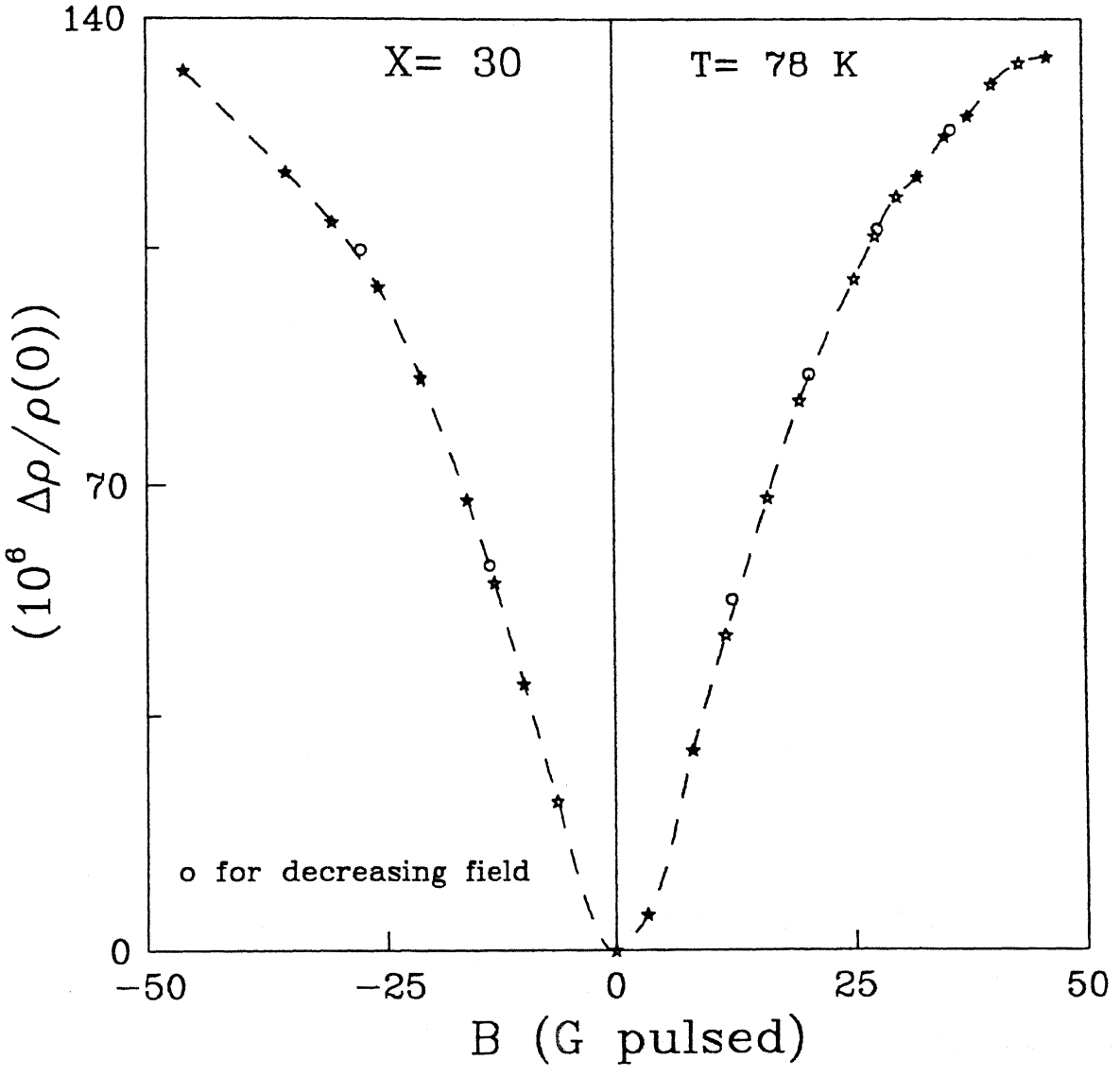

Figure 4.11: Variation of the LFMR with pulsed square-wave field for X=30 (FM) measured at 78 K in a field of 38 Hz.

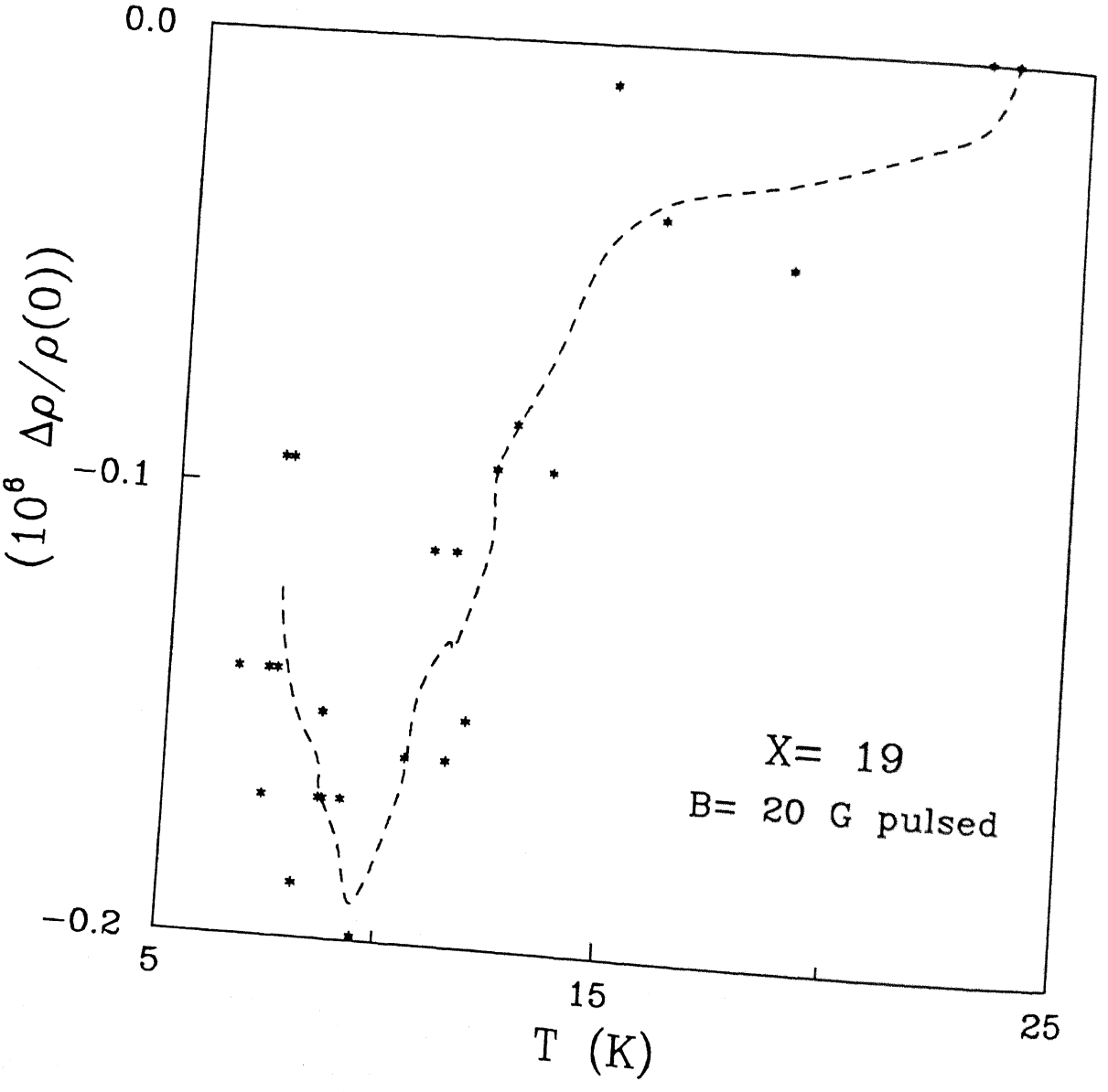

Figure 4.12: Temperature variation of the LFMR for X=19 (SG) measured in a 20 gauss pulsed square-wave field.

the FM clusters allowing the SG component, which is less affected by dc fields, to be revealed. This results in a negative LFMR. We measured the non-linear ac-susceptibility, which shows a peak around T_g[7]. This peak can only be observed if a spontaneous magnetization is present. Moreover, the presence of small internal fields, causing a shift of the *static point* in the LFMR curve at the lower temperature, supports the above proposition in the RSG. Thus the lower temperature phase of the sample with X=26 consists of both SG and FM type of orderings. In this phase small FM clusters are embedded in a matrix of frustrated SG-like spins. We define this phase as the RSG which is distinctly different from the SG.

At temperatures above T_g, the LFMR becomes positive for both nonzero and zero biasing fields, indicating a pure FM phase. However, at higher temperatures, close to the critical temperature T_C, we observed a tendency towards a negative LFMR for higher fields. In the presence of biasing fields, the LFMR can have both positive and negative values. We know that the positive LFMR arises out of the FM clusters, and the negative contribution comes from either the SG or the PM type of orderings. If the FM ordering coexists with the PM (SG) type of random spins, then the resultant LFMR can be of either sign, determined by the relative contributions of the different spin orderings. Normally for smaller fields, the contribution from the FM component dominates, but at higher fields or in the presence of biasing fields, the FM part is locked, and then the negative contribution becomes more prominent. We observed similar behaviour around T_C in the RSG (X=26). So, near the critical point, both above and below, when the sample (X=26) passes from the PM to the FM phase with the lowering of temperature, it passes through an intermediate phase where FM clusters coexist with PM (SG) spins. It is a new kind of phase which exists for a very narrow temperature interval prior to the onset of the FM phase. A similar kind of phase was also predicted earlier near T_C in $FeNiMn$ RSG[1]. At 78 K ($T > T_C$), the LFMR becomes negative, indicative of a PM (SG) phase. So from the present LFMR measurements, we propose a new phase of FeNiCr alloys which exists for a very narrow temperature interval near T_C. This kind of phase is possible where there are very strong competing interactions in a

magnetic system. The final nature of the phase depends upon the more dominant interaction. If the strengths of the interactions are comparable, then this kind of mixed phase may be possible. However, we could not trace this kind of phase from our earlier dc and ac magnetic measurements. So from these LFMR measurements, we conclude that the sample with X=26 passes through diverse magnetic phases like, $PM \rightarrow (PM(SG) + FM) \rightarrow FM \rightarrow RSG(=$ FM + SG) with the lowering of temperature.

4.3 Conclusion

We have measured the LFMR in different magnetic phases of $Fe_{80-x}Ni_xCr_{20}$ alloys. We observe that the LFMR is negative in the SG(X=19) and the PM phases and positive in the FM (X=30) phase. In the RSG (X=26), at the lowest temperature (4.5 K), the intrinsic LFMR is positive for zero biasing field, but the presence of a 18.2 gauss static biasing field makes the LFMR negative, a feature generally associated with the SG state. This suggests that the lowest temperature phase of the RSG has mixed FM and SG-type of orderings. We believe that small FM clusters are embedded in a matrix of frustrated spins of the SG. We observe hysteresis effects in the LFMR for small applied fields at the lowest temperature for the RSG sample. But such small fields do not produce any hysteresis effect in the FM phase(X=30). We find that the LFMR becomes negative around T_C for a +4 gauss pulsed field in the RSG. From the LFMR measurements, we conclude that when the RSG sample(X=26) goes from the PM to the FM phase with lowering temperature, it passes through an intermediate phase. Here the PM(SG) phase coexists with the FM phase for a very narrow temperature interval. So with the reduction of temperature, the RSG sample passes through various magnetic phases like, $PM \rightarrow (PM(SG) + FM) \rightarrow FM \rightarrow RSG(= FM + SG)$. We also find a close resemblance between the temperature variation of the LFMR and the ac susceptibility in the RSG(X=26).

References

[1] R. D. Barnard, Ch Bottger, S. Thamm, and J. Hesse, J. Phys. Condens. Matter **4**, 7219(1992).

[2] R. D. Barnard, J. Phys. Condens. Matter **2**, 5191(1990); J. Appl. Phys. **73**, 6846(1993).

[3] L. D. Rakers and Paul A. Beck, Phys. Rev. B **36**, 8622(1987).

[4] G. Sinha, R. Chatterjee, M. Uehara, and A. K. Majumdar, J. Magn. Magn. Mater **164**, 345(1996).

[5] T. K. Nath and A. K. Majumdar, J. Appl. Phys. **70**, 5828(1991).

[6] S. Banerjee and A. K. Raychaudhuri, Phys. Rev. B **52**, 3452(1995).

[7] G. Sinha and A. K. Majumdar, J. Magn. Magn. Mater **185**, 18(1998).

Chapter 5

Low-field ac susceptibility

In this chapter we present the low-field ac susceptibility and its dc field dependence in four different magnetic phases of $Fe_{80-X}Ni_XCr_{20}(14 \leq X \leq 30)$ alloys within the same crystallographic phase. In the spin-glass(SG) phase(X=19) the transition temperature(T_g) varies with frequency(ν) and follows Fulcher's law of the form $\nu = \nu_0 \exp[-\frac{E_a}{k(T_g - T_0)}]$ while the non-linear susceptibility(χ_2) shows a peak at T_g. In the reentrant spin glasses(RSG) (X=26 and 23), double transitions are clearly seen from the imaginary part of the linear susceptibility(χ_0''). The peak near the upper transition vanishes in the presence of a small dc biasing field. We compare the lower transition of the RSG with that of an SG and the upper one with that of a ferromagnet(FM). Critical exponents, γ, β, and δ are obtained from χ_0 and its dc field dependence in the RSG(X=26). They follow the scaling law obtained from the mean-field theory(MFT) although the values of the exponents are not in agreement with it. The non-linear susceptibility (χ_1) shows a peak near T_g in both the RSG's which is indicative of a long-range order. This is never observed in a pure SG, including X=19. The value of the critical exponent γ increases with the increase in Ni concentration (X=23

[1]This chapter is mainly based on the published work by G. Sinha and A. K. Majumdar, J. Magn. Magn. Mater **185**, 18(1998).

to 30) as the system moves towards the FM phase(X=30). In the antiferromagnet(X=14), the transition temperature (T_N) shifts towards higher temperatures in the presence of small dc fields.

5.1 Results and discussion

5.1.1 Spin glass (X=19)

Generally, the transition temperature of an SG (T_g) depends upon the frequency of measurement. Figure 5.1 shows the variation of the real part of the ac susceptibility(χ_0') with temperature for the SG (X=19) for different frequencies. Although we have taken the data at an interval of 2 mK down to 1.2 K, to show the effect more clearly near T_g we plot the data around it and shift the curves arbitrarily on the vertical axis. It is observed that T_g shifts towards higher temperatures with the increase of frequency (19.23 K at 37 Hz and 19.34 K at 726 Hz). The value of $\chi(T_g)$ reduces for higher frequencies. The sharp peak of $\chi(T)$ at T_g for lower frequencies gradually becomes rounded with the increase of frequency. For temperatures below T_g the curves for different frequencies are separated and approach different non-zero frequency-dependent values as T $\rightarrow$ 0 as observed earlier[1]. In $Eu_{0.2}Sr_{0.8}S$ it was found that these curves converged to a non-zero frequency-independent value as T $\rightarrow$ 0. In the case of the SG Co-Ga, $\chi(T)$ smoothly approaches zero as T $\rightarrow$ 0 for a frequency range of 15 to 5000 Hz.

The variation of T_g with frequency can be described by either the Arrhenius law or the Fulcher law. Fitting our experimental data to the Arrhenius law, $\nu = \nu_0 \exp[-E_a/kT_g]$, we get an unphysical value of $\nu_0 (\approx 10^{30}$ Hz). The Arrhenius law is applicable for a system of non-interacting moments and thus it is not able to represent the SG properly. A better description of our data can be obtained by using the Fulcher law[2] of the form

$$\nu = \nu_0 \exp\left[-E_a/k(T_g - T_0)\right], \tag{5.1}$$

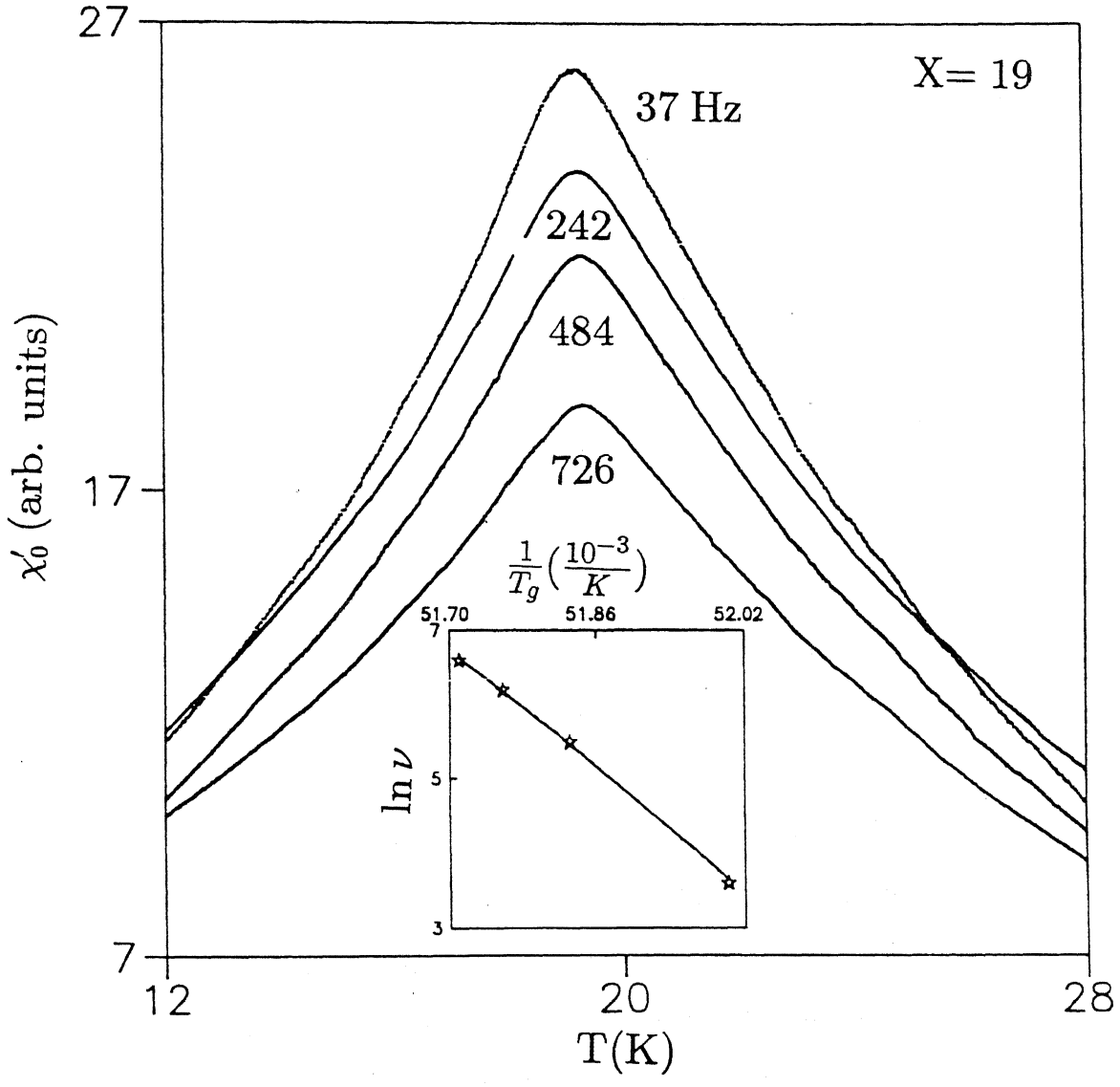

Figure 5.1: Temperature variation of the real part of the linear susceptibility (χ_0') of the SG(X=19) for different frequencies (ν). ν = 37, 242, 484, and 726 Hz from top to bottom, respectively. Curves are arbitrarily displaced on the vertical axis for clarity. The inset shows the variation of the inverse of T_g with $\ln \nu$. The two indistinguishable solid lines are the best fits to the Fulcher law for T_0 = 18.3 and 18.5 K, respectively.

where ν_0 is a characteristic frequency, E_a the activation energy, and T_0 a fitting parameter which formally represents a transition temperature to an equilibrium state and is related to an interaction energy of the system. The value of ν_0 is extremely sensitive to the choice of T_0. Fitting the data to Eq. (5.1) with T_0= 18.3 and 18.5 K yields widely different ν_0 with values of 7.8×10^{13} and 3.5×10^{11} Hz, respectively ($\chi^2 \simeq 4 \times 10^{-5}$). To show both the fits we plot $\ln \nu$ *vs* $1/T_g$ in the inset of Fig. 5.1. Since the values of χ^2 are of the same order, the curves are not distinguishable. The values of ν_0 and E_a/k (26.3 and 16.7 K for T_0= 18.3 and 18.5 K, respectively) are of the same order as found earlier in different SG systems[3]. However, much smaller values were observed in the Co-Ga SG. From the variation of T_g with frequency one can experimentally distinguish a SG from a superparamagnet where simply blocking of energy barriers occur. In case of the superparamagnet $[(Ho_2O_3)(B_2O_3)]$ the Arrhenius law holds good and the change of T_g is at least an order of magnitude larger than that of the SG. To observe any detectable change of $T_C(T_N)$ with frequency in FM (AF) the measuring frequency should be very high(mega or giga Hz).

The imaginary part of the susceptibility(χ_0'') is the Fourier transform of the two spin correlation function which characterizes the dynamics of the magnetic system. So it is expected that this should show an anomalous behaviour near magnetic phase transitions. Figure 5.2 shows the temperature variation of χ_0'' in this SG for different frequencies. These curves are also shifted along the vertical axis for clarity. On extrapolation to lower temperatures ($T \rightarrow 0$) it is found that χ_0'' for lower frequencies attains non-zero values which are $\approx 50\%$ of their maximum values. This percentage also increases with the increase in frequency. Similar behaviour was observed in $CuMn$ and $AgMn$ whereas in $Eu_{0.2}Sr_{0.8}S$, χ_0'' extrapolated to a nearly zero value as $T \rightarrow 0$. From Fig. 5.2 we also observe very distinct peaks in χ_0'' at temperatures just below T_g. The peaks show very small shifts towards higher temperatures with the increase of frequency. For temperatures greater than T_g, χ_0'', which is the absorptive part of the susceptibility, approaches a nearly zero value (note that the curves are shifted along the vertical axis) as T increases for all measuring frequencies.

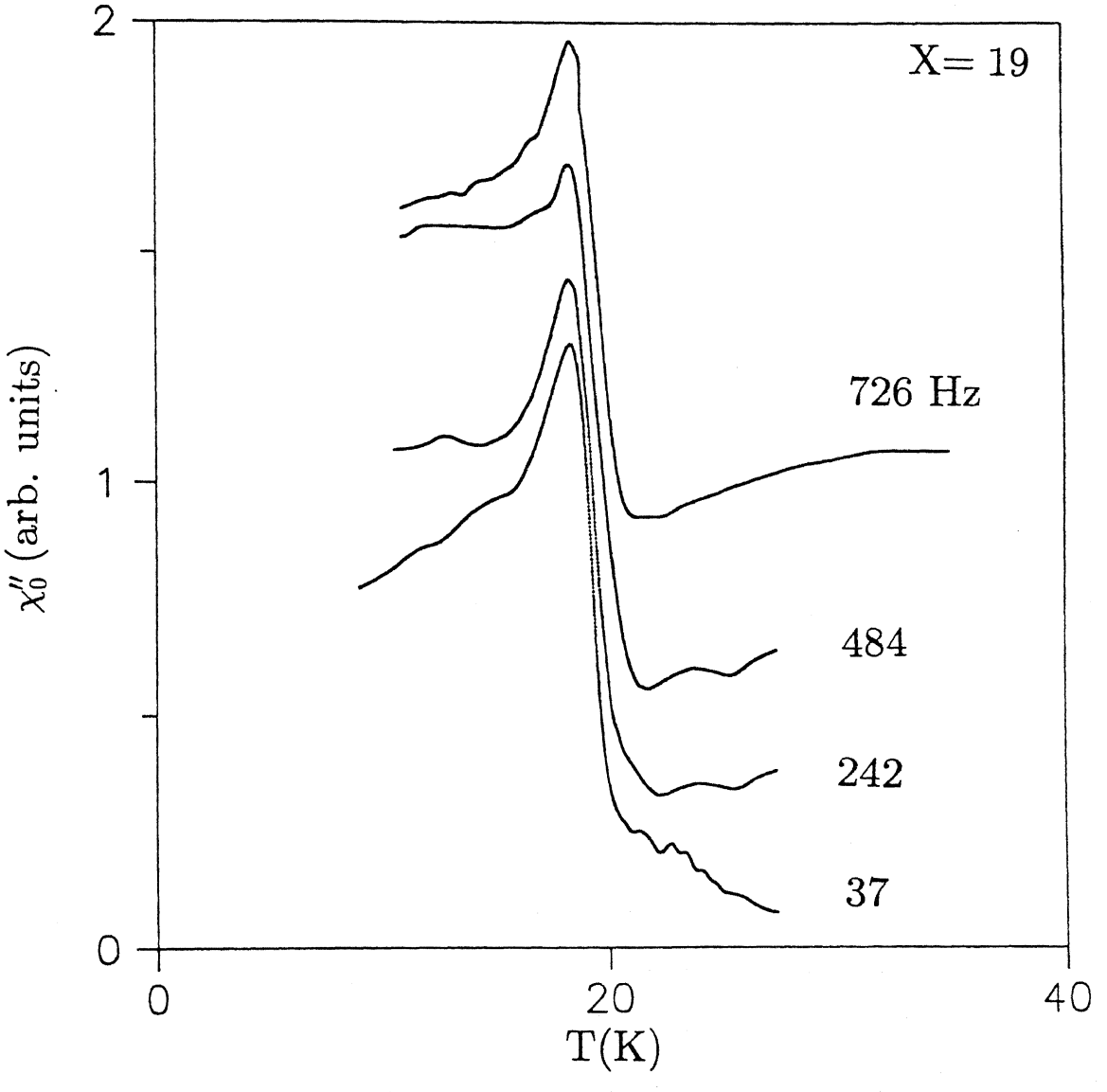

Figure 5.2: Temperature variation of the imaginary part of the linear susceptibility (χ_0'') of the SG(X=19) for different frequencies (ν). ν = 726, 484, 242, and 37 Hz from top to bottom, respectively. Curves are arbitrarily displaced on the vertical axis for clarity.

The effect of a dc biasing field on the SG transition is depicted in Fig. 5.3 where the temperature variation of the real part of the susceptibility (χ_0') is plotted for different dc biasing fields. The maxima of χ_0' are very sensitive to the external field. The value of $\chi_{0,max}'$ decreases and the peak position shifts towards lower temperatures with the increase of external field (inset of Fig. 5.3). Similar behaviour was found in most of the spin glasses but in $Eu_{0.4}Sr_{0.6}S$, $GdAl$, $FeMnPBAl$, and $CuMn$ it was found that the position of the peak initially shifted towards higher temperatures and then at somewhat higher fields, it showed a shift back towards lower temperatures[4]. An explanation for this behaviour was given in terms of a competition between the noncritical linear susceptibility and the critical non-linear susceptibility[5]. The above non-mean-field theory predicted scaling exponents and scaling functions which can explain both the above behaviours. However, a simple equilibrium mean-field theory, under certain conditions, can also explain such behaviour[6]. We should mention here that T_g, derived from dc magnetization (12K)[7], varies from that obtained in ac measurements. However, very small dc field measurements are needed for proper comparison. It was observed in several other SG's that T_g measured by different methods vary from one another[8].

We have measured the dc-field dependence of the imaginary part as well of the ac susceptibility (χ_0'') (Fig. 5.4). The magnitude of χ_0'' reduces and the peak moves towards lower temperatures with the increase of external dc field. The sharp peak in χ_0'' without a dc field vanishes in the presence of it. χ_0'' shows a rounded maximum at a temperature which is lower than T_g, obtained from the peak of χ_0' (Fig. 5.3). However, $d\chi_0''/dT$ shows a dip (inset of Fig. 5.4) at a temperature which coincides with that where χ_0' shows a peak corresponding to the same dc field of 80 Oe. We can understand the decrease of the ac susceptibility in the presence of external dc biasing fields in the framework of Néel's superparamagnetic model[9]. The external dc field defines the quantization axis of the spins and the ac field excites the spins. In order to respond to the ac field the spins or clusters of spins have to change their orientation continuously. In this process the spins interact with the lattice and give rise to a

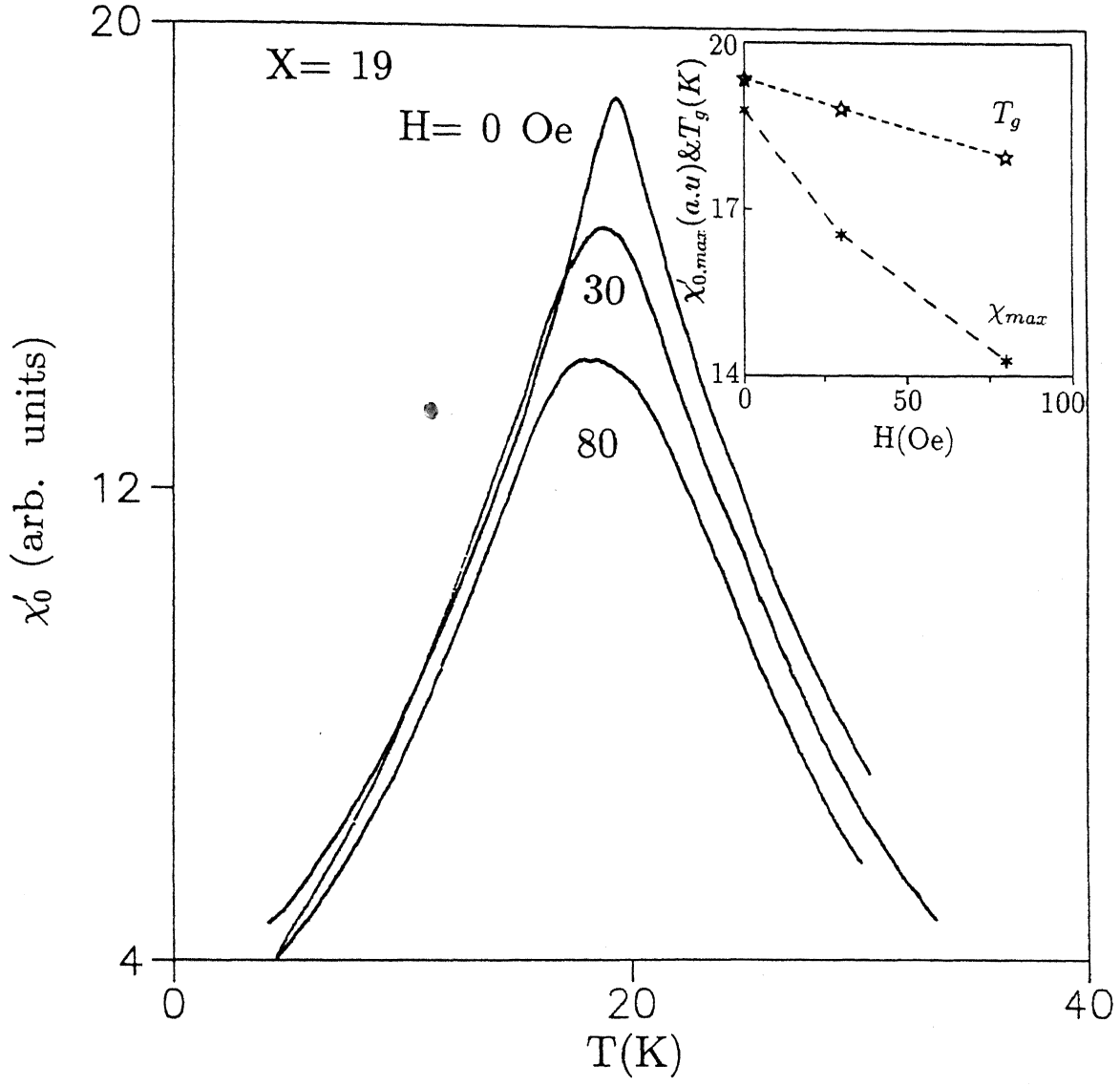

Figure 5.3: Temperature variation of the real part of the linear susceptibility (χ_0') of the SG(X=19) for different dc biasing fields (H). H = 0, 30, and 80 Oe from top to bottom, respectively. The inset shows the variation of the maximum value of χ_0' ($\chi_{0,max}'$) and the temperature at which maximum occurs (T_g) with dc biasing field, H.

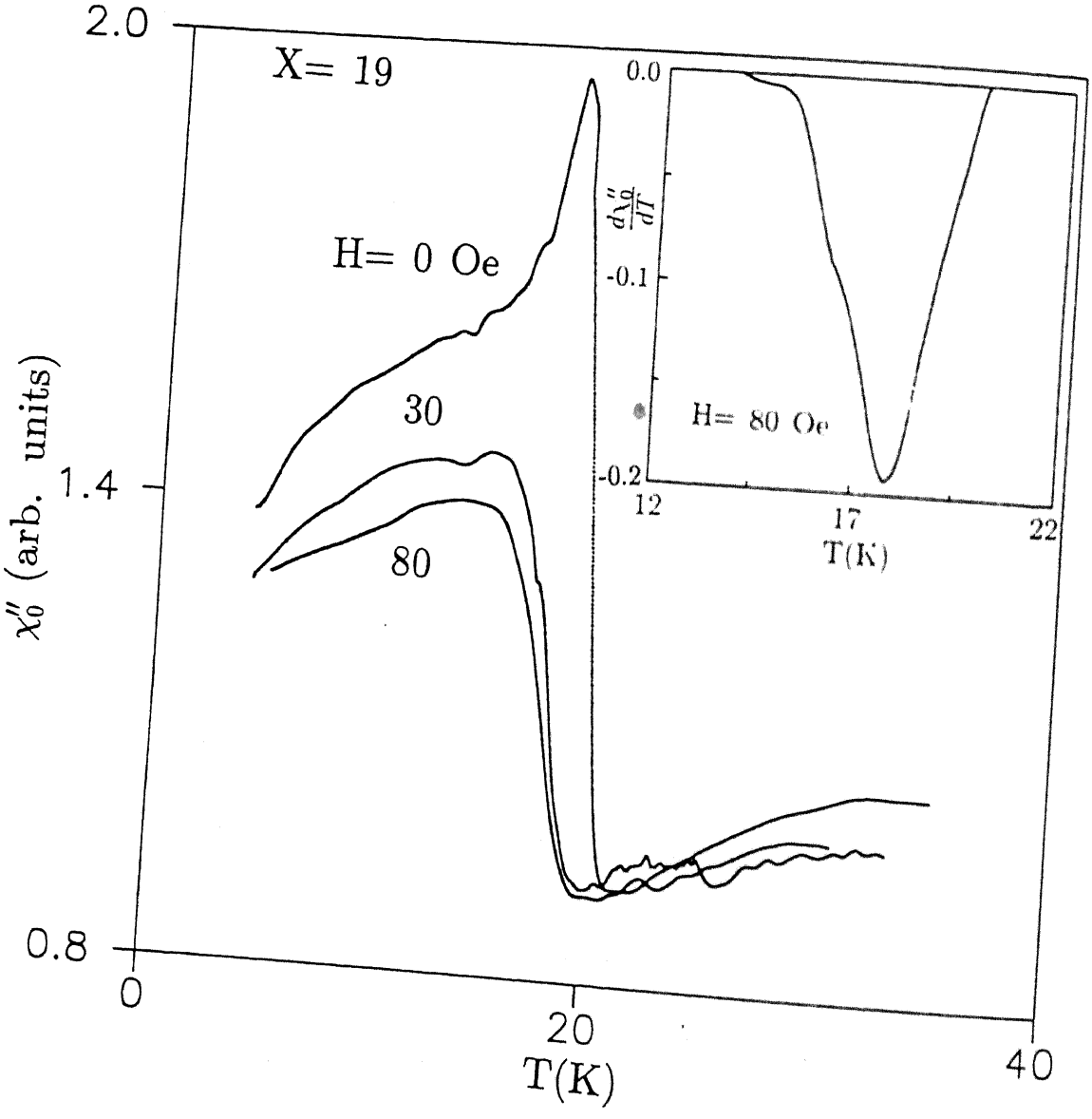

Figure 5.4: Temperature variation of the imaginary part of the linear susceptibility (χ_0'') of the SG(X=19) for different dc biasing fields(H). H = 0, 30, and 80 Oe from top to bottom, respectively. The inset shows the derivative of χ_0'' with respect to T for H=80 Oe. It shows a dip which coincides with the peak in χ_0' (H=80 Oe) as shown in Fig. 5.3.

characteristic relaxation time. This relaxation time depends upon the height of the potential barrier which is proportional to the external dc field. Application of a dc field parallel to the ac field increases the relaxation time. Hence those clusters having relaxation times greater than the time constant of the exciting ac field cease to contribute to the ac susceptibility, thus causing its reduction.

Studies of non-linear susceptibilities lead to a better understanding of phase transitions. Several theoretical models[10, 11] predict that the non-linear susceptibility, $\chi_2 = \partial^3 m/\partial h^3$, should diverge at T_g for an SG. In fact, this is one of the ways of accurately measuring T_g. If there is no spontaneous magnetization, as in case of a SG, the non-linear susceptibility, $\chi_1 = \partial^2 m/\partial h^2$, should not be present (Eq. (1.25)). Hence measurements of χ_1 and χ_2 will provide important information about the nature of the phase transition and the magnetic state. The temperature variations of χ_1 and χ_2 are measured in an ac field of 0.6 Oe at a fundamental frequency of 242 Hz($\omega/2\pi$). χ_1 and χ_2 are detected at frequencies 484 Hz ($2\omega/2\pi$) and 726 Hz ($3\omega/2\pi$), respectively (Fig. 5.5). Here we present the total susceptibility, the real and imaginary parts are not shown separately. χ_2 shows a very distinct peak at T_g (19.3 K) whereas χ_1 shows only diffuse background signals. The peak in χ_2 and the absence of χ_1 imply an SG transition and the absence of any spontaneous magnetization at lower temperatures. Earlier we had measured the time-dependent magnetization in the SG (X=19) which revealed a stretched exponential relaxation[12]. Hence the sample with X=19 shows all the features of an SG, viz., slow relaxation, frequency and field-dependent susceptibility, and peak in the odd harmonics of the susceptibility.

5.1.2 Reentrant spin glass (X= 26 and 23)

The samples with X=26 and 23 show sequential magnetic phase transitions, PM $\rightarrow$ FM $\rightarrow$ RSG with decreasing temperature. Such sequential phase transitions are clearly seen from the ac susceptibility measurements (Fig. 5.6 for X=26) at a frequency of 242 Hz and 0.6 Oe ac field. As we reduce the temperature, the ac susceptibility increases very sharply around

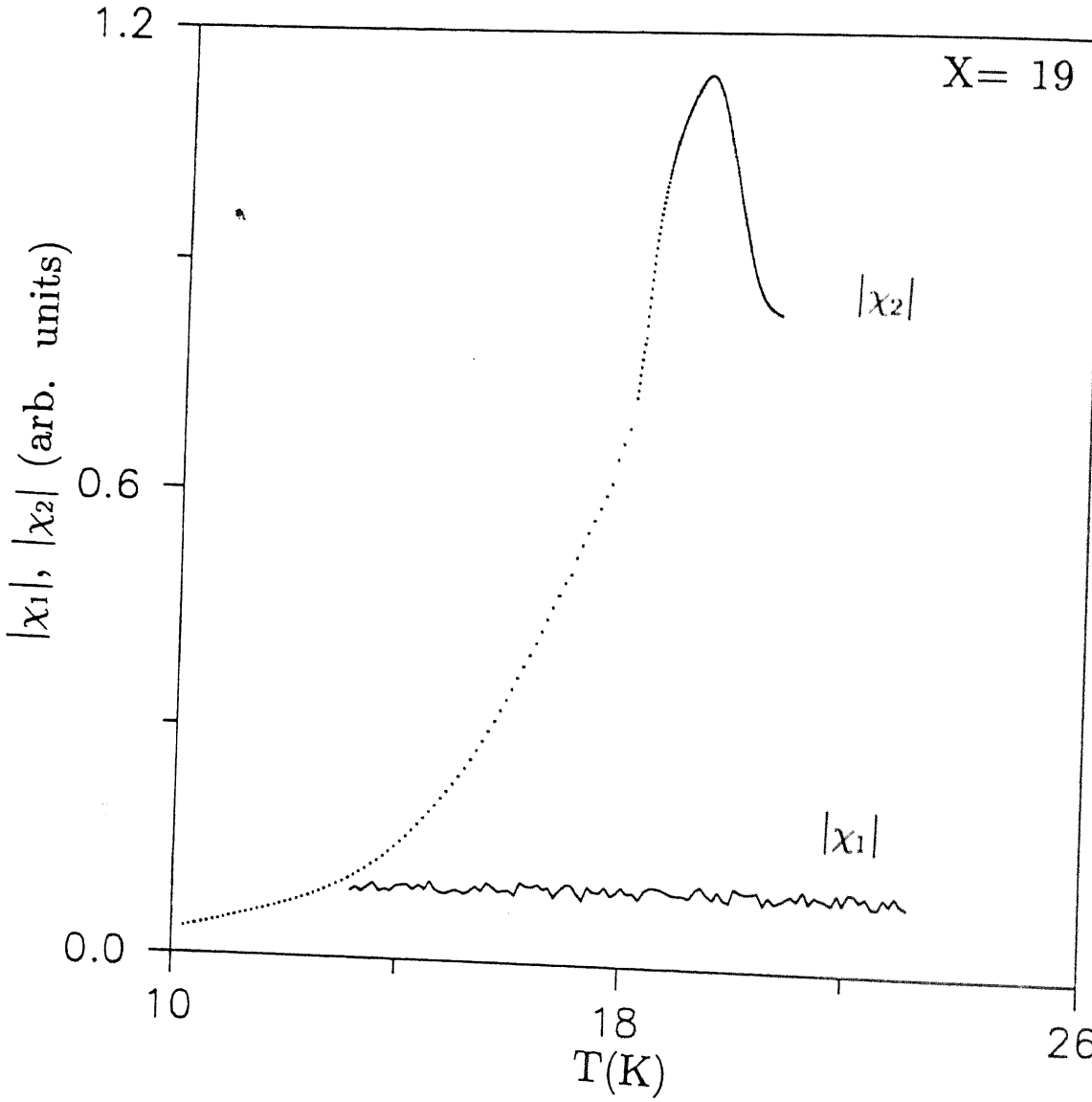

Figure 5.5: Temperature variation of the non-linear susceptibilities, $\chi_1 = \frac{\partial^2 m}{\partial h^2}$ and $\chi_2 = \frac{\partial^3 m}{\partial h^3}$, of the SG(X=19) measured in a 0.6 Oe ac field.

70 K indicating a PM → FM phase transition. However, it is difficult to determine the exact value of T_C from this curve. For this purpose as well as to understand the nature of the phase transition we derive the critical exponent (γ) using the Kouvel-Fisher(KF) analytical method[13]. KF plots have several advantages; the most important one is that T_C and γ can be determined simultaneously without any prior knowledge of T_C. Since the value of γ is extremely sensitive to the choice of T_C, its exact determination is very important. According to KF, the zero-field ac susceptibility(χ_0) near T_C varies as

$$Y = \left[\frac{d}{dT}(\ln \chi_0^{-1})\right]^{-1} = \frac{T - T_C}{\gamma}. \tag{5.2}$$

In Fig. 5.6 we have also plotted Y vs T. The inverse slope and the intercept on the T- axis give $\gamma = 0.90 \pm 0.02$ and $T_C = (68.89 \pm 0.04)$ K.

We also know that the temperature variation of the zero field susceptibility (χ_0) just above T_C can be expressed by a power law, $\chi_0 \propto (\frac{T-T_C}{T_C})^{-\gamma}$. By using the above value of T_C and plotting $\log \chi_0$ *vs* $\log(\frac{T-T_C}{T_C})$ (inset of Fig. 5.6) we get the value of γ as 0.94, which is quite close to its value obtained from the KF method. Using $T_C = 68.89$ K and plotting(not shown) $\log \chi_0$ *vs* $\log(\frac{T-T_C}{T_C})$ from a second set of $\chi_0(T)$ data at 726 Hz in a 1.5 Oe field, we get a value of γ= 0.91. Hence we find that in our limited frequency and ac field ranges, γ does not vary significantly and is quite close to the mean-field value of 1. However, in typical PM to FM transitions, γ is found to be greater than 1 and close to the 3D-Heisenberg prediction of 1.38. In Table 5.1 we present the values of γ predicted by different theories and observed experimentally in some FM's and RSG's.

On lowering the temperature below T_C (Fig. 5.6), χ_0 follows a weakly temperature-dependent plateau in the FM regime and then it decreases very sharply around T_g. This brings the system into a new phase known as the RSG, where FM and SG-like orderings coexist. The value of χ_0 approaches a temperature-independent non-zero value as T → 0. The imaginary part of the susceptibility (χ_0'') characterizes the dynamics of a magnetic system and should show anomaly near magnetic phase transitions. We observe very distinct peaks

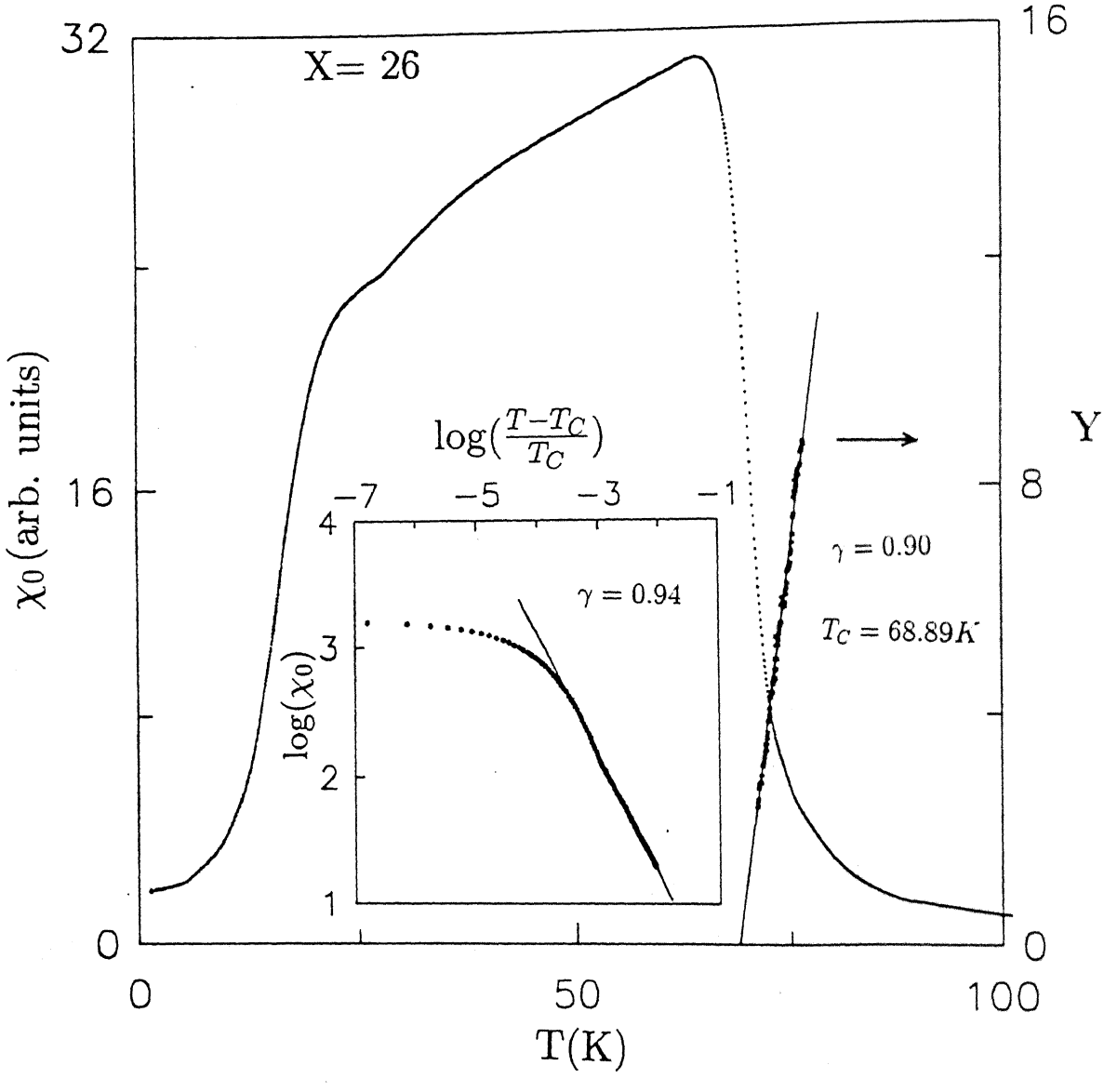

Figure 5.6: Temperature dependence of the linear susceptibility, χ_0, and $Y = [\frac{d}{dT}(\ln \chi_0^{-1})]^{-1}$ of the RSG (X=26) measured at $h_0 = 0.6$ Oe and at 242 Hz. The straight line is the best fit of the data to Eq. (5.2). The inverse slope and its intercept on the temperature axis, give γ and T_C, respectively. The inset shows the double logarithmic plot of χ_0 versus the reduced temperature, $\frac{T-T_C}{T_C}$, above T_C. The slope of the straight line again gives γ.

in $\chi_0''(H_{dc} = 0)$ at T_C and T_g indicating PM to FM and FM to RSG transitions, respectively (Fig. 5.7). The value of χ_0'' start falling very sharply around 68.5 K which coincides with the T_C obtained from the KF plot. In the PM regime ($T > T_C$), the absorptive part χ_0'' approaches zero with increasing temperature. We observed a similar behaviour in the SG(X=19). We find a small hump below T_C around 61.5 K but its origin is not clear. On further decreasing the temperature χ_0'' shows a very sharp peak at 16.68 K indicating an FM to RSG transition. At the lowest temperature χ_0'' approaches a small non-zero value in contrast to the case of the SG(X=19) where χ_0'' approaches a value which is $\approx$ 50% of its peak value.

χ_0'' is very sensitive to the external dc field. With the application of a small dc field of 20 Oe, a dramatic change is observed (Fig. 5.7). The peak near T_C vanishes. However, a dip is observed at 58.2 K. This dip occurs around the temperature where we observe a hump in χ_0'' without any dc field. Around T_g, the peak value of χ_0'' reduces and the peak shifts towards higher temperatures (16.72 K for 20 Oe field), whereas in the SG (X=19) we observe a shift towards lower temperatures with fields(Fig. 5.4). On further increase of the dc field (40 Oe) the sharpness and the amplitude of the peak at 16.94 K reduce. At higher temperatures (T > 25 K) χ_0'' approaches a small value which is independent of temperature. The low-temperature peak, at 17.35 K, becomes more rounded and reduced with further increase of the dc field till 65 Oe. Thus we observe in the RSG (X=26) that the external dc field reduces the peak value of χ_0'' near T_g and shifts it towards higher temperatures. The variations of the peak amplitude and the peak temperature (defined as T_g) with dc field are shown in Fig. 5.8. In contrast, for the SG (X=19) χ_0'' shows rather broad maxima instead of peaks, which move towards lower temperature with the application of dc fields(Fig. 5.4).

It should be mentioned here that from our earlier dc measurements(50 Oe field) we found T_C and T_g as 56 and 7 K, respectively[7]. So there is a marked difference between the transition temperatures obtained from low-field ac and comparatively high-field dc measurements. However, the low-field ac susceptibility method is, in principle, a more reliable

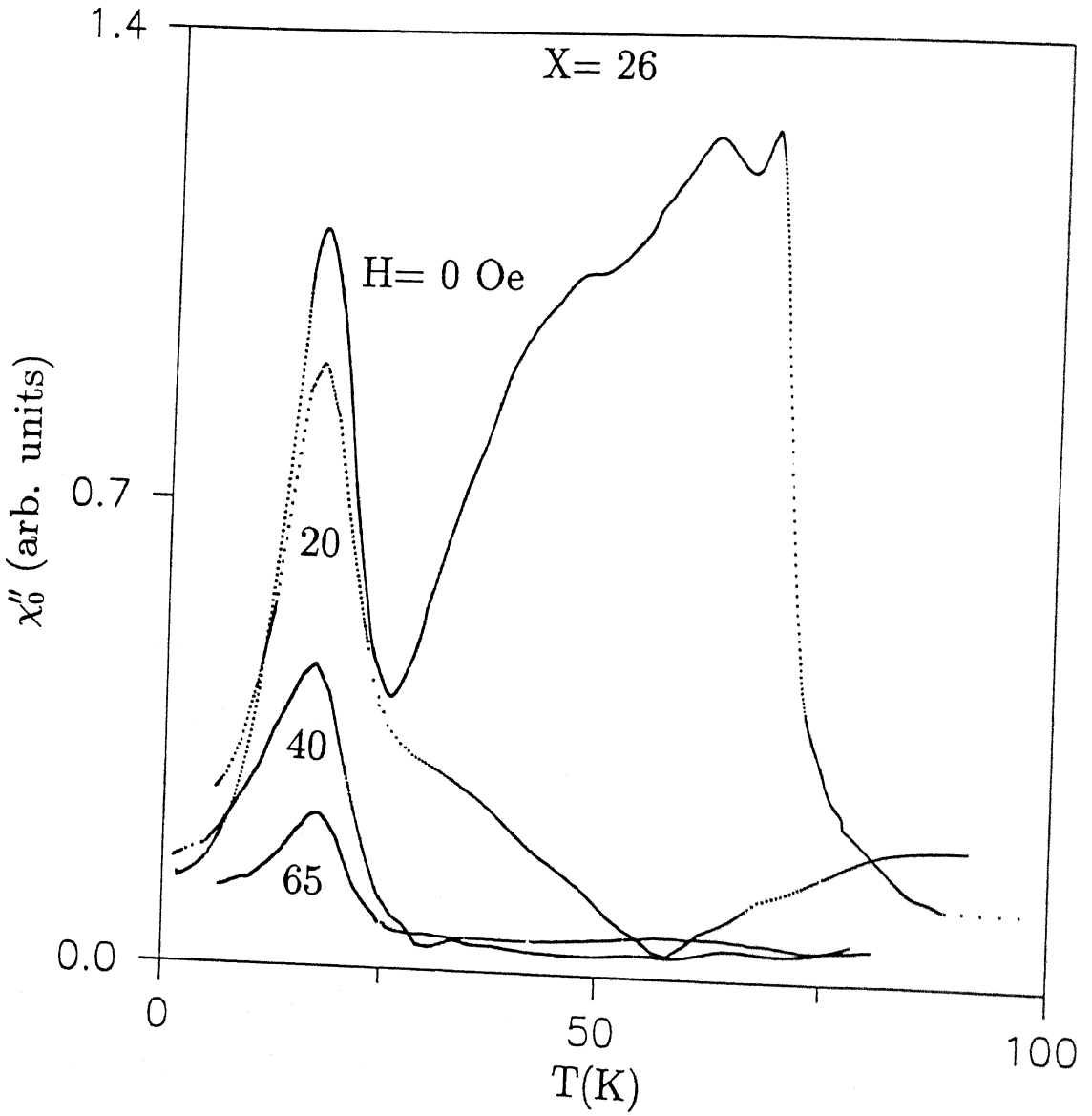

Figure 5.7: Temperature variation of the imaginary part of the linear susceptibility (χ_0'') of the RSG(X=26) for different dc biasing fields (H) measured at $h_0 = 0.6$ Oe and at 242 Hz. H = 0, 20, 40 and 65 Oe from top to bottom, respectively.

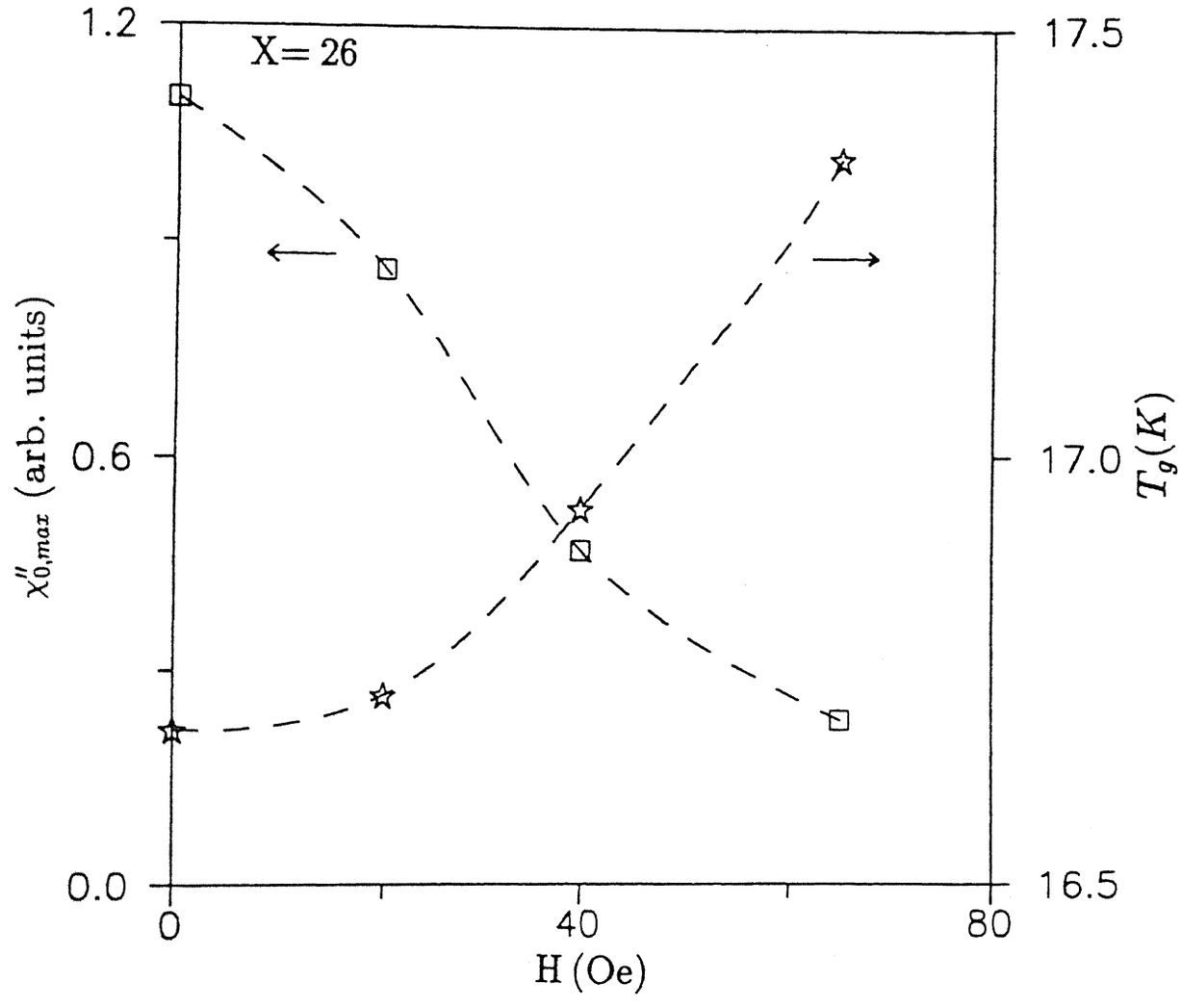

Figure 5.8: DC biasing field dependences of the maximum value of χ''_0 ($\chi''_{0,max}$) and the temperature at which the maximum occurs (T_g).

one for getting transition temperatures. When we superpose external dc fields on the small ac field, we observe that χ_0'' shows an anomaly near 58 K which is somewhat closer to the earlier findings of T_C at 56 K. To the best of our knowledge this is the first report where such interesting features in χ_0'' around T_C are observed.

Figure 5.9 depicts the temperature variation of the linear susceptibility (χ_0) in external dc fields and measured at 242 Hz and 0.6 Oe ac field. The zero dc field susceptibility shows a principal maximum near T_C, known as Hopkinson peak[14]. In many FM systems, static biasing fields suppress the amplitude of Hopkinson maxima which shift towards lower temperatures and also give rise to secondary peaks at higher temperatures. This is exactly what we find in Fig. 5.9. The usual static scaling laws, $\chi(h,t) = t^{-\gamma}F(\frac{h}{t^{\gamma+\beta}}) = h^{1-\frac{1}{\delta}}G(\frac{h}{t^{\gamma+\beta}})$, where $h \propto \frac{H}{T_C}$ *and* $t = \frac{T-T_C}{T_C}$, predict such peaks at higher temperatures with a field-dependent amplitude[14]. The variation of χ_0 can be expressed as a power law in H

$$\chi_0(H, T_m) \propto H^{\frac{1}{\delta}-1}, \tag{5.3}$$

where T_m is the temperature where the secondary peak occurs. We have also made additional measurements for different dc biasing fields around T_C which are not shown in Fig. 5.9. From these measurements and Fig. 5.9 we find the height of the secondary peaks ($\chi_0(H, T_m)$) for different fields. By plotting $\log \chi_0(H, T_m)$ *vs* $\log H$ we get the value of δ as 4.7 ± 0.4 (Fig. 5.10) which is greater than the value predicted by the mean-field theory ($\delta = 3$) and those found experimentally[15, 14].

The other critical exponent β can also be derived from a prior knowledge of γ and using the power law, $t_m = \frac{T_m - T_C}{T_C} \propto H^{(\gamma+\beta)^{-1}}$[21]. We can rewrite this as

$$T_m = K_1 H^n + T_C\,, \tag{5.4}$$

where K_1 is a constant and $n = (\gamma + \beta)^{-1}$. By varying the power of H, i.e., n, we find that for $n = 0.83$ the above equation gives an excellent straight line. In Fig. 5.10 we plot T_m *vs* $H^{0.83}$ and from the best fit ($\chi^2 = 1.37 \times 10^{-7}$) the coefficient of H^n and T_C are obtained as (0.245 ± 0.001) and (64.94 ± 0.01) K, respectively. Using the value of γ as 0.92 (average

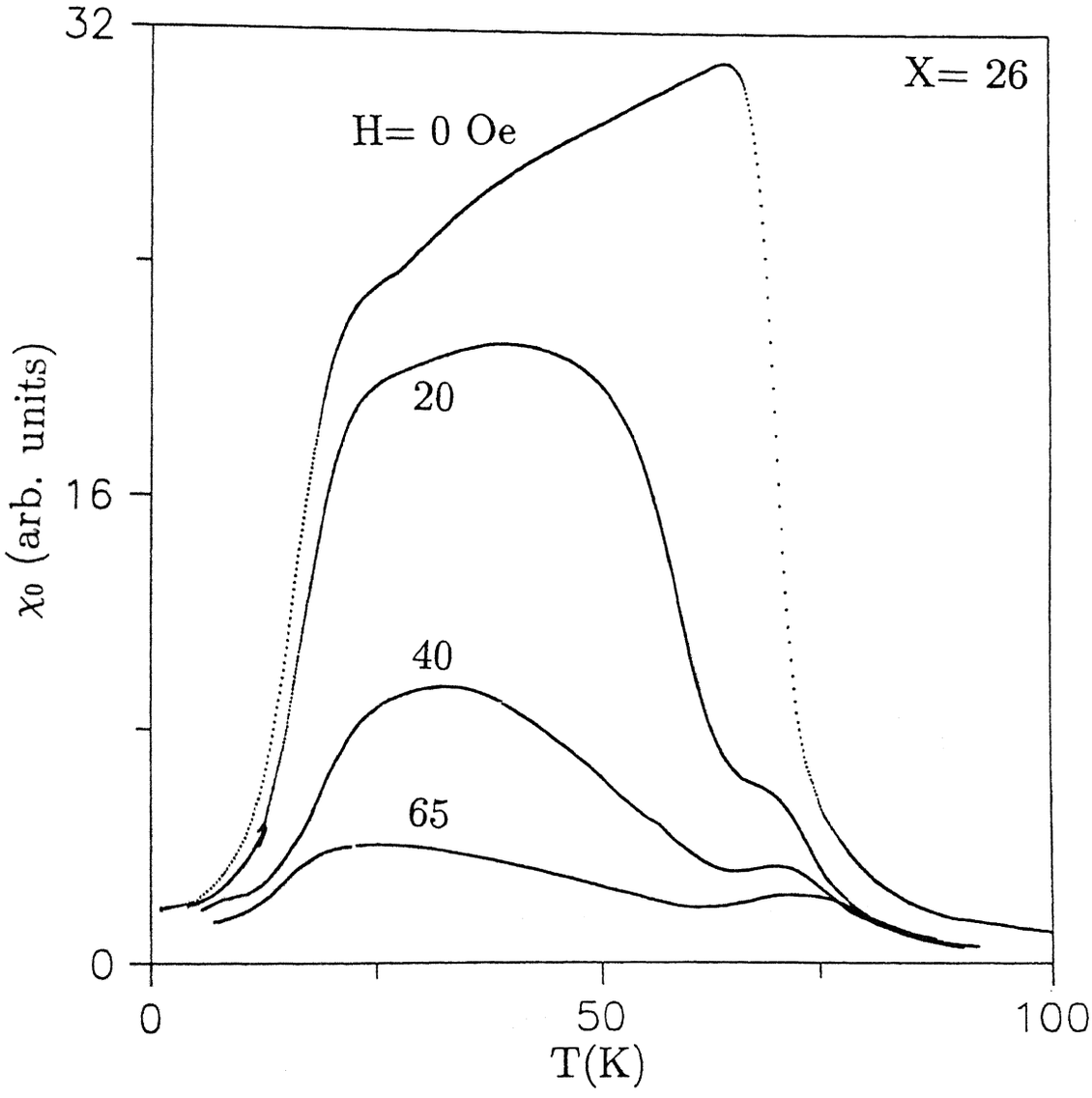

Figure 5.9: Temperature variation of the linear susceptibility (χ_0) for different dc biasing fields (H) of the RSG(X=26) measured at $h_0 = 0.6$ Oe and at 242 Hz. H = 0, 20, 40, and 65 Oe from top to bottom, respectively. χ_0 shows a secondary peak around T_C in the presence of H.

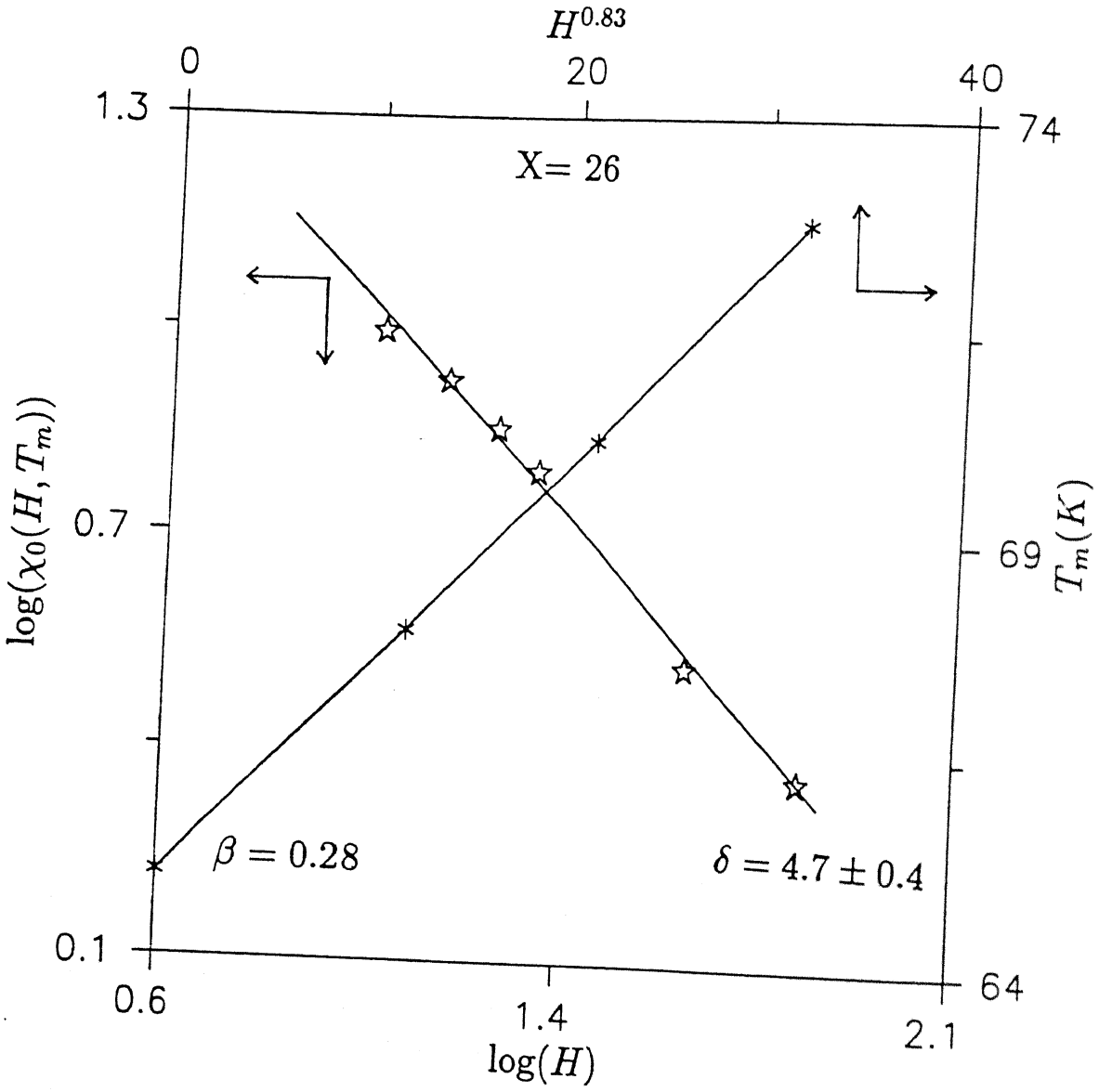

Figure 5.10: The value of the susceptibility at the secondary peak ($\chi_0(H, T_m)$) plotted against dc biasing field (H) on a double logarithmic plot of the RSG(X=26). The best-fitted straight line gives δ. The temperature at which the secondary peak occurs (T_m) is plotted against H^n. The data show an excellent fit to a straight line when n= 0.83. β is found using the relation $n = (\gamma + \beta)^{-1}$.

Table 5.1: Values of the critical exponents obtained from theories and experiments in some FM's and RSG's.

Theory/ Material	β	γ	δ	Reference
Mean field theory	1/2	1	3	D. J. Amit[16]
Ising model (d=2)	1/8	7/4	-	,,
Ising model (d=3)	0.31	1.25	-	,,
Heisenberg model (d=3)	0.36	1.38	4.8	,,
$(Pd_{99.66}Fe_{0.34})_{95}Mn_5$	-	1.8 ± 0.2	-	Sato et al.[17]
$Au_{82}Fe_{18}$	-	1.33 ± 0.05	-	Bitoh et al.[18]
$(Pd_{99.65}Fe_{0.35})_{95}Mn_5$	0.53 ± 0.08	1.64 ± 0.07	4.1 ± 0.1	Kunkel et al.[21]
$Pd_{0.930}Fe_{0.015}Mn_{0.055}$	0.464	1.4	-	Sato et al.[19]
$Au_{82}Fe_{18}$	0.46 ± 0.03	1.13 ± 0.06	4.0 ± 0.1	Gangopadhyay et al.[20]
$Fe_{85}Mn_5Zr_{10}$	0.39 ± 0.02	1.63 ± 0.05	5.3 ± 0.1	Nicolaides et al.[22]
X=23	-	0.72	-	Present work
X=26	0.28	0.92 ± 0.02	4.7 ± 0.4	Present work
X=30	-	1.06 ± 0.01	-	Present work

value), β comes out to be 0.28 which is less than the mean-field prediction(β =0.5). Here we get a value of T_C (64.94 K) which is less than the measured T_C (68.89 K). The reason for this discrepancy is not clear. The maximum of the zero dc-field susceptibility occurs at a temperature which is less than T_C and we have used the position of this maximum in the above calculation. This may be one of the reasons for the discrepancy. From the scaling law we know that the critical exponents, δ, β, and γ are related by the equation $\gamma = \beta(\delta - 1)$. If we use the values of β and γ as 0.28 and 0.92, respectively, then δ comes out to be 4.3 ± 0.2 instead of 4.7 ± 0.4 (Fig. 5.10). So the scaling laws of the mean-field theory are valid within the limits of our experimental error. However, the individual value of the exponents are at variance with the theoretical prediction ($\beta = 0.5, \gamma = 1.0, \delta = 3.0$). Similar results were also found by Kunkel et al.[21] and Nicolaides et al.[22] [Table 5.1].

We have not seen any well-defined structure in χ_0 near T_g for various dc biasing fields. However, χ_0 shows a very sharp fall around T_g and its(χ_0) value is suppressed in the presence of biasing fields. We tried to compare(Fig. 5.9) the shift of the sharp fall of χ_0 with temperature in the presence of different biasing fields with theoretical models. If we assume that the temperature where χ_0 starts falling very sharply is the possible location of the GT (or AT) phase boundary, then we find $\tau = \frac{T_G(H=0)-T_G(H)}{T_G(H=0)} = C\, h^{1.24}$, where $h = \frac{g\mu_B H}{kT_G(H=0)}$ and $C = 0.043$. So we find that τ varies with H faster than expected from the AT line(2/3) and slower than expected from the GT line(2) and the prefactor is also less than the predicted values (C= $(\frac{3}{4})^{1/3}$ and 0.23(m=3) for AT and GT lines, respectively).

To summarize, for the RSG(X=26) the linear ac susceptibility and its dc field dependence give T_C and the critical exponents for the PM to FM transition. The values of the exponents are different from those of typical FM's. However, they are related through the scaling relation. We also observe SG-like behaviour at lower temperatures. Now the important question arises - is there any difference between the SG and the RSG ? We claim that the FM ordering persists in the RSG down to the lowest temperature. To what extent is this true?

To answer such subtle and debatable questions we need to probe into the non-linear susceptibilities. If FM ordering exists in the RSG then it must be reflected in the non-linear susceptibility $\chi_1(\partial^2 m/\partial h^2)$. In fact, we indeed observe a broad but distinct peak around T_g in χ_1 along with a very sharp peak at T_C (Fig. 5.11). The peak near T_g arises because of the breaking of time reversal symmetry of m (spontaneous magnetization) with respect to the applied field. This peak indicates FM ordering and is never observed in any SG including X=19. We believe that the occurrence of this peak near T_g is an intrinsic feature of the RSG and can be regarded as one of the criteria for identifying the RSG phase. Several other investigators also found the existence of FM ordering down to the lowest temperature in NiMn, $(NiFe)_{25}Au_{75}$, and AuFe[23]. Senoussi et al.[24] observed the existence of a well-defined *macroscopic* domain structure well below T_g in $Ni_{81}Mn_{19}$. They also observed similar domain structure and the associated magnetic properties in the FM and the RSG phases. However, a faster time response of these domains was found in the FM while in the RSG it was considerably slower. On the other hand Aeppli et al.[25] found no evidence for the coexistence of FM order with freezing of the transverse spin components, as predicted by the GT model, in the EuSrS and FeMnPBAl systems from neutron scattering studies.

The effect of a dc biasing field on χ_1 also shows interesting features. Application of a small dc field (5 Oe) increases the value of χ_1 significantly (Fig. 5.11) compared to the zero dc-field value and shows double transitions. The peak near T_C shifts towards lower temperatures, its magnitude reduces and it becomes rounded with the increase of dc field from 5 to 20 Oe, whereas the amplitude of the peak near T_g increases and it broadens with field. In Eq. (1.24), instead of putting $h = h_0\, cos\omega t$, if we use $h = H + h_0\, cos\omega t$, then the non-linear susceptibility can be written as

$$\chi_1^t h_0 = \chi_1 h_0 + 3\chi_2 H h_0 + \chi_3(6H^2 + h_0^2)h_0 + ... , \tag{5.5}$$

instead of Eq. (2.2). Hence, in the presence of an external dc field(H), higher order terms also contribute to χ_1^t. This may be one of the reasons for the above enhancement.

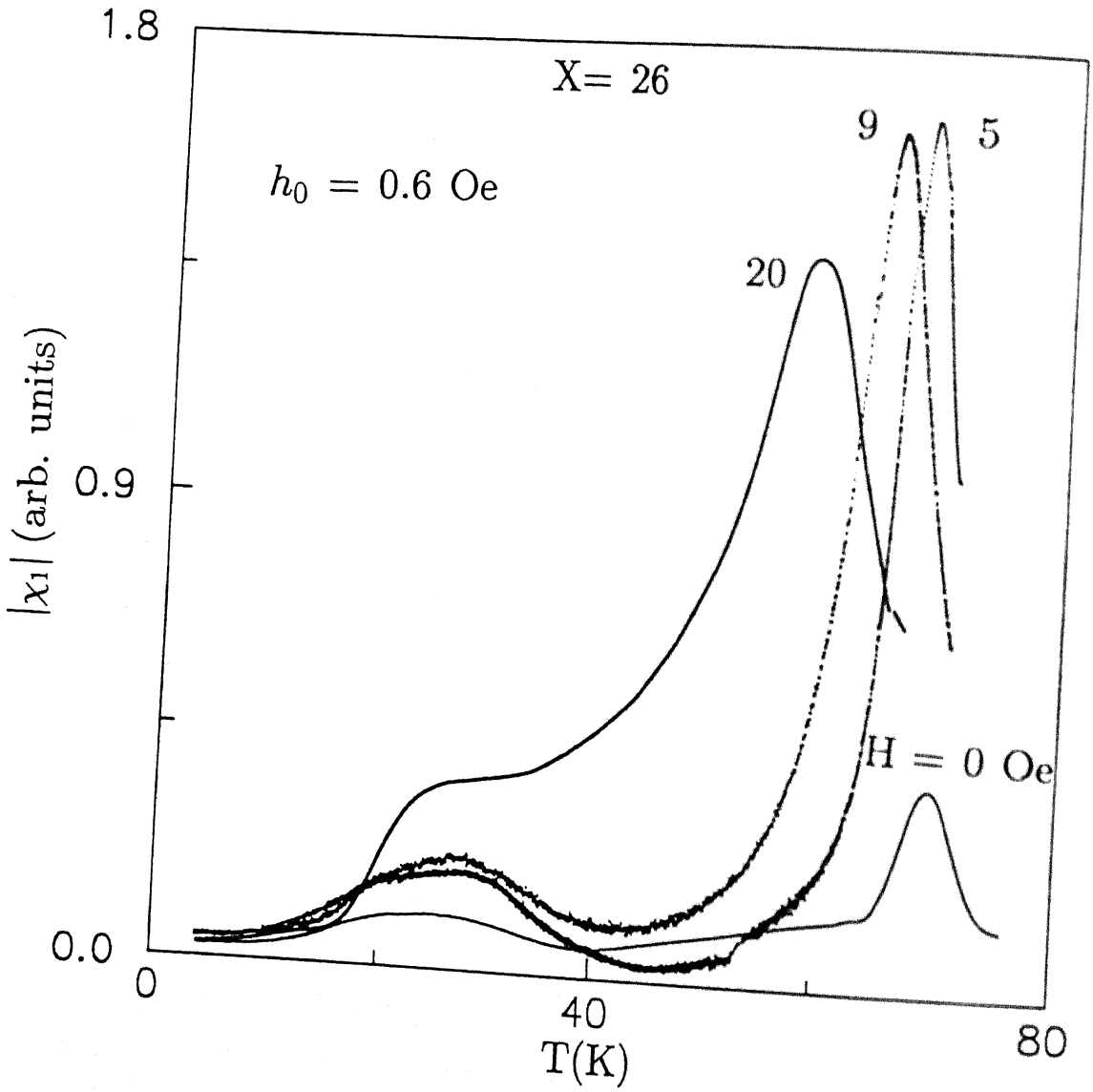

Figure 5.11: Temperature variation of the non-linear susceptibility, $\chi_1 = \frac{\partial^2 m}{\partial h^2}$ of the RSG (X = 26) for zero and different dc biasing fields (H= 5, 9, and 20 Oe).

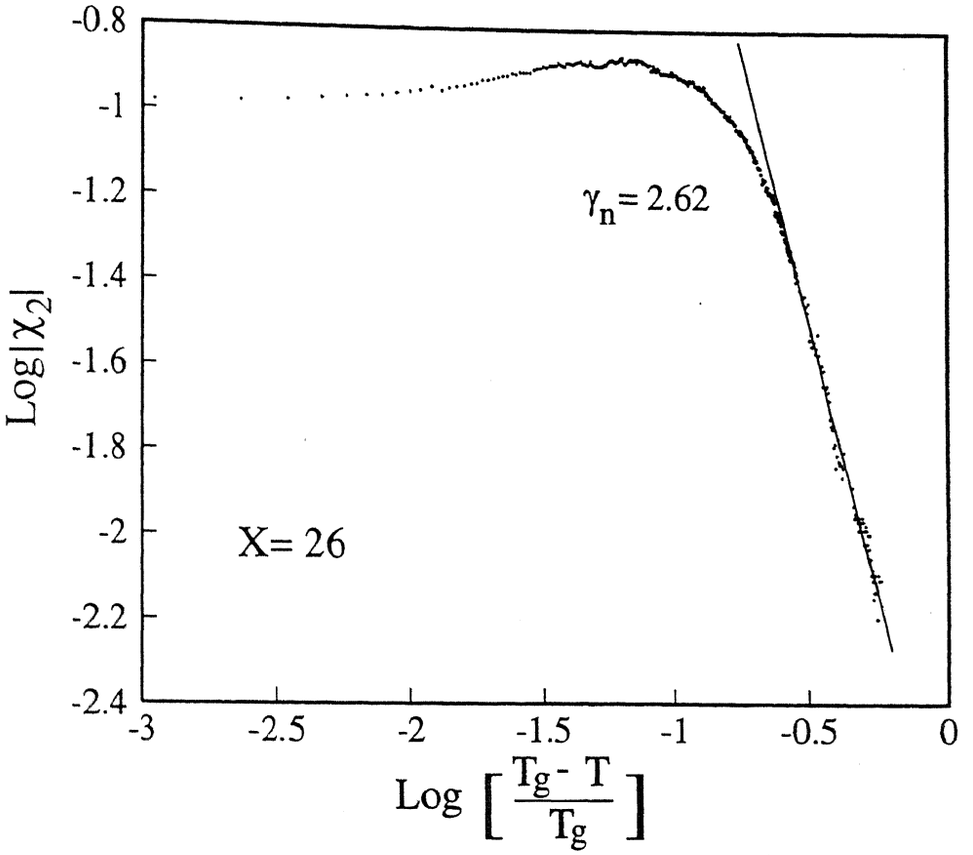

Figure 5.12: Double logarithmic plot of the non-linear susceptibility, $|\chi_2|$, versus the reduced temperature, $\frac{T_g-T}{T_g}$, below T_g for X= 26. The slope of the straight line gives $\gamma_n = 2.62 \pm 0.03$.

In the case of PM to SG transition it was predicted that χ_2 should follow a power law behaviour near T_g and the value of the exponent γ_n could have a wide variation(1 - 3.6) depending on the system and temperature[10, 5, 26]. In the case of RSG, the system goes from the FM to the SG phase with the reduction of temperature. Hence in our case we fit χ_2 to $(\frac{T_g-T}{T_g})^{-\gamma_n}$ instead of $(\frac{T-T_g}{T_g})^{-\gamma_n}$ [Fig. 5.12] for temperature less than T_g as in the FM region the power law is not valid. We get γ_n= 2.62 $\pm$ 0.03 which is, however, less than those observed by others[5, 21]. We also find that γ_n does not vary with the biasing field up to 20 Oe.

The sample with X=23 is also known to be an RSG[7]. It undergoes similar kinds of phase transitions as those of sample X=26. We have plotted the temperature variation of

the real (χ_0')[Fig. 5.13] and imaginary (χ_0'')[Fig. 5.14] parts of the linear susceptibility and their dc field dependence measured at 37 Hz and 0.6 Oe ac field. The variation of χ_0' does not show any double transition. Here the two transition temperatures, T_C and T_g, are not substantially separated. Hence, the intervening weakly temperature-dependent plateau is not seen here, unlike the other RSG sample with X=26. χ_0' shows a broad maximum around 28 K. However, the double transition is quite clear from the temperature variation of χ_0'' (Fig. 5.14). It shows a very sharp peak at T_g (23.5 K) indicating an RSG to FM transition. On further increase of temperature it shows a broad peak at 35 K, where the system enters the PM phase. In the case of the sample X=26, the fall in χ_0'' near T_C is very sharp, unlike in X=23. For example, an increase of temperature by 3 K near T_C changes χ_0'' by 55% for X=26 and by only 7% for X=23. This may be an indication that the upper transition is a gradual one in comparison with X=26. We plot $\log\chi_0$ against $\log(\frac{T-T_C}{T_C})$, with T_C=35 K for calculating γ from the slope (inset of Fig. 5.13, curve a) which changes gradually with temperature. So, instead of calculating some average γ we plot γ vs the reduced temperature (inset of Fig. 5.13, curve b). The value of γ becomes unusually small (0.15) very near T_C and then it starts increasing slowly with the increase of temperature and ultimately saturates at a value of 0.72. The value of γ is considerably smaller compared to that of other FM's and the sample with X=26.

The value of χ_0' reduces and the maximum broadens with the increase of the dc biasing field(Fig. 5.13). Only at 50 Oe dc field χ_0' does show a second maximum at a higher temperature (36 K). In the case of X=26 we observed the second maximum for an external dc field as small as 20 Oe. The position of the principal maximum shows a shift towards lower temperatures with the increase in the dc field, similar to that observed in X=26.

The dc field dependence of χ_0'' of X= 23 shows some striking features (Fig. 5.14). We observe that at lower temperatures χ_0'' approaches a small value which is independent of the external dc field (upto 50 Oe). It shows near T_g distinct peaks whose amplitude and sharpness reduce with the dc field. The position of the peak in χ_0'' near T_g shifts to lower

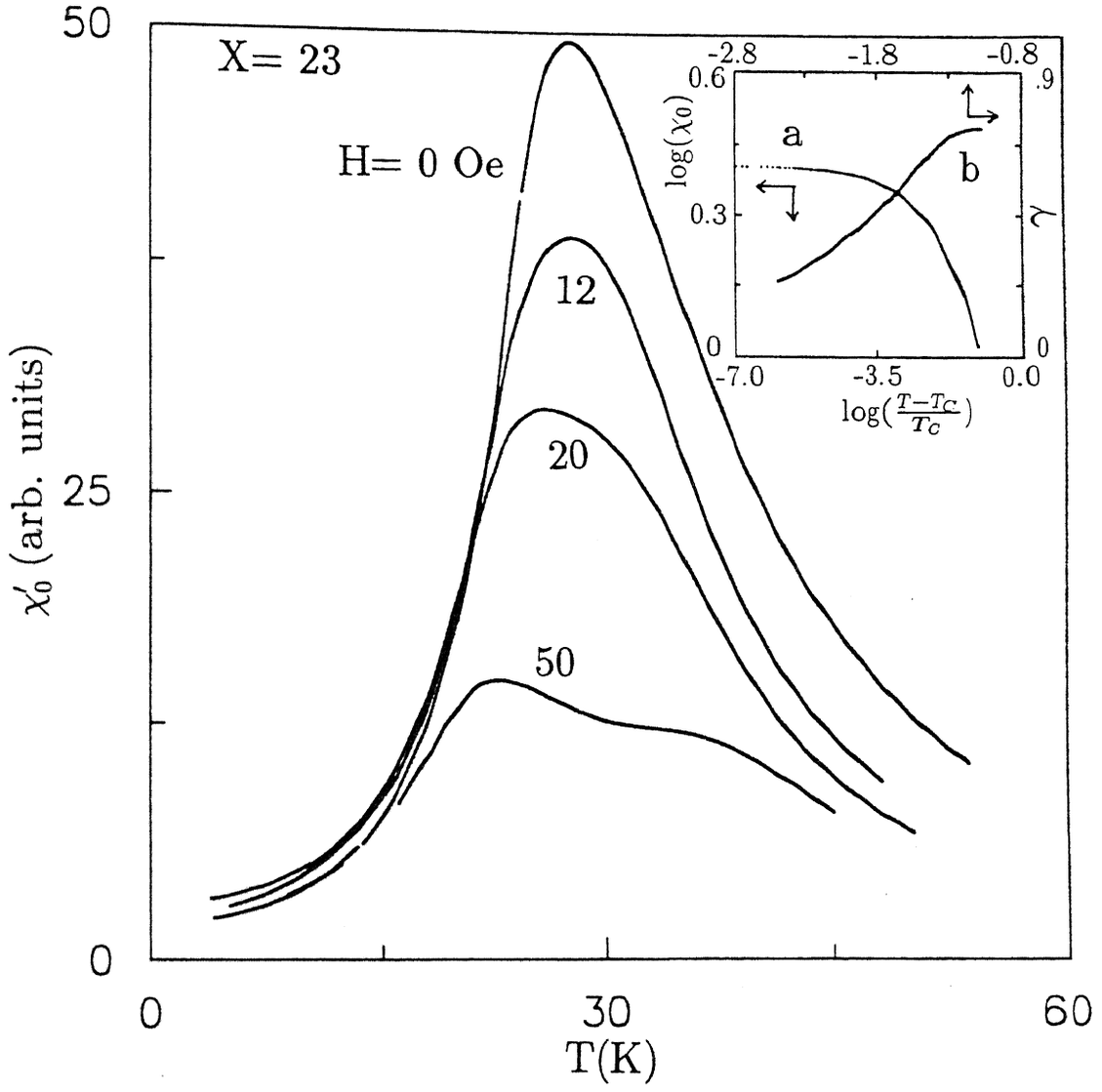

Figure 5.13: Temperature variation of the real part of the linear susceptibility (χ_0') of the RSG(X=23) for different dc biasing fields(H) measured at $h_0 = 0.6$ Oe and at 242 Hz. H = 0, 12, 20, and 50 Oe from top to bottom, respectively. The inset shows the double logarithmic plots of χ_0 and the critical exponent, γ, vs the reduced temperature, $\frac{T-T_C}{T_C}$ ($T_C = 35$ K), for $T > T_C$.

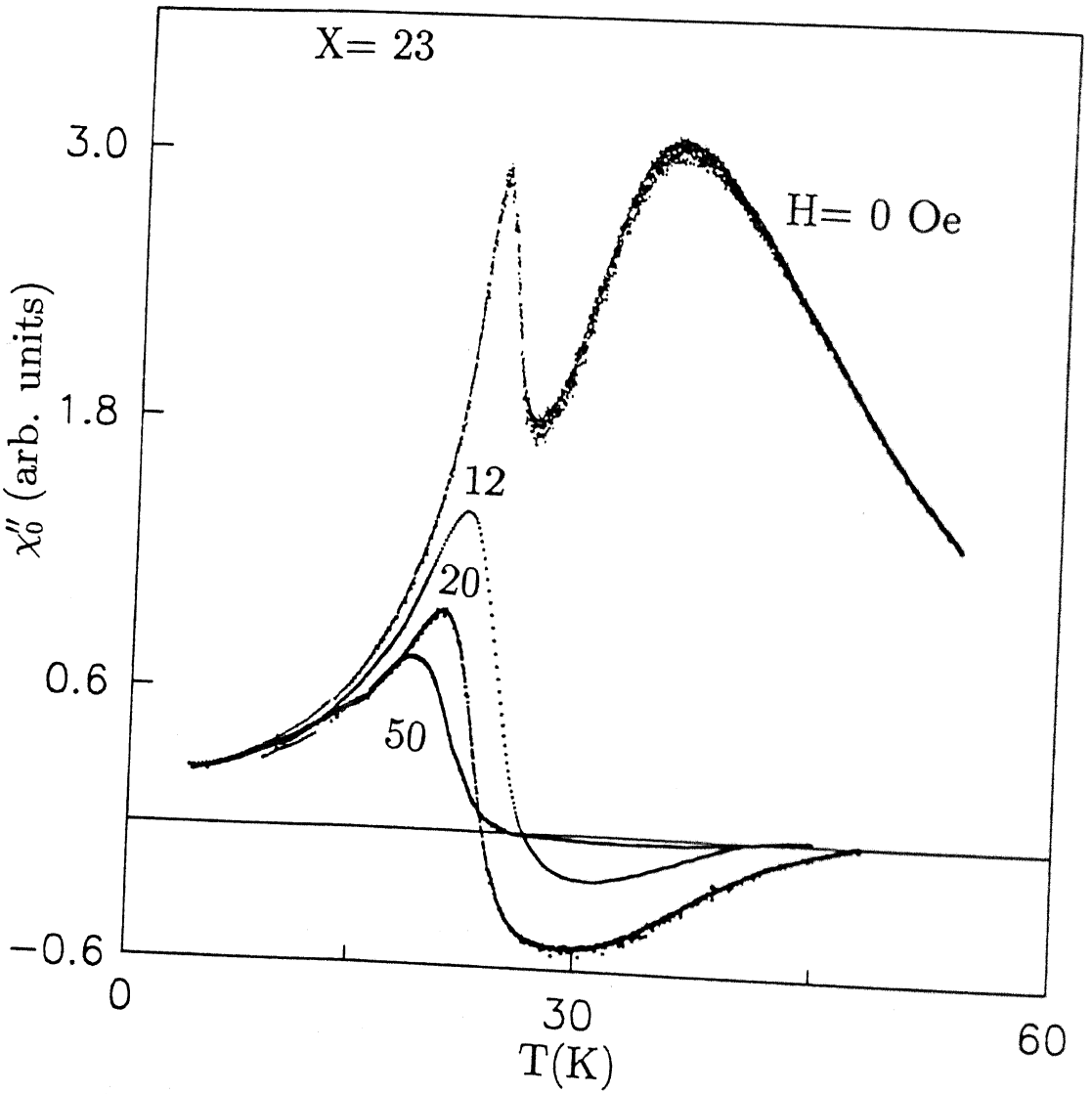

Figure 5.14: Temperature variation of the imaginary part of the linear susceptibility (χ_0'') of the RSG(X=23) for different dc biasing fields(H) measured at $h_0 = 0.6$ Oe and at 242 Hz. H = 0, 12, 20, and 50 Oe from top to bottom, respectively.

temperatures by a considerable amount (23.6, 22.1, 20.7, and 18.7 K for 0, 12, 20, and 50 Oe, respectively). In contrast, we observed (Fig. 5.4) small shifts of the peak in χ_0'' towards lower temperatures in the SG (X=19) in the presence of dc fields, whereas the other RSG (X=26) showed an opposite shift(Fig. 5.7).

We have stated earlier that the non-linear susceptibility (χ_1) should show an anomaly near T_g if a spontaneous magnetization persists below T_g. We observe (inset of Fig. 5.15a, for X= 23) a peak in χ_1 at T_g (23.6 K) which clearly indicates the presence of a spontaneous magnetization at lower temperatures. We believe that this peak in χ_1 is a definitive signature of an RSG which distinguishes it from an SG. Here the peak is sharper than that of X= 26(Fig. 5.11). χ_1 increases with the increase of temperature above T_g showing a broad maximum and then it starts falling slowly above 39 K, which is higher than its T_C. We also did not observe any sharp peak in χ_0'' near its T_C of 35 K (Fig. 5.14). Normally, it is expected that if a system goes from an FM to a PM state with the increase of temperature, then its magnetization (m) also reduces with temperature. But from our magnetic relaxation data[12] we observed that m reduces with temperature up to T_C, then around 38 K it suddenly increases to a higher value for the sample with X=23. We tried to explain this unusual behaviour in terms of the presence of a strong anisotropy. However, this is not observed in the case of the other RSG sample, X=26. The amplitude of χ_1 increases dramatically by an order of magnitude with the application of a dc field as small as 3 Oe (Fig. 5.15 and its inset a). Here χ_1 shows a broad peak instead of a double peak as in the zero dc-field case. Application of external dc fields broadens both the peaks near T_g and T_C, which are not widely separated. They might overlap and produce a single broad peak. To demonstrate this we break up the peak in χ_1 for H= 3 Oe dc field into two peaks (α and β) in inset b of Fig. 5.15. However, the shape and position of the individual curves are not unique. For sample X=26, the transition temperatures are far apart, so although the peaks are broadened in the presence of dc fields, we could still observe two distinct peaks(Fig. 5.11). The above decomposition holds for H= 6 and 12 Oe as well. With further increase of the dc field, χ_1

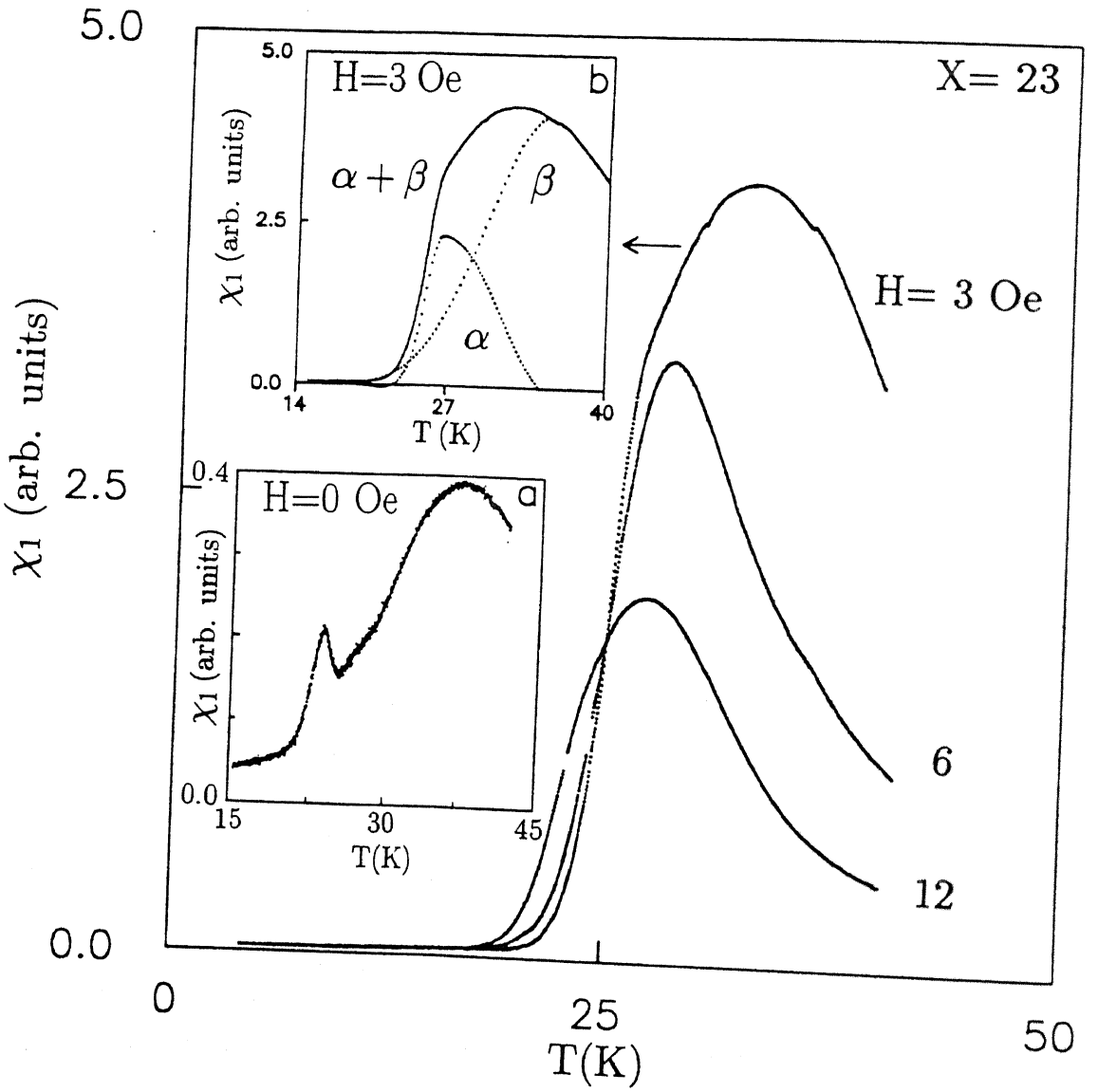

Figure 5.15: Temperature variation of the non-linear susceptibility, $\chi_1 = \frac{\partial^2 m}{\partial h^2}$, of the RSG (X=23) for different external dc biasing fields(H). H = 3, 6, and 12 Oe from top to bottom, respectively. Inset (a) shows the variation for H= 0 and (b) shows that for H= 3 Oe, χ_1 is the superposition of two peaks, α and β. Similarly superposition could be shown for H=6 and 12 Oe as well.

reduces and at lower temperatures it approaches a very small value independent of the field and temperature. Similar observations are made for X=26.

We have measured χ_2 which shows a negative dip around T_g as observed in the case of X=26. We have fitted the dip in χ_2 with the power law. From the slope of the log-log plot of χ_2' and $(\frac{T_g-T}{T_g})$ [Fig. 5.16] we find the exponent $\gamma_n = 2.31 \pm 0.03$ which is slightly less than that observed for X=26.

We find several differences between the behaviour of the samples X=23 and X=26, though they undergo similar kinds of phase transitions. We observe for sample X=23 that the imaginary part of the linear susceptibility (χ_0'') shows broad peaks at temperatures higher than T_C which is not the case for X=26. For sample X=23, the transition near T_g is sharp and somewhat similar to that of the SG (X=19) rather than that of the other RSG (X=26) whereas the transition around T_C is not very sharp for X=23. Nevertheless, both the RSG samples (X=23 and 26) show some features which are distinctly different from the SG (X=19). For the sample X=26, the transition near T_C is quite sharp and the features are closer to typical FM's. The value of the critical exponent γ increases with the increase of Ni concentration. So a gradual change over from an SG (X=19) to an RSG (X=23 and 26) phase is observed in this alloy system within the same crystallographic phase by increasing Ni concentration from 19 to 26.

5.1.3 Ferromagnet (X=30) and Antiferromagnet (X=14)

In the preceding sections we presented a detailed study of the properties of the SG (X=19) and the RSG (X=26 and 23) phases. In this section we present the magnetic properties of the FM (X=30)[7] and compare them with those of the high temperature transition of the RSG's. Figure 5.17 depicts the temperature variation of the real (χ_0') and imaginary (χ_0'') parts of the linear susceptibility of the FM(X=30). At lower temperatures χ_0' remains almost a constant and around 125 K it starts decreasing sharply with the increase of temperature, indicating a phase transition (FM to PM). We plot $Y = [\frac{d}{dT}(\ln \chi_0^{-1})]^{-1}$ against

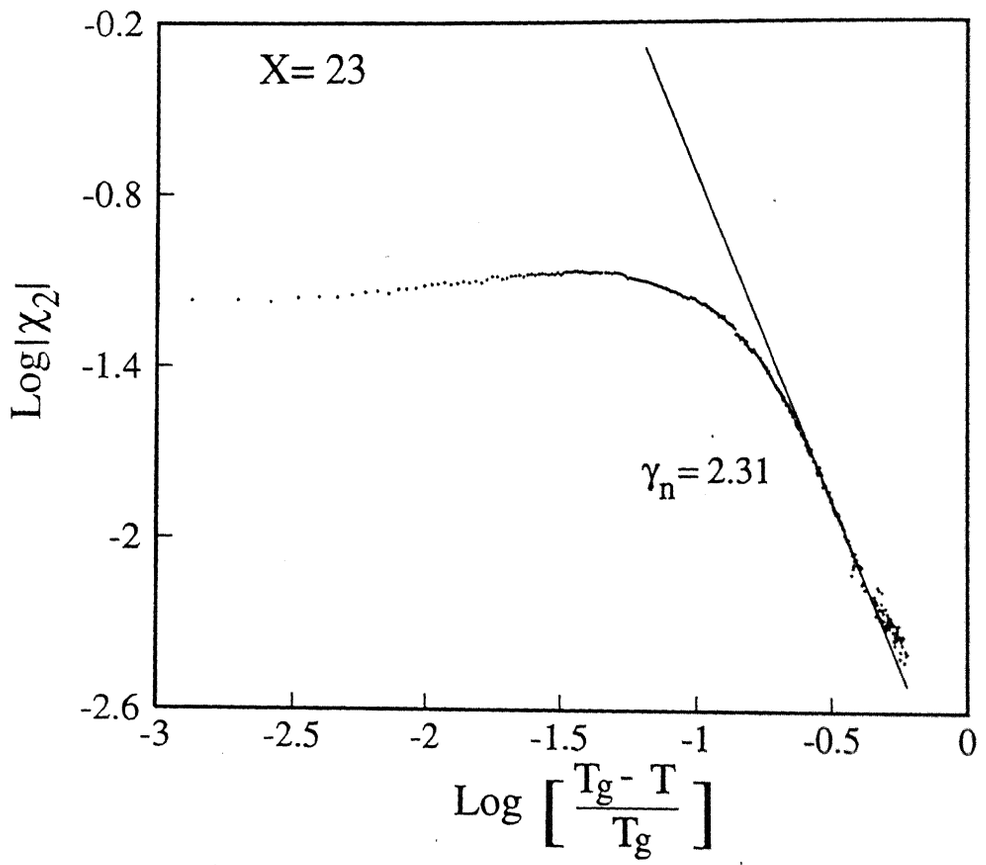

Figure 5.16: Double logarithmic plot of the non-linear susceptibility, $|\chi_2|$, versus the reduced temperature, $\frac{T_g - T}{T_g}$, below T_g for X= 23. The slope of the straight line gives $\gamma_n = 2.31 \pm 0.03$.

T (Fig. 5.17) whose inverse slope gives $\gamma = 1.10 \pm 0.01$ and the point of intersection on the temperature axis, $T_C = (126.7 \pm 0.2)$ K. The value of T_C is substantially smaller than that found earlier from dc magnetization[7]. χ_0'' shows a small peak and then it starts decreasing very sharply around T_C with the increase of temperature. It approaches zero as the system enters the PM phase. We also observe that the ratio of χ_0' to χ_0'' is ≈ 30 in this FM. It reduces to ≈ 25 in the RSG and to ≈ 22 in the SG. It means that the relative value of the absorptive component (χ_0'') increases with the increase of randomness as the system goes from the ordered FM phase to the disordered SG phase with the reduction in Ni concentration (X) from 30 to 19.

To cross check the value of γ we use the other method which requires a prior knowledge of T_C. We plot $\log \chi_0$ against $\log(\frac{T-T_C}{T_C})$ (inset of Fig. 5.17) and using the formula, $\chi_0 \propto (\frac{T-T_C}{T_C})^{-\gamma}$, we get $\gamma = 1.06 \pm 0.01$. Thus, the values of γ obtained from the two different methods are in good agreement. The mean-field theory predicts the value of γ as 1 whereas in the 3D Heisenberg model it is 1.38. Most of the real systems are 3D in nature and the values of γ obtained in pure FM's Ni[13] and Fe[27] are 1.35 and 1.33, respectively. However, the value of γ can vary widely in different ferromagnetic systems[28]. We observe that in the present alloy system the value of γ increases with the increase in Ni concentration (X) (0.72, 0.92 and 1.1 for X=23, 26 and 30, respectively) as the system goes towards the FM phase. We have measured the temperature variation of γ and found that it does not vary much in the case of the FM, X= 30(inset of Fig. 5.18), while in the RSG (X=26, inset of Fig. 5.18 and X= 23, curve b of the inset of Fig. 5.13) it shows wide variations.

We have seen that with the increase in Ni concentration the system moves towards ferromagnetic order. On the other hand, for low Ni concentration (X=14) it shows an antiferromagnetic behaviour. Figure 5.18 depicts the temperature variation of the linear susceptibility (χ_0) of the sample X=14 (AF), measured at 0.6 Oe and at 726 Hz. It shows a peak at 30 K which indicates a possible AF to PM transition. Earlier, T_N was found to be (26 ± 1) K from dc magnetization data(dc field = 1 kOe) and (30 ± 10) K from neutron

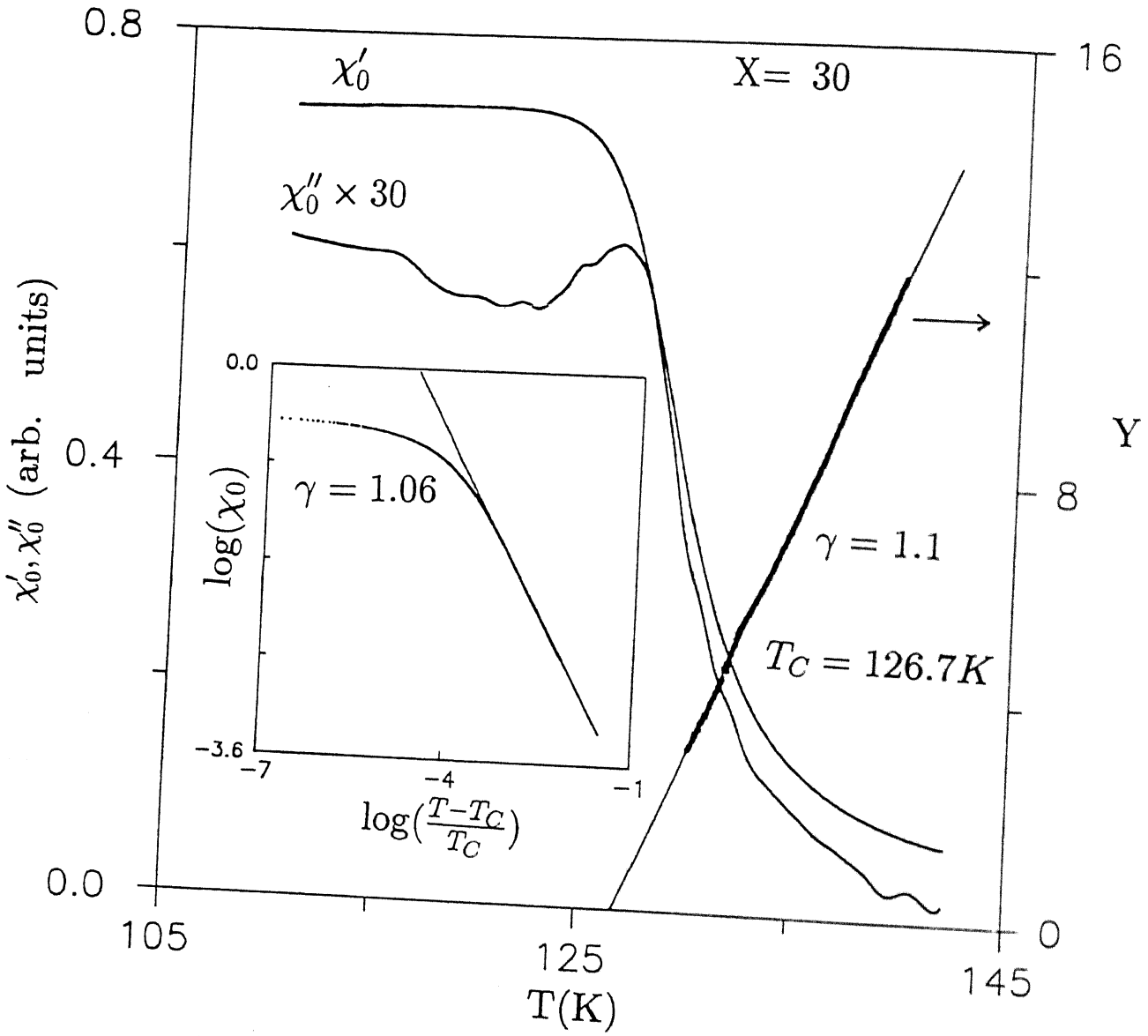

Figure 5.17: Temperature dependence of the linear susceptibility, χ_0 (real and imaginary) and $Y = [\frac{d}{dT}(\ln \chi_0^{-1})]^{-1}$ of the FM (X=30) measured at $h_0 = 0.6$ Oe and at 242 Hz. The straight line is the best fit of the data to the KF relation. The inverse of the slope gives γ and its intercepts on the temperature axis, T_C. The inset shows the double logarithmic plot of χ_0 versus the reduced temperature ($\frac{T-T_C}{T_C}$) for $T > T_C$. The slope of the straight line again gives γ.

diffraction measurements[7]. So we find discrepancies in the value of T_N obtained from different measurements for the AF (X=14). This kind of discrepancy was also reported by a large number of investigators in different AF's[29]. It is believed that in an AF the susceptibility shows a maximum a little above T_N[30]. The positions of the peak in susceptibility and specific heat are reported to differ by as much as 10 K in some AF's[31, 32]. For a 20 Oe dc biasing field, χ shows a peak at a higher temperature of 31 K (Fig. 5.18). The mean-field theory predicts a decrease in $T_N(H)$ with increasing H[33]. On the other hand, Kosterlitz et al.[34] theoretically predicted that $T_N(H)$ first increases with H, passes through a maximum at some value of H, and then it decreases when H is increased still further. Oguchi and Blume had shown that $T_N(H)$ increases in a uniform magnetic field of appropriate magnitude when the spin entropy at T_N is large[35].

5.2 Conclusion

We have measured the low-field ac susceptibility in four different magnetic phases of $Fe_{80-x}Ni_xCr_{20}(14 \leq x \leq 30)$ alloys. In the SG (X=19), T_g varies with measuring frequency obeying a Fulcher law of the form $\nu = \nu_0 \exp[-\frac{E_a}{k(T_g - T_0)}]$. External dc biasing fields shift T_g towards lower temperatures and reduce the susceptibility. The variation of T_g can be understood in terms of a non-mean-field theory[5] and the decrease of susceptibility can be explained in the framework of Néel's superparamagnetic model. Both of above features could also be explained in terms of a mean-field theory[6]. A very distinct peak in χ_2 and the absence of χ_1 in the SG are consistent with theoretical predictions. The values of the critical exponent γ near T_C, obtained by two different methods, in the RSG (X=26) are closer to the mean-field prediction while the other two exponents β and δ are at variance. However, they satisfy the static scaling law within the experimental error. χ_0'' in the RSG shows a double transition with two distinct peaks at T_C and T_g. A dc biasing field shifts T_g towards higher temperatures in the RSG(X=26) in contrast to the opposite shift in the SG (X=19). As

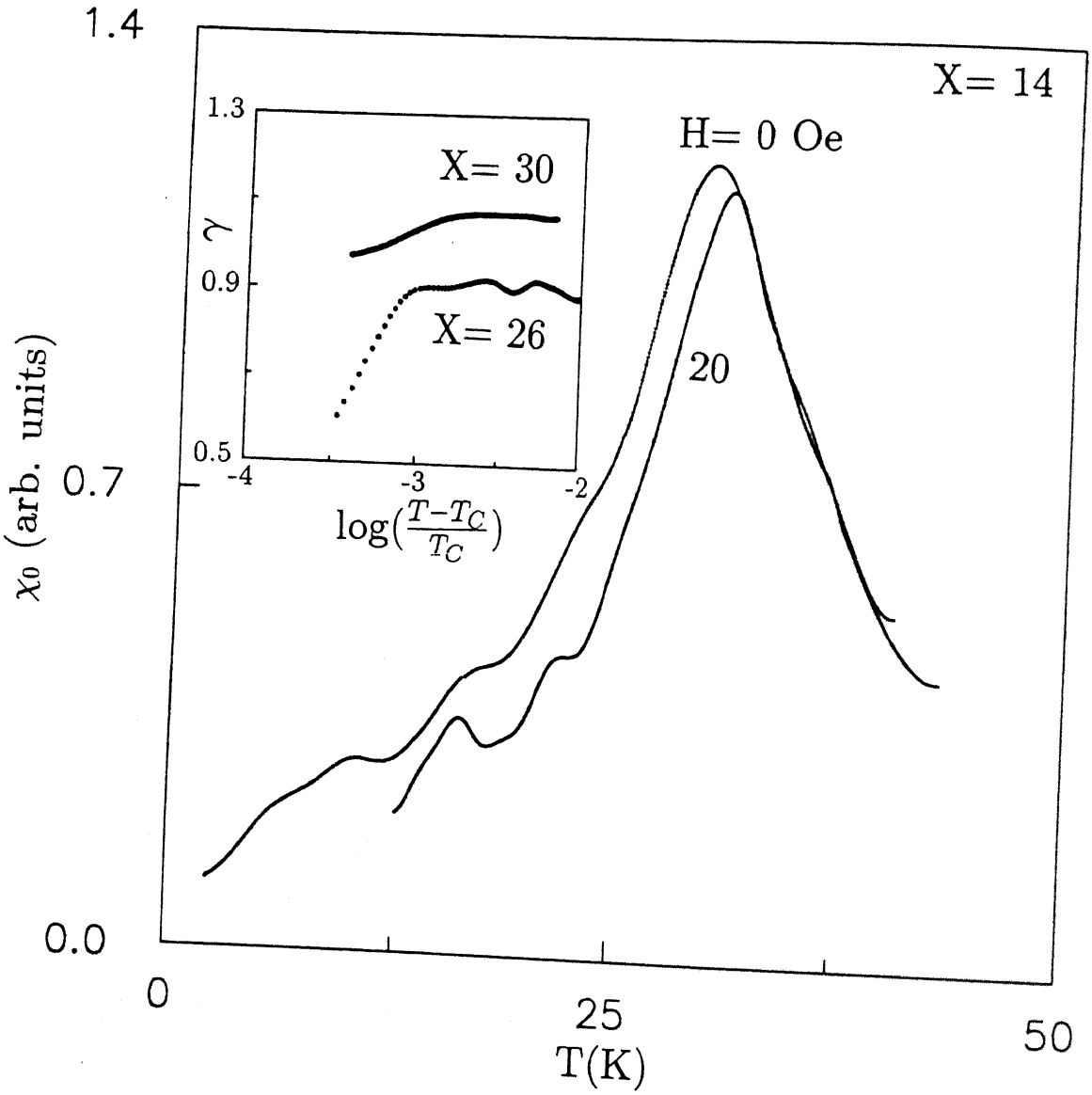

Figure 5.18: Temperature variation of the linear susceptibility (χ_0) and its dc field dependence (H=20 Oe) of the AF (X=14) measured at $h_0 = 0.6$ Oe and at 726 Hz. The inset shows the variation of γ with $\log(\frac{T-T_C}{T_C})$ of the FM (X=30) and the RSG (X=26).

$T \rightarrow 0$. χ_0'' approaches a very small non-zero value in the RSG while in the SG it approaches a value which is $\approx 50\%$ of its peak value. The non-linear susceptibility, χ_1, shows a peak near T_g in both the RSG's (X=26 and 23) indicative of a long-range order. This has never been observed in any SG including X=19. This distinguishes the RSG from the SG. However, we observed some different features in the two samples X=23 and 26 although they undergo similar kinds of phase transitions. We find that the transition near T_g for X=23 is sharper than that near T_C. But the reverse is observed for X=26, whose composition is somewhat closer to the FM (X=30). We also find that the value of the critical exponent γ increases with the increase of Ni concentration, X, from 23 to 30 as the system moves towards the FM phase. In the AF (X=14), around T_N, χ_0 shows a peak which shifts towards higher temperatures in the presence of small dc fields in agreement with the prediction of Kosterlitz et al.[34]. The present detailed, high-resolution data are expected to attract the attention of theorists in the field. Several findings remain unexplained in the light of existing theories.

References

[1] L. E. Wenger, C. A. M. Mulder, and A. J. Van Duyneveldt, Phys. Lett. **87A**, 439(1981).

[2] G. I. Fulcher, J. Am. Ceram. Soc. **8**, 339 and 789(1925).

[3] J. L. Tholence, Solid State Commun. **35**, 113(1980).

[4] H. Maletta and W. Felsch, Phys. Rev. B **20**, 1245(1979).

[5] B. Barbara, A. P. Malozemoff, and S. E. Barnes, J. Appl. Phys. **55**, 1655(1984); B. Barbara, A. P. Malozemoff, and Y. Imry, Phys. Rev. Lett. **47**,1852(1981).

[6] C. Loewen and R. M. Roshko, Phys. Rev. B **31**, 4663(1985).

[7] A. K. Majumdar and P. v. Blanckenhagen, Phys. Rev. B **29**, 4079 (1984); J. Magn. Magn. Mater. **40**, 227(1983).

[8] A. P. Murani and J. L. Tholence, Solid State Commun. **22**, 1402(1978).

[9] L. Néel, Adv. Phys. **4**, 191(1955).

[10] M. Suzuki, Prog. Theor. Phys. **58**, 1151(1977).

[11] S. F. Edwards and P. W. Anderson, J. Phys. F **5**, 965(1975).

[12] G. Sinha, R. D. Barnard, and A. K. Majumdar, Phys. Rev. B **55**, 8982(1997); G. Sinha, R. Chatterjee, M. Uehara, and A. K. Majumdar, J. Magn. Magn. Mater. **164**, 345(1996).

[13] J. S. Kouvel and M. E. Fisher, Phys. Rev. **136**, A1626(1964).

[14] H. P. Kunkel, M. S. Westmore, and G Williams, Phil. Mag. B **65**, 1215(1992) and the references therein.

[15] V. G. Bar'yakhtar, A. B. Surzhenko, and G. A. Takzeĭ, Sov. Phys. JETP **75**, 905(1992).

[16] D. J. Amit, Field Theory, The Renormalization Group, and Critical Phenomena (World Scientific, 1993).

[17] T. Sato and Y. Miyako, J. Phys. Soc. Jpn. **51** (1982) 1394.

[18] T. Bitoh, T. Shirane, and S. Chikazawa, J. Phys. Soc. Jpn. **62** (1993) 2837.

[19] T. Sato, T. Nishioka, Y. Miyako, Y. Takeda, S. Morimoto, and A. Ito, J. Phys. Soc. Jpn.**54** (1985) 1989.

[20] A. K. Gangopadhyay, S. B. Roy, and A. K. Majumdar, Phys. Rev. B**33** (1986) 5010.

[21] H. P. Kunkel and G. Williams, J. Phys. F **18**, 1271(1988); J. Magn. Magn. Mater. **75**, 98(1988); Anita G. Berndt, X. Chen, H. P. Kunkel, and Gwyn Williams, Phys. Rev. B **52**, 10160(1995).

[22] G. K. Nicolaides, G. C. Hadjipanayis, and K. V. Rao, Phys. Rev. B **48**, 12759(1993).

[23] A. P. Murani, Solid State Commun. **34**, 705(1980); Phys. Rev. Lett. **37**, 450(1976).

[24] S. Senoussi, S. Hadjoudj, and R. Fourmeaux, Phys. Rev. Lett. **61**, 1013(1988).

[25] G. Aeppli, S. M. Shapiro, H. Maletta, R. J. Birgeneau, and H. S. Chen, J. Appl. Phys. **55**, 1628(1984).

[26] M. Fähnle and T. Egami, J. Appl. Phys. **53**, 7693(1982).

[27] J. E. Noakes, N. E. Tornberg, and A. Arrott, J. Appl. Phys. **37**, 1264(1966).

[28] S. N. Kaul, J. Magn. Magn. Mater. **53**, 5(1985).

[29] S. Ikeda and Y. Ishikawa, J. Phys. Soc. Jpn **39**, 332(1975).

[30] N. W. Ashcroft and N. D. Mermin, Solid State Physics(Saunders College Publishing, International Edition, 1988), p 699.

[31] T. Hashimoto and Y. Ishikawa, J. Phys. Soc. Jpn. **23**, 213(1967).

[32] J. E. Zimmerman, A. Arrott, H. Sato, and S. Shinozaki, J. Appl Phys. **35**, 942(1964).

[33] Y. Shapira and C. C. Becerra, Phys. Rev. Lett. **38**, 358(1977).

[34] J. M. Kosterlitz, D. R. Nelson, and M. E. Fisher, Phys. Rev. **13**, 412(1976); M. E. Fisher, Phys. Rev. Lett. **34**, 1634(1975).

[35] T. Oguchi and M. Blume, J. Phys. Soc. Jpn. **50**, 2547(1981); T. Oguchi, Prog. Theor. Phys. **13**, 148(1955).

Chapter 6

Hall Effect

In this chapter we are reporting Hall effect data of $Fe_{80-X}Ni_XCr_{20}(14 \leq X \leq 30)$ alloys for four different magnetic phases within the fcc $\gamma - phase$. In the spin-glass phase(SG) (X=19) the Hall resistivity(ρ_H) increases with the field and does not saturate till 1.6 T. The temperature variation of ρ_H shows broad peaks around T_g for lower fields (< 0.1 T) which disappear at higher fields(1 T). We separate the ordinary(OHC) and the extra-ordinary Hall coefficient(EHC) in the ferromagnetic sample(X=30) and show their temperature variation. In the reentrant spin-glass(RSG) (X=26) ρ_H shows non-linear variation with field. The temperature variation of ρ_H shows anomaly near both T_g and T_C. In the antiferromagnetic phase(AF) (X=14) ρ_H increases more or less linearly with field and its temperature variation shows broad peaks around T_N for lower fields.

6.1 Results and Discussion

Hall effect in magnetic alloys exhibits some unusual features. It is observed that ρ_H increases rather sharply and linearly with field for lower fields, followed by a non-linear increase and at still higher fields it varies linearly with a relatively smaller gradient. It is

clear that the above behaviour is not due to the the Lorentz force alone. This is called extra-ordinary or anomalous Hall effect arising because of spin-orbit interaction present in an FM[1]. This anomalous behaviour can be found in any material having large and/or localized magnetic moments, for example, in FM, RSG, SG, AF, and strongly paramagnetic materials[2].

Hall effect can be undrestood in terms of the behaviour of itinerant current carriers moving under the influence of external electric and magnetic fields. These carriers interact asymmetrically with the scattering center in the metal. In other words, the carriers find it energetically favourable to move to one side of the scattering center rather than to the other. This process gives rise to a transverse current in the sample which produces the anomalous Hall voltage. Various theoretical models and scattering processes are described in details in chapter 1.

We have measured ρ_H in FM(X=30), SG(X=19), RSG(X26), and AF(X=14) phases of $Fe_{80-X}Ni_XCr_{20}$ alloys. Hall resistivity in magnetic alloys is given by

$$\rho_H = R_0 B + R_s M_s, \tag{6.1}$$

where R_0 and R_s are the ordinary (OHC) and extra-ordinary Hall(EHC) coefficients, respectively, M_s is the saturation magnetization, and B is the magnetic induction. In our Hall geomery $B = \mu_0 H$. We find that the sign of the Hall coefficients(HC) is positive for all the alloys in the temperature range of 1.4 K to 300 K up to 1.6 T. The sign of Hall coefficient(HC) is generally determined by the shape of the E(K) dispersion curve at the Fermi surface. A positive Hall coefficient was observed in various transition metal alloys. This can be understood as the effect of hybridization between the free electrons and the d-band which gives rise to an anomalous 'S' shaped dispersion curve[3]. If the Fermi surface lies in the region where the slope of the dispersion curve ($\frac{\partial E}{\partial K}$) is negative, then the Hall coefficient will become positive.

Figure 6.1 shows the field dependence of the Hall resistivity, ρ_H for X= 19 for various

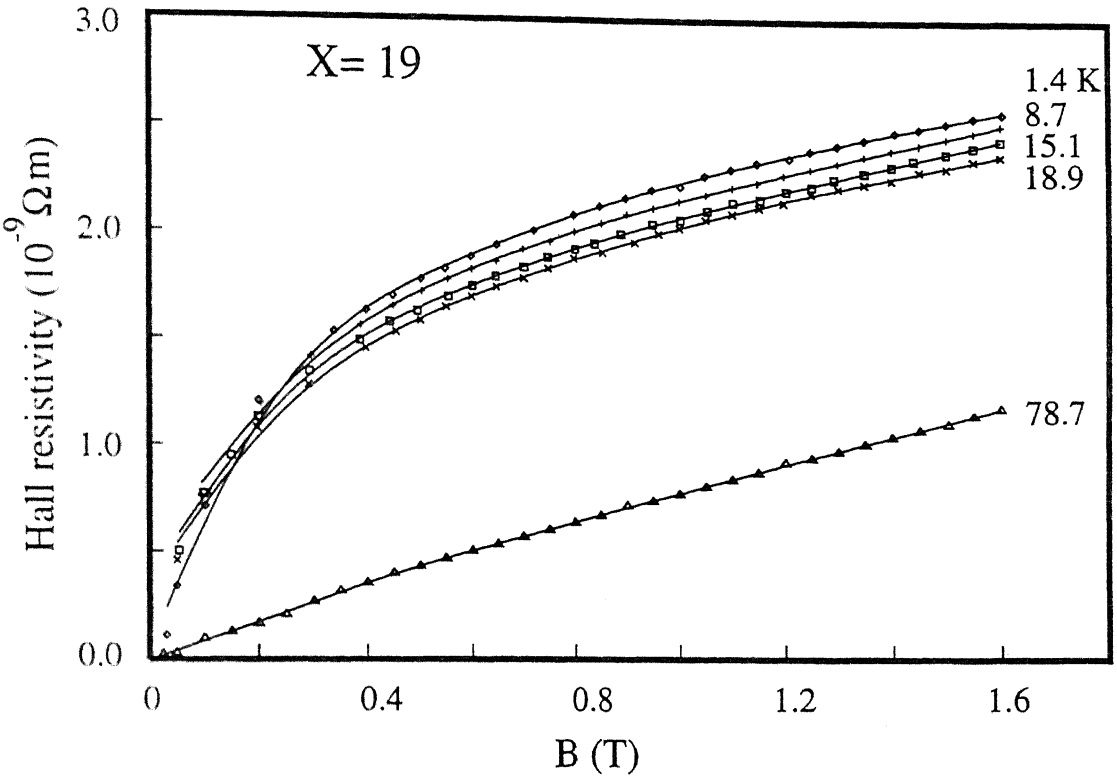

Figure 6.1: Field variation of the Hall resistivity, ρ_H, in the SG (X= 19) for various temperatures, T= 1.4, 8.7, 15.1, 18.9, and 78.7 K, from top to bottom, respectively. Solid lines are just guides to the eye.

temperatures, T = 1.4, 8.7, 15.2, 18.9, and 78.7 K, from top to bottom, respectively. We have measured ρ_H for various other temperatures but for clarity showing only a few of them in Fig. 6.1. The non-linear behaviour and the magnitude of ρ_H indicate the presence of extra-ordinary Hall component which arises because of spin-orbit interaction. In most of the cases the magnitude of the extra-ordinary component is at least one order of magnitude larger than that of the ordinary Lorentz component. Therefore, we are not attempting to separate the small Lorentz term from the ρ_H but consider the total ρ_H for analysis. We have also studied the temperature variation of ρ_H(Fig. 6.2) which shows broad peaks around T_g for lower fields. For fields of 0.03 and 0.05 T the peaks are prominent. However, around a field of 0.1 T it starts smearing out and finally disappears at 1 T. At 1 T ρ_H decreases monotonically with the increase of temperature. Similar behaviour was also reported in other SG's[4, 5]. The peaks around T_g in ρ_H for lower fields are somewhat similar to that observed in the temperature variation of susceptibility[6].

In a SG, at the lowest temperature($T < T_g$) the spins are frustrated, randomly distributed and undergo cooperative freezing. Hence, they find it difficult to orient themselves along the applied field, specially if the field is small. Therefore, the spin-orbit scattering events additively can not produce any significant extra-ordinary Hall component. This is why at the lowest temperature the value of ρ_H is small. With the increase of temperature, thermal energy tries to unlock some of the weakly coupled spins which, in tern, try to align along the applied field. This enhances the spin-orbit scattering events that eventually add coherently to give a larger ρ_H. So, up to T_g, ρ_H increases with the increase of temperature. However, above T_g all orderings are disrupted and the spins behave in a Curie-like fashion and further increase of temperature increases the disorder. Because of this, the spin-orbit scattering events are not added coherently and ρ_H reduces with the increase of temperature above T_g. This we think is a plausible reason for the peaks in ρ_H with temperature in the SG(X=19).

If the applied field is strong enough(say 1 T) then it can unlock some of the frozen spins

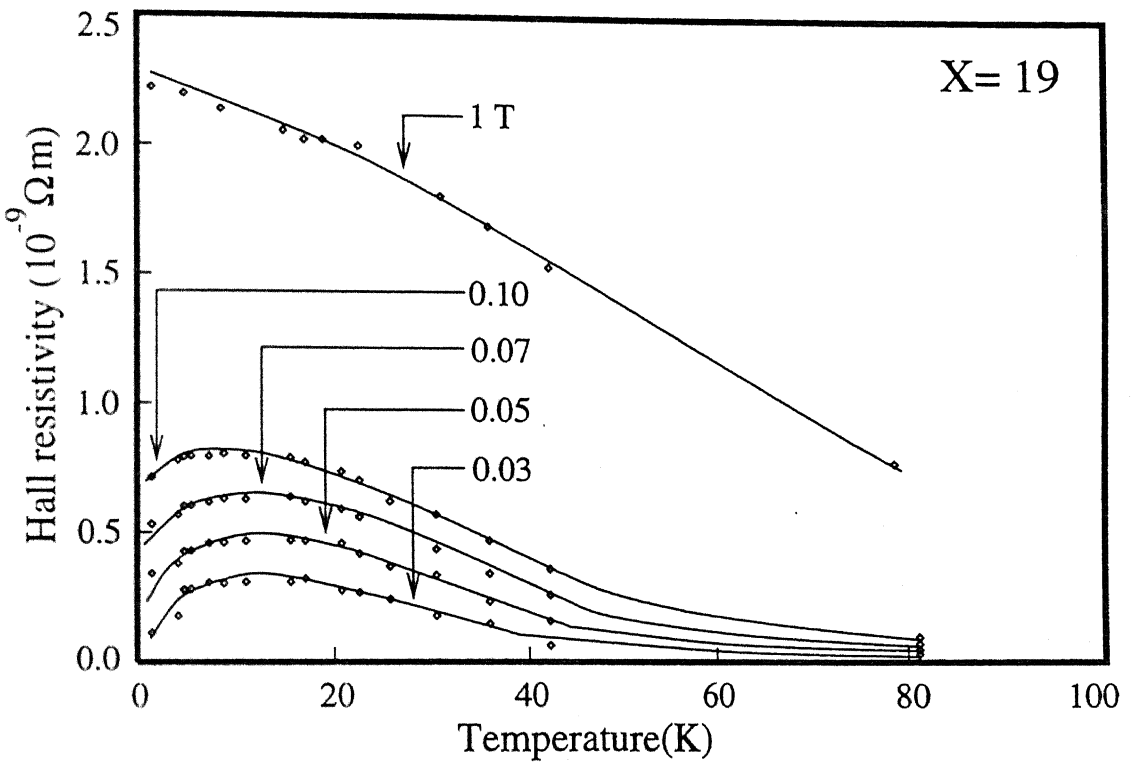

Figure 6.2: Temperature variation of the Hall resistivity, ρ_H, in the SG (X= 19) for various fields. B= 1, 0.1, 0.07, 0.05, and 0.03 T, from top to bottom, respectively. Solid lines are just guides to the eye.

and align them along the field even at the lowest temperature. In other words, strong fields can disrupt the cooperative SG state and force the spins to align along the field. Because of this alignment of the spins, ρ_H is larger at lower temperature for higher fields. So, any further alignment of spins with the increase of temperature is not possible because there are no more weakly coupled spins which thermal energy can decouple for the field to align them. However, in weak fields, magnetic energy is not strong enough to align the frozen spins at lower temperatures. Then the thermal energy can play a crucial role to unlock the weakly coupled spins and helps in aligning them in the presence of the field. Thus, we observed different behaviour of ρ_H with temperature for high and low fields. In high fields thermal energy tries to increase the disorder and hence ρ_H reduces with the increase of temperature. This reduction of ρ_H is even faster beyond T_g.

We have shown the variation of ρ_H with field for X= 30, an FM with $T_C = 130K$, for various temperatures(Fig. 6.3). It shows the usual ferromagnetic behaviour. We have also calculated the value of R_0 from the high field slope of the ρ_H vs B curve whose intersection on the ρ_H axis gives R_sM_s. From the intersection of the low and high field slope of the ρ_H vs B curve we get the value of M_s. We find that the value of M_s at T= 0 K obtained in this method after extrapolation is quite close to that obtained from our earlier M vs T data[7]. Using our earlier $M_s(T)$ data we calculate the value of R_s. We find that the value of R_s increases sharply with the increase of temperature (Fig. 6.4). It was reported that this sample shows resistivity minimum around 10 K[8]. However, we do not observe its effect on the temperature variation of R_s. This prevents us from finding any simple correlation between its R_s and resistivity. The variation of R_0 with temperature shows some unusual behaviour(Fig. 6.4). It shows a marginal rise with temperature from 2 K to 6 K and then it decreases with the increase of temperature till 20 K. Then it again starts rising with temperature.

ρ_H in the RSG (X= 26) shows a non-linear behaviour with field. It is somewhat similar to that of the FM with a marked difference that it does not show any definite tendency of

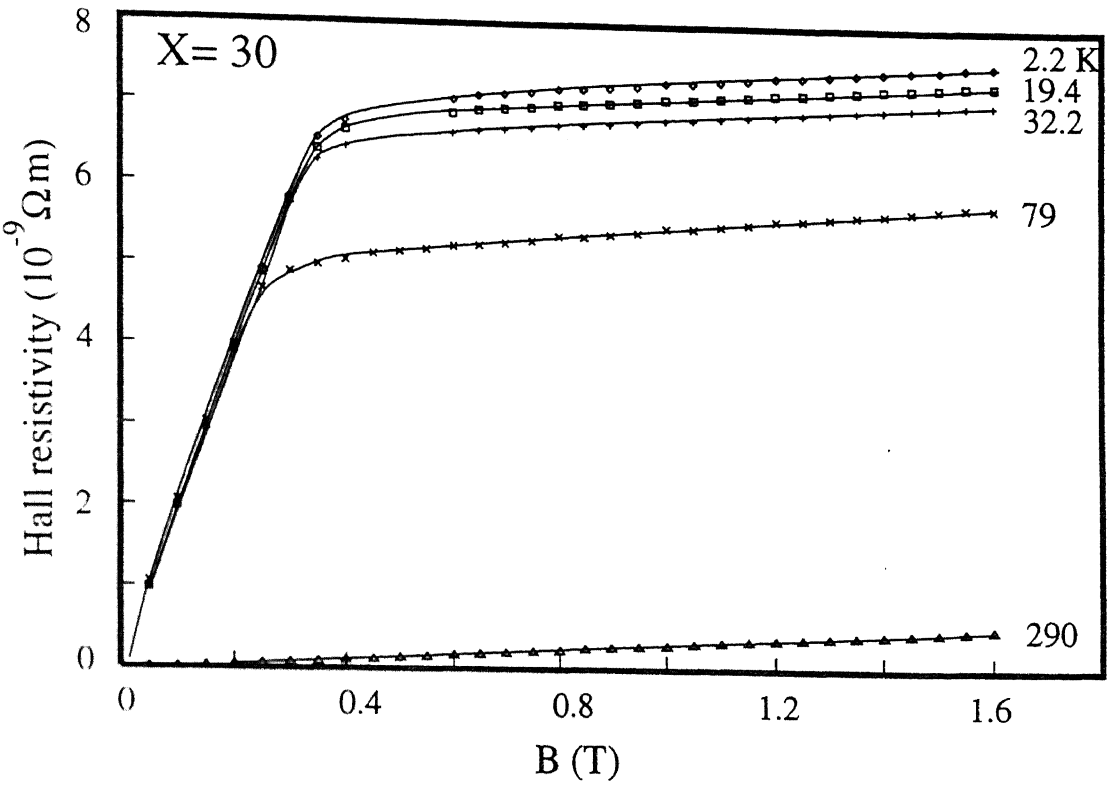

Figure 6.3: Field variation of the Hall resistivity, ρ_H, in the FM (X= 30) for various temperatures. T= 2.2 , 19.4, 32.2, 79, and 290 K, from top to bottom, respectively. Solid lines are just guides to the eye.

saturation even at the field of 1.6 T (Fig. 6.5). The variation of ρ_H shows an interesting feature(Fig. 6.6). It shows anomaly near both the transition temperatures, first when it goes to the FM phase from the mixed phase around 7 K and the second when it goes to the PM phase from the FM one around 56 K. Somewhat similar behaviour has been observed in the temperature variation of the susceptibility[9].

In the AF (X=14) ρ_H varies almost linearly with the field for various temperatures above and below the transition temperature($T_N = 26K$) (Fig. 6.7). However, perfect linearity is only seen at higher temperatures for example, at 44 K and 78 K as shown in Fig. (6.7). However, at the lowest temperature(1.7 K) ρ_H shows two distinct slopes for lower and higher fields. It increases linearly with field till 0.9 T and then continues to increase with the further

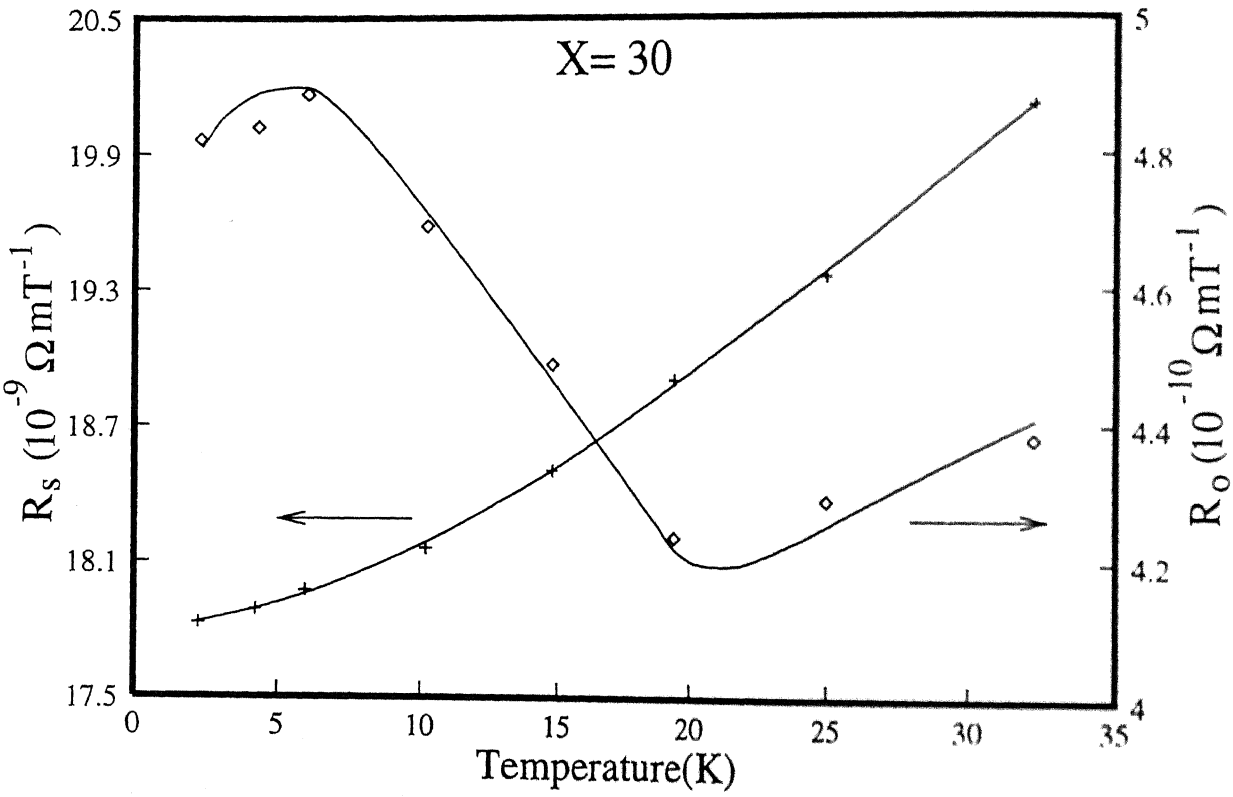

Figure 6.4: Temperature variation of the extra-ordinary, R_s and the ordinary, R_0, Hall coefficients in the FM (X= 30). Solid lines are just guides to the eye.

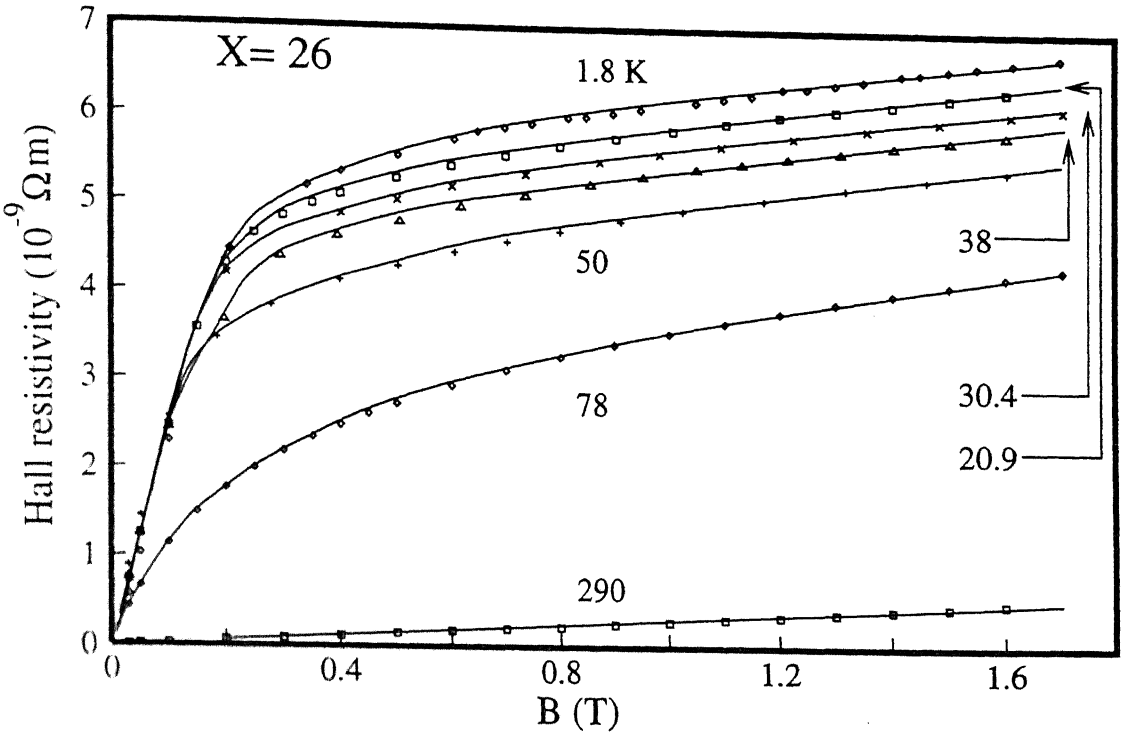

Figure 6.5: Field variation of the Hall resistivity, ρ_H, in the RSG (X= 26) for various temperatures. T= 1.8, 20.9, 30.4, 38, 50, 78 and 290 K, from top to bottom, respectively. Solid lines are just guides to the eye.

increase of field with a relatively higher slope. In an AF ρ_H consists of both the ordinary and the extra-ordinary Hall components. However, in the absence of M_s (M_s is zero in AF) both of them vary linearly with field since for an AF Eq. (6.1) could be rewritten as

$$\rho_H = R_0\mu_0 H_{applied} + R_s\chi H_{applied}, \tag{6.2}$$

where $\chi = \frac{\partial M}{\partial H_{applied}}$ is the susceptibility and $B = \mu_0[H_{applied} + 4\pi(1-N)M]$. For our Hall geometry, the demagnetization factor, $N \approx 1$ and hence $B \approx \mu_0 H_{applied}$. Hence, a linear variation of ρ_H is expected.

The variation of ρ_H with temperature in the AF (X= 14) shows some interesting features(Fig. 6.8). It shows broad peaks around T_N(26 K) for 0.3, 0.4, and 0.5 T fields. However, this feature becomes smeared for the field of 1 T and finally it disappears at 1.6 T. For the field of 1.6 T ρ_H decreases monotonically with the increase of temperature. M(T) curves for

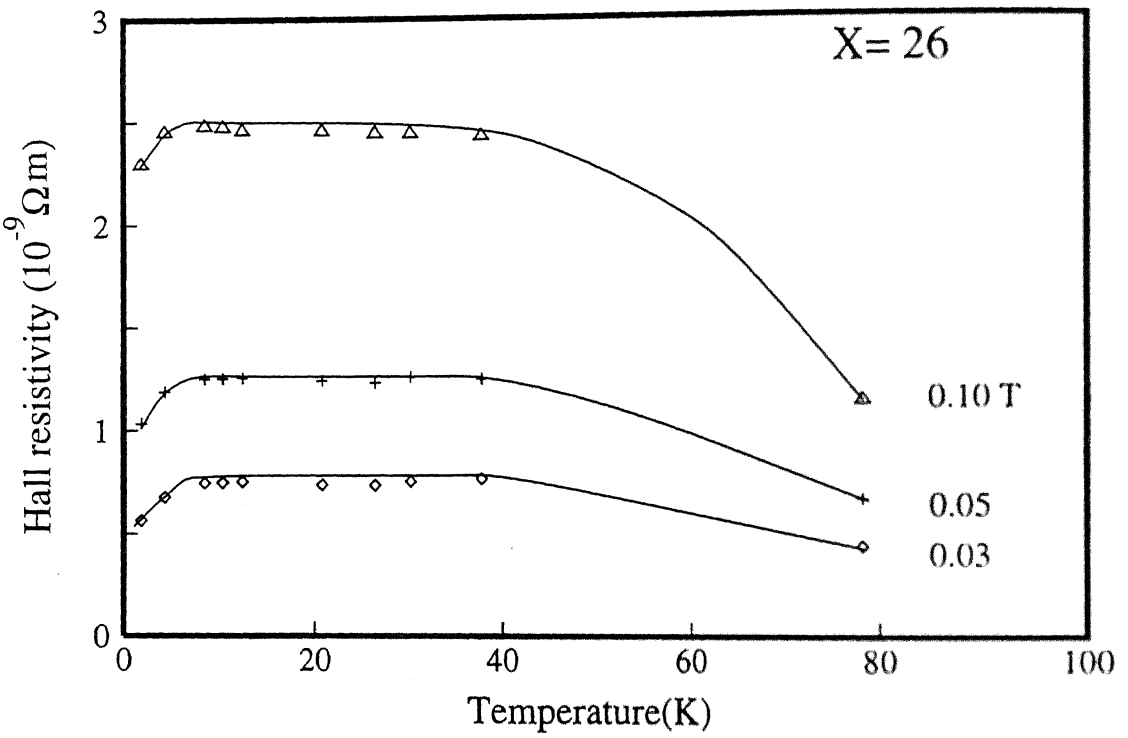

Figure 6.6: Temperature variation of the Hall resistivity, ρ_H, in the RSG (X= 26) for various fields, B= 0.1, 0.05, and 0.03 T, from top to bottom, respectively. Solid lines are just guides to the eye.

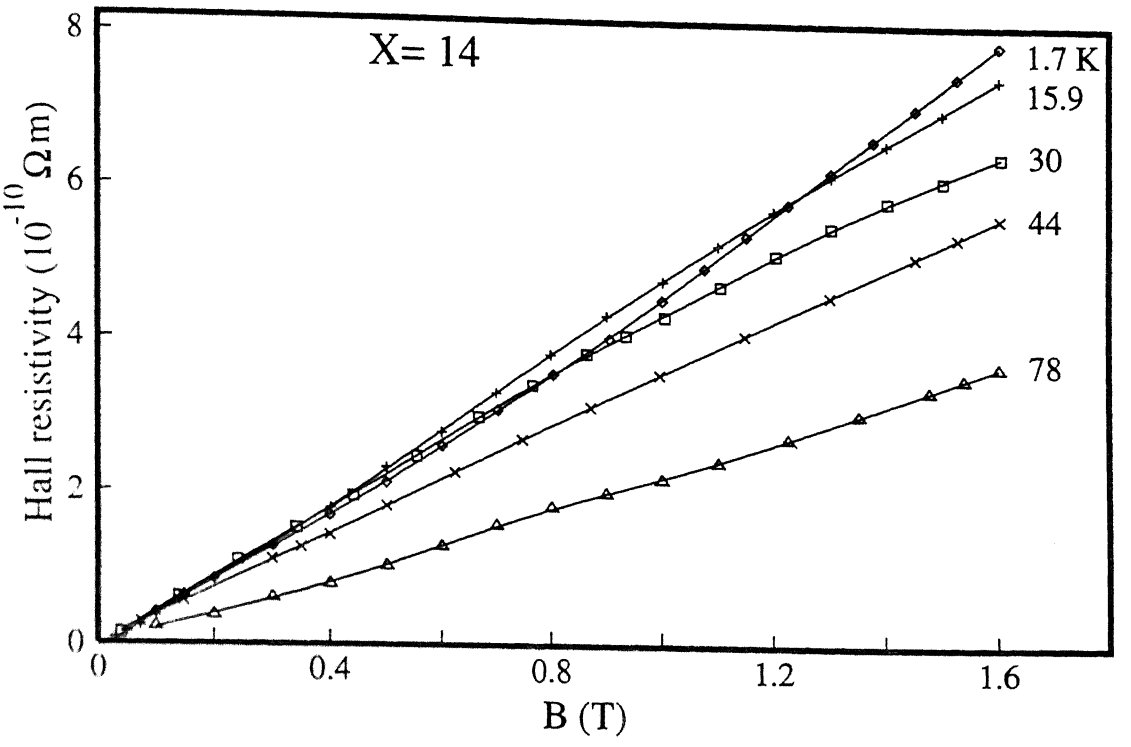

Figure 6.7: Field variation of the Hall resistivity, ρ_H, in the AF (X= 14) for various temperatures. T= 1.7, 15.9, 30, 44 and 78 K, from top to bottom, respectively. Solid lines are just guides to the eye.

X= 14[6] look very similar to those of Fig. 6.8. Similar observation was also reported for various other AF's[10, 11].

Finally, we have compared the variation of ρ_H with field at 4.2 K in various magnetic phases of $Fe_{80-X}Ni_XCr_{20}(X = 30, 26, 19, and\ 14)$ alloys(Fig. 6.9). ρ_H in X= 30 shows a typical FM-like behaviour. It increases sharply at lower fields and saturates at higher fields. On the other extreme X= 14, an AF, shows the usual linear behaviour of ρ_H with field and its magnitude is an order of magnitude smaller compared to that of the FM(X= 30). ρ_H in X= 19 shows a non-linear variation with field. It increases gradually with field without saturation as expected in a typical SG. The magnitude of ρ_H for X= 19 is smaller compared to that of the FM(X= 30) and larger than that of the AF(X= 14). The ρ_H in X= 26 shows the behaviour of both the FM and the SG phases showing their coexistance in this RSG.

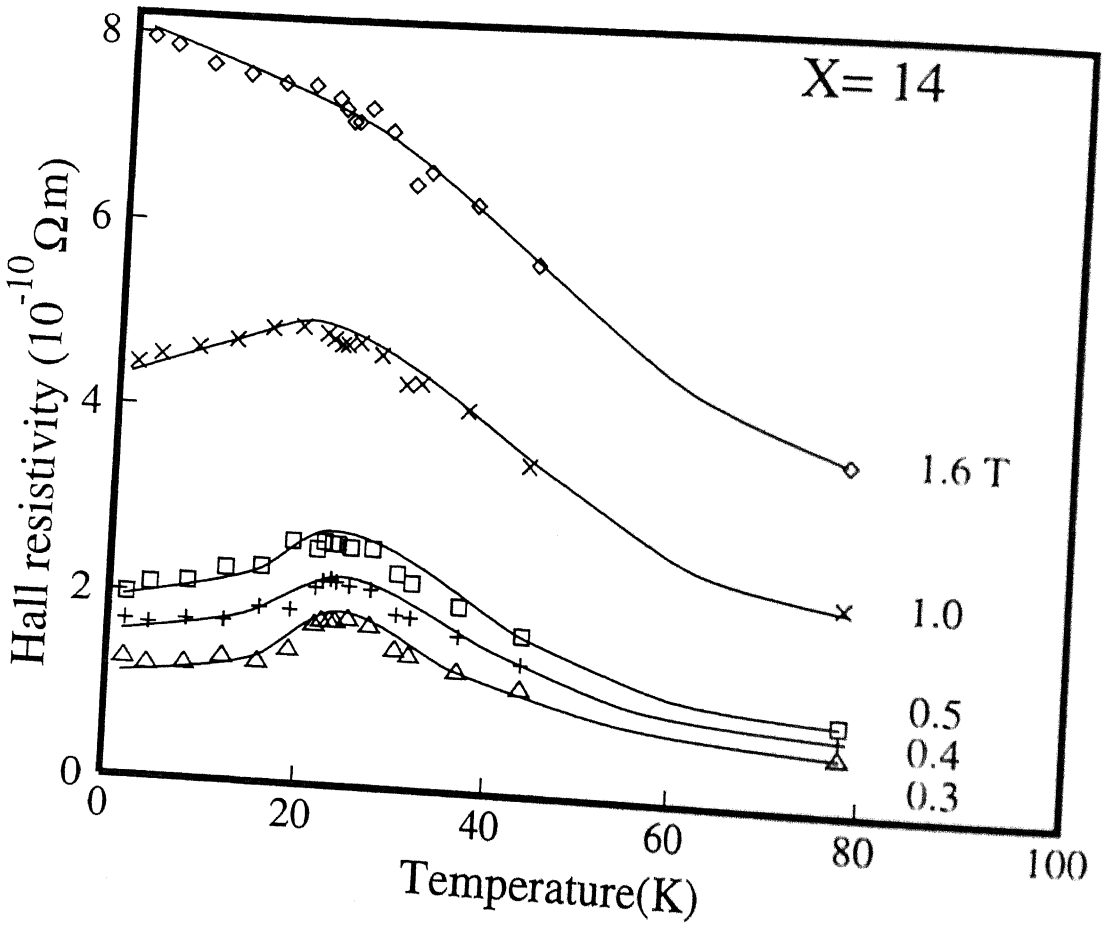

Figure 6.8: Temperature variation of the Hall resistivity, ρ_H, in the AF (X= 14) for various fields, B= 1.6, 1, 0.5, 0.4, and 0.3 T, from top to bottom, respectively. Solid lines are just guides to the eye.

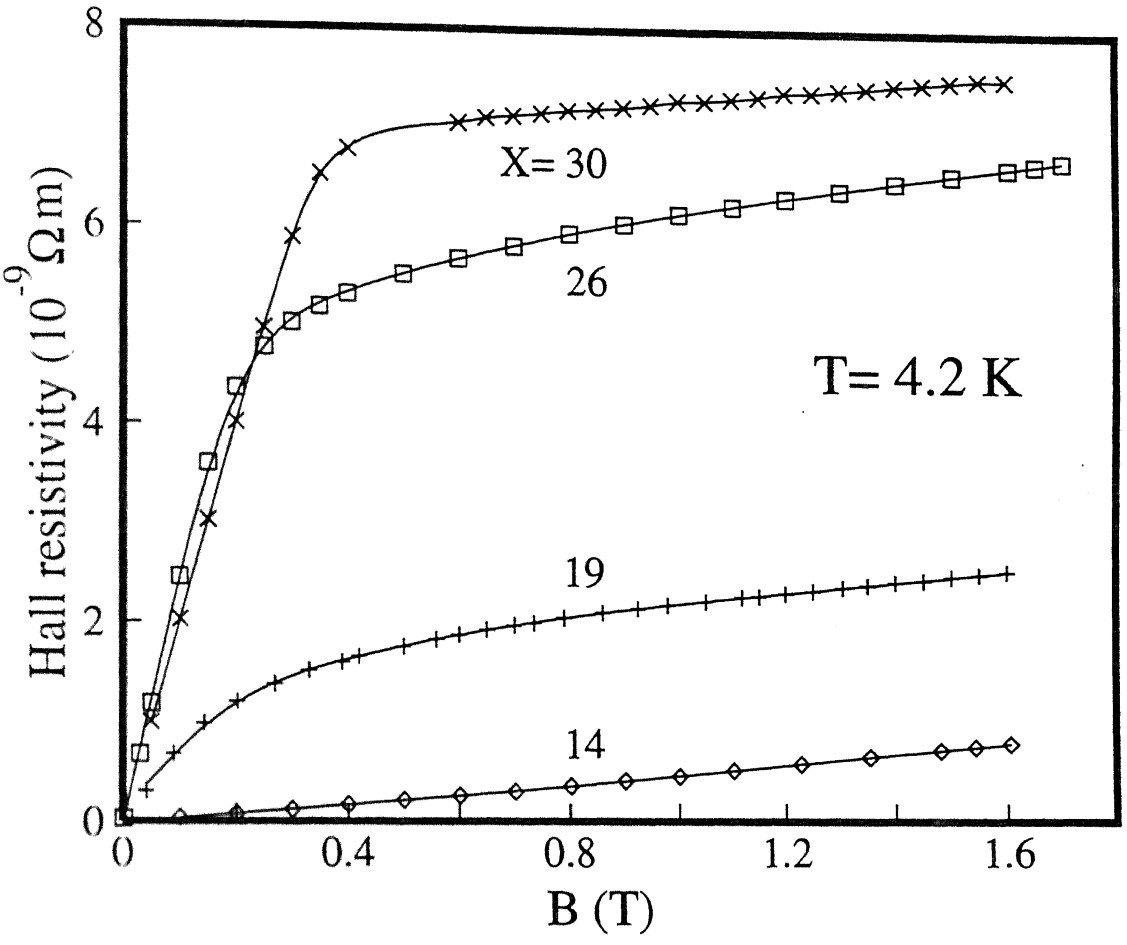

Figure 6.9: Field variation of the Hall resistivity, ρ_H, in all the four different phases of $Fe_{80-X}Ni_XCr_{20}(14 \leq X \leq 30)$ alloys, viz., FM(X= 30), RSG(X= 26), SG(X=19), and AF(X= 14), from top to bottom, respectively. Solid lines are just guides to the eye.

ρ_H increases sharply at lower fields as in the case of the FM but at higher fields it has some tendency of saturation which is however not complete even at a field of 1.6 T, unlike in an FM. This behaviour as well as the magnitude of ρ_H for $X = 26$ lies in between the SG (X= 19) and the FM (X= 30)samples.

In conclusion, we have studied the Hall effect in four different magnetic phases of the $Fe_{80-X}Ni_XCr_{20}(14 \leq X \leq 30)$ alloys. In the SG(X= 19) the Hall resistivity(ρ_H) shows a non-linear behaviour with field which arises because of the spin-orbit scattering. The temperature variation of ρ_H shows broad peaks around T_g for lower fields (< 0.1 T) but they disappear at higher fields(1 T). We have given an explanation for different behaviour of ρ_H with temperature for low and high fields in the SG. We have separated the ordinary(OHC) and the extra-ordinary(EHC) Hall coefficients in the ferromagnetic sample(X=30) and shown their temperature variations. In the RSG (X=26) ρ_H shows a non-linear variation with field. The temperature variation of ρ_H shows anomaly near both T_g and T_C. In the antiferromagnetic phase (X=14) ρ_H increases almost linearly with field and its temperature variation shows broad peaks around T_N for lower fields.

References

[1] A. K. Gangopadhyay, *Thesis*, Indian Institute of Technology, Kanpur, India.

[2] J. J. Rhyne, J. Appl. Phys. **40**, 1001(1969), Phys. Rev. **172**, 523(1968).

[3] J. S. Dugdale, Contemp. Phys. **28**, 547(1987).

[4] S. P. McAlister and C. M. Hurd, Phys. Rev. Lett. **37**, 1017(1976).

[5] S. P. McAlister and C. M. Hurd, Solid State Commun. **19**, 881(1976).

[6] A. K. Majumdar and P.v. Blanckenhagen, Phys. Rev. B **29**, 4079(1984); J. Magn. Magn. Mater. **40**, 227(1983).

[7] T. K. Nath, *Thesis*, Indian Institute of Technology, Kanpur, India.

[8] S. Banerjee, *Thesis*, Indian Institute of Science, Bangalore, India.

[9] G. Sinha, R. D. Barnard, and A. K. Majumdar, Phys. Rev. B **55**, 8982(1997);

[10] P. Haen, F. Lapierre, J. M. Mignot, and R. Tournier, J. Magn. Magn. Mater. **15**, 909(1980).

[11] F. E. Maranzana, Phys. Rev. **160**, 421(1967).

Chapter 7

Conclusions

We have started writing this thesis by asking whether there are any differences between an SG and an RSG? Various investigations on $Fe_{80-X}Ni_XCr_{20}$ ($14 \leq X \leq 30$) alloys have given us enough experimental evidences to conclude that there are differences between the SG and the RSG phases. We have found two different analytical forms for the time decay of the thermo-remanent magnetization(TRM) in the SG(X= 19) and the RSG(X= 23 and 26). In the RSG(X= 26), at the lowest temperature, the intrinsic LFMR is positive for zero biasing field, as observed in a FM, but the presence of a 18.2 gauss static biasing field makes the LFMR negative, a feature generally associated with a SG state. This suggests that the lowest temperature phase of the RSG has mixed FM and SG type of orderings. We believe that small FM clusters are embedded in a matrix of frustrated spins of the SG. We have observed a peak in non-linear susceptibility near T_g in the RSG that indicates the presence of a long-range order which has never been observed in a pure SG, including X=19. We also found that the behaviour and the magnitude of the Hall resistivity, ρ_H, for RSG lie in between the SG and the FM samples. In this Chapter we present some of the other conclusions of the present work.

We have measured the TRM in $Fe_{80-X}Ni_XCr_{20}$ ($14 \leq X \leq 30$) alloys for four different

magnetic phases within the *same crystallographic phase* and from their wait time and temperature variations tried to establish a correspondence with the magnetic phase diagram. We find distinct differences between the SG and the RSG phases with two different analytical forms for the time decay of the TRM. In the SG(X=19) very distinct ageing effects are observed where M(t) can be described as $M(t) = M_0(t/t_w)^{-\gamma}\exp[-(t/\tau)^{1-n}]$ for the entire time domain. In the RSG(X= 23 and 26), M(t) can be better represented by the stretched exponential with an addition of a constant term which can be explained well by the Gabay-Toulouse(GT) model. We also report the remarkable observation of the local maximum of the TRM just above T_C in the RSG (X=23) when it passes to the PM phase from the FM phase. This is found for the first time in any polycrystalline RSG. However, it's exact theoretical justification is unclear. We also observe that the values of the exponents show anomaly near the phase transitions. We observe some different features in the samples X=23 and X=26, though they undergo similar kinds of phase transitions. We find the conventional power law decay in the FM phase. The value of the magnetization is found to increase with the Ni concentration. In the AF phase the power law decay is indistinguishable from the stretched exponential as a description of the TRM. More experimental work is needed to arrive at a more definite conclusion about the decay of TRM in AF.

We have measured the LFMR in different magnetic phases of $Fe_{80-x}Ni_xCr_{20}$ alloys. We observe that the LFMR is negative in the SG(X=19) and the PM phases and positive in the FM (X=30) phase. In the RSG (X=26), at the lowest temperature (4.5 K), the intrinsic LFMR is positive for zero biasing field, but the presence of a 18.2 gauss static biasing field makes the LFMR negative, a feature generally associated with the SG state. This suggests that the lowest temperature phase of the RSG has mixed FM and SG-type of orderings. We believe that small FM clusters are embedded in a matrix of frustrated spins of the SG. We observe hysteresis effects in the LFMR for small applied fields at the lowest temperature for the RSG sample. But such small fields do not produce any hysteresis effect in the FM phase(X=30). We find that the LFMR becomes negative around T_C for a +4 gauss

pulsed field in the RSG. From the LFMR measurements, we conclude that when the RSG sample(X=26) goes from the PM to the FM phase with lowering of temperature, it passes through an intermediate phase. Here the PM(SG) phase coexists with the FM phase for a very narrow temperature interval. So with the reduction of temperature, the RSG sample passes through various magnetic phases like, $PM \rightarrow (PM(SG) + FM) \rightarrow FM \rightarrow RSG(= FM + SG)$. We also find a close resemblance between the temperature variation of the LFMR and the ac susceptibility in the RSG(X=26).

We have measured the low-field ac susceptibility in four different magnetic phases. In the SG (X=19), T_g varies with measuring frequency obeying a Fulcher law of the form $\nu = \nu_0 \exp[-\frac{E_a}{k(T_g - T_0)}]$. External dc biasing fields shift T_g towards lower temperatures and reduce the susceptibility. The variation of T_g can be understood in terms of a non-mean-field theory and the decrease of susceptibility can be explained in the framework of Néel's superparamagnetic model. Both the above features could also be explained in terms of a mean-field theory. A very distinct peak in χ_2 and the absence of χ_1 in the SG are consistent with theoretical predictions. The values of the critical exponent γ near T_C, obtained by two different methods, in the RSG (X=26) are closer to the mean-field prediction while the other two exponents β and δ are at variance. However, they satisfy the static scaling law within the experimental error. χ_0'' in the RSG shows a double transition with two distinct peaks at T_C and T_g. A dc biasing field shifts T_g towards higher temperatures in the RSG(X=26) in contrast to the opposite shift in the SG (X=19). As $T \rightarrow 0$, χ_0'' approaches a very small non-zero value in the RSG while in the SG it approaches a value which is $\approx 50\%$ of its peak value. The non-linear susceptibility, χ_1, shows a peak near T_g in both the RSG's (X=26 and 23) indicative of a long-range order. This has never been observed in any SG including X=19. This distinguishes the RSG from the SG. However, we observed some different features in the two samples X=23 and 26 although they undergo similar kinds of phase transitions. We find that the transition near T_g for X=23 is sharper than that near T_C. But the reverse is observed for X=26, whose composition is somewhat closer to the FM (X=30). We also find

that the value of the critical exponent γ increases with the increase of Ni concentration, X, from 23 to 30 as the system moves towards the FM phase. In the AF (X=14), around T_N, χ_0 shows a peak which shifts towards higher temperatures in the presence of small dc fields in agreement with the prediction of Kosterlitz et al. The present detailed, high-resolution data are expected to attract the attention of theorists in the field. Several findings remain unexplained in the light of existing theories.

The Hall effect for the four different phases of these alloys is also measured. In the SG(X= 19) the Hall resistivity(ρ_H) shows a non-linear behaviour with field which arises because of spin-orbit scattering. The temperature variation of ρ_H shows broad peaks around T_g for lower fields (< 0.1 T) but they disappear at higher fields(1 T). We have given an explanation for different behaviour of ρ_H with temperature for low and high fields in SG. We have separated the ordinary(OHC) and the extra-ordinary(EHC) Hall coefficients in the ferromagnetic sample(X=30) and shown their temperature variations. In the RSG (X=26) ρ_H shows a non-linear variation with field. The temperature variation of ρ_H shows anomaly near both T_g and T_C. In the antiferromagnetic phase (X=14) ρ_H increases linearly with field and its temperature variation shows broad peaks around T_N for lower fields.